AFFDL-TR-67-94

ANALYSIS AND EXPERIMENT OF RADIANT HEAT EXCHANGE BETWEEN SIMPLY ARRANGED SURFACES

R. VISKANTA
J. R. SCHORNHORST
J. S. TOOR

SCHOOL OF MECHANICAL ENGINEERING
PURDUE UNIVERSITY
LAFAYETTE, INDIANA

FOREWORD

This report was prepared by the School of Mechanical Engineering, Purdue University, under Contract No. AF 33(615)-2362 as part of Project 6146, Task 614616. The program was administered by the Air Force Flight Dynamics Laboratory, Wright-Patterson Air Force Base, Ohio. The Technical Monitor was Mr. C. J. Feldmanis.

The study presented herein, which began in May 1965 and was concluded in June 1967, was performed by R. Viskanta, J. T. Schornhorst, and J. S. Toor.

The manuscript was released by the authors June 30, 1967 for publication as an AFFDL Technical Report.

This technical report has been reviewed and is approved.

William C. Savage
Environmental Control Branch
Vehicle Equipment Division
AF Flight Dynamics Laboratory

ABSTRACT

The work reported herein covers the effort to improve the accuracy and to provide some confidence in the analytical methods for predicting radiant heat exchange among surfaces having nonelementary emission and reflection characteristics. The study consisted of an examination of the validity of commonly used simplified methods of radiant heat transfer analysis, measurements of local irradiation at a surface, and Monte Carlo calculations to estimate what level of detail is important in the description of the radiation characteristics of surfaces.

The radiant heat transfer problem was first formulated for a general enclosure with as few simplifying assumptions as possible and then specialized to a very simple configuration. Solutions for the local radiant heat flux and incident flux were obtained for seven different models approximating the radiation characteristics of surfaces. The models ranged from the simple diffuse, specular, and diffuse-specular constant property models to the very detailed directional emission and bidirectional reflection model.

The local irradiation was measured for five different materials and two simple configurations. The materials tested were sandblasted stainless steel, electropolished stainless steel, rough electroplated gold, smooth electroplated gold, and PV 100 white paint. Measurements were made over the temperature range from 50°F to 850°F for each of four sets of geometric parameters. The predictions of the local incident flux using the diffuse, specular, and diffuse-specular models have been compared with experimental results.

The Monte Carlo method was found to yield radiant heat transfer results of acceptable engineering accuracy. The results showed that under some conditions the choice of the model for radiation surface characteristics can be very critical for both the local heat transfer and overall radiant interchange claculations.

The effort has advanced the general technology and developed a number of important technical areas which are worthy of further study. The detailed results, discussion, and conclusions are given in the body of the report.

Distribution of this abstract is unlimited.

TABLE OF CONTENTS

LIST OF TABLES

LIST OF FIGURES

LIST OF SYMBOLS

Symbol	Definition
A	Area
a_o	Autocorrelation distance
BP	Abbreviation for directional emission and bidirectional reflection properties (model G)
CP	Abbreviation for constant properties
DP	Abbreviation for direction dependent properties
E	Emitted radiant energy flux
$\mathcal{F}_{ij}$	Hottel's radiation exchange factor defined by Eq. (6.5)
$\mathcal{F}'_{ij}$	Overall absorption factor defined by Eq. (6.4)
$\mathcal{F}'_{di-j}$	Local absorption factor defined by Eq. (6.3)
$\mathcal{F}''_{j-di}$	Local absorption factor defined by Eq. (6.16)
f	Reflection distribution function
f_∞	Reflection distribution function for an infinite electrical conductor
G	Irradiation (incident radiant flux) defined by Eq. (3.3)
G*	Dimensionless irradiation, $G/\epsilon\sigma T^4$
H,L,W,Z	Dimensions of surfaces, see Fig. 22
h	Plate separation distance, Fig. 3
I	Intensity of radiation
I_b	Black body intensity of radiation given by Planck's function
J	Radiosity (leaving radiant energy flux) defined by Eq. (3.4)
K_{12}, K_{21}	Kernels defined by Eqs. (A.18) and (A.19)

k	Imaginary part of the complex index of refraction
L	Plate width, Fig. 3
N	Number of energy bundles emitted
$\tilde{n}$	Complex index of refraction, $\tilde{n} = n-ik$
n	Real part of the complex index of refraction
Q	Overall radiant heat transfer rate
$Q_{i\rightleftarrows j}$	Overall radiant heat exchange between two finite surfaces i and j defined by Eq. (6.12)
q	Local heat flux
q^*	Dimensionless local heat flux, $q/\epsilon\sigma T^4$
R	Random number
$\vec{r}$	Position vector
T	Temperature
U	Function defined by Eq. (3.17)
x,y,z	Coordinates, see Figs. 3 and 22
α	Absorptivity
β	Included angle between plates, see Figs. 3 and 22
γ	Separation to width ratio, h/L
δ_1	Dimensionless distance, d_1/L
δ_2	Dimensionless distance, d_2/L
ϵ	Emissivity
η	Dimensionless coordinate, y/L
θ	Polar angle
λ	Wavelength
ξ	Dimensionless coordinate, x/L
ρ	Reflectivity

σ	Stefan-Boltzmann constant
σ_o	Optical root mean square roughness
σ_m	Mechanical root mean square roughness
ϕ	Azimuthal angle
$\vec{\Omega}$	Unit vector in direction (θ,ϕ) of the pencil of radiation, see Fig. 1
Ω	Solid angle

Subscripts

c	Refers to cold plate
h	Refers to hot plate
1,2,3	Refers to surfaces, see Figs. 3 and 22

Superscripts

d	Diffuse component of reflectivity
s	Specular component of reflectivity
'	Incident intensity or direction

1. INTRODUCTION

An understanding of heat transfer has become increasingly important for modern day technology. Contemporary applications have called for systems capable of operating at high temperatures or in the absence of convection, e.g., free space. Specific examples of these applications include space vehicles, solar energy conversion devices, power plants for space exploration needs, propulsion systems, etc. In these applications radiation heat transfer may be the major or the only means of energy transfer and its determination is of considerable practical importance.

In the design of the more complex space vehicles capable of penetrating into unfamiliar thermal environments the engineer must rely more than ever on the thermal control of the vehicle for optimum reliability and performance. This control can be achieved by passive or active means, but essential to either method is an accurate prediction of the radiant heat transfer. This particular application as well as others has called for more reliability, higher precision, and greater detail in radiant heat transfer predictions than were considered necessary in the past. Therefore a need has been generated for a more complete understanding of the basic principles of radiation heat transfer, more realistic methods of analysis, and more detailed knowledge of the radiation characteristics of surfaces.

The present study was conceived as an analytical and experimental evaluation of the validity and accuracy of the simplified models for approximating radiation surface characteristics and the different methods of radiant heat transfer analysis. Specifically, the purpose of the investigation conducted was twofold and can best be described by briefly summarizing the essential elements of the research program:

1. Using a more realistic and refined analysis, examine the accuracy of the commonly used simplified models for predicting radiation interchange between real surfaces.
2. Experimentally check the validity of the simplified methods of radiant heat transfer analysis.

The program as stated above is too ambitious and too inclusive to be treated thoroughly within the limits of the time and funding of the program. The specific tasks undertaken were therefore based upon the following steps:

1. Predict radiant heat transfer between representative simply arranged surfaces taking into account the dependence of radiation surface characteristics on wavelength, direction, and roughness.

2. Measure radiant heat transfer between simply arranged surfaces.

3. Compare analytical predictions with experimental data and examine the validity of the commonly used simplified methods of radiant heat transfer analysis.

4. Determine what level of detail is important in the prediction of overall and local heat transfer rates using the Monte Carlo method and estimate the accuracy of this computational procedure.

5. Estimate the useful range of the commonly used approximate methods for radiant heat transfer analysis and suggest simplified models and procedures which should be employed for more realistic radiant heat transfer design calculations.

2. LITERATURE SURVEY

The aim of this chapter is to present a review of the literature of the topics relevant to the present study. Emphasis is placed on contributions describing the most recent achievements. Most of the earlier work is referred to by way of textbooks or previous survey articles. The survey of literature covers two general areas: 1) analysis of radiant heat interchange, and 2) experimental measurement of radiant heat transfer.

2.1 Analysis of Radiant Heat Interchange

Until recently it had been a common engineering practice to predict radiant heat transfer by assuming that the participating surfaces are gray, perfectly diffuse,and non-polarizing. A number of computational procedures have been devised for calculating radiation interchange between gray diffuse surfaces. A review and comparison of these methods has been given by Sparrow [1]*. With the approximation that the radiosity or irradiation is uniform on each constant temperature surface (or zone), the standard methods permit the calculation of radiant heat exchange between n-surfaces with no greater difficulty than solving a system of n-algebraic equations. Unfortunately, the accuracy of the results obtained is uncertain due to the departure of the basic assumptions from actual conditions. Experiments performed some time ago [2,3] have shown that emission and reflection is not diffuse for actual materials. In spite of the experimental evidence, the postulate that the surfaces are diffuse has remained standard until recently. The justification for retaining the diffuse assumption has been computational simplicity. Another deficiency of the methods is that only the overall heat transfer rate for each surface (or a zone) can be calculated; local heat flux can not be predicted.

The emphasis on precision and greater detail demanded by newer applications to modern technology has brought forth new approaches and more realistic methods for computing radiant heat transfer. The assumption that the radiosity over a given surface is uniform has been relaxed by formulating the radiation exchange problems in terms of integral equations. A number of solutions for different geometrical arrangements has been reported in the literature. A

*Numbers in brackets donote references.

summary of some of these studies can be found in the review articles by Sparrow [1,4] and in the textbook by Sparrow and Cess[5].

As an alternate to the diffuse model the image method for calculating radiation interchange between plane surfaces which emit diffusely and reflect specularly has been developed by Eckert and Sparrow [6] and extended by Sparrow et al. [7]. This method has been employed in a number of studies to facilitate computation of radiation interchange in enclosures consisting of plane surfaces. The image method has also been applied for calculating radiation interchange in an axisymmetric configuration formed by specularly reflecting surfaces [8]. A more complete review of the literature concerning the diffuse emission and specular reflection model can be found in Reference [5].

Real surfaces are neither purely diffuse nor specular reflectors. A model which probably approaches more closely to physical reality has been suggested by Seban [9]. It involves a subdivision of the hemispherical reflectance into diffuse and specular components, such that

$$\rho = \rho^{d} + \rho^{s}$$

This approximation coupled with the assumption of diffuse emission also lends itself readily to analytical treatment. This model has been adopted by Sparrow and Lin [10] and by Sarofim and Hottel [11] for calculating radiation interchange between surfaces. The approach is more realistic than the methods already discussed; however, it is still not completely satisfactory since the radiation characteristics of surfaces are assumed to be independent of direction.

The radiation exchange problem between real surfaces can be formulated quite generally in terms of integral equations. Introduction of the reflection distribution function (bidirectional, biangular, or partial reflectance) permits a rigorous formulation of the radiation interchange problem [12,13]. There is, however, insufficient knowledge of the bidirectional reflectance for actual engineering materials, and even with such data available the solution of the radiation interchange equations is too formidable to be generally of practical use. Three approximate methods of increasing exactness for calculating radiation interchange within a multisurface enclosure made up of actual surfaces have been proposed by Bevans and Edwards [13]. Radiant heat exchange between two infinitely long specularly reflecting plates sharing a common edge and having direction dependent radiation surface properties has been analyzed by Hering [14].

The numerical solution of rigorously formulated radiation interchange problems is often impractical even on the very fast digital computers. As an alternate to the analytical formulation a statistical method known as Monte Carlo has recently been used and appears to be promising for evaluation of radiation interchange in complex systems and where radiation surface characteristics depend on direction as well as wavelength. The application of the Monte Carlo method to the analysis of radiation interchange between surfaces has been discussed by Howell [15] and Corlett [16]. A more complete and up to date survey of the literature dealing with the application of Monte Carlo and related methods to radiation interchange is given by Toor [17].

The review of the literature has revealed that few attempts have been made to analyze radiant heat transfer between actual surfaces with direction and wavelength dependent properties. The validity of the simplified methods of analysis has not been verified either by more realistic calculation schemes or by experimental measurements. It is clear that there is a definite need for more refined and yet manageable methods of prediction of radiant heat transfer.

2.2 Experiments on Radiant Heat Interchange

The experimental measurement of radiation interchange between surfaces, i.e., the overall radiant heat loss, the irradiation, etc., has received very little attention. Most of the research effort in the past has been devoted to the experimental determination of radiation surface characteristics. In a large number of experiments the overall radiant heat interchange was measured between simply arranged surfaces, such as two parallel plates or two concentric cylinders, and from these data the total hemispherical emittance was calculated. Other studies have involved the measurement of equilibrium temperatures of surfaces which are exchanging heat by radiation only. Reference [18] is one example of such studies.

To the authors' knowledge measurements of radiant heat exchange have been made by only a few investigators [19-21]. The overall heat transfer between two eccentric spheres having different surface properties was measured by Elser [19]. He found that heat transfer increased with eccentricity and attributed this finding to the increase in importance of specular reflection. A similar test arrangement was employed by Münch [20]. The inner sphere was made of copper and the outer of brass and both were highly oxidized. Münch found that the overall radiant heat transfer increased slightly with eccentricity and that the radiation interchange factor based on a diffuse-specular model for reflection agreed well with the experimental data. Radiant heat interchange between

two one square foot parallel, type 302 stainless steel, plates maintained at different temperatures was measured by Love and Gilbert [21]. For close spacings the measured overall heat transfer agreed within few percent with the predictions based on the diffuse model.

3. ANALYSIS OF RADIANT HEAT TRANSFER

The purpose of this chapter is threefold. First, to present a method of radiant heat transfer analysis which accounts for the spectral, directional, and mechanical (such as roughness) characteristics of engineering materials. Second, to focus attention on radiation interchange between some simply arranged surfaces and predict radiant heat transfer on the basis of more realistic models for radiation surface properties than has heretofore been attempted. Third, to compare the radiant heat transfer predictions based on the widely used idealized diffuse, specular, and diffuse-specular models for radiation surface properties with more refined models and thereby ascertain their validity and accuracy.

To this end, the general radiation interchange problem in a real enclosure is formulated and then specialized to a particular configuration. The radiation surface characteristics required in the implementation of the heat transfer analysis and the models for radiation surface properties adopted for consideration are discussed in some detail. Finally, the results are presented and analyzed.

3.1 Formulation of the Radiation Interchange Problem

A sufficiently general radiant heat transfer analysis between surfaces can best be given by considering radiation interchange in an enclosure. The "enclosure" may be fictitious and the concept as used here denotes a hypothetical region completely bounded by real surfaces of known radiation characteristics at which either the local temperature or the heat flux are prescribed and/or by imaginary surfaces over which the incident radiation field is completely specified. An enclosure defined in this manner encompasses practically all radiant heat transfer problems of engineering interest. This concept is introduced only for the purpose of making certain that all radiation, whether incident or leaving the system, is accounted for in the analysis.

The intent here is to formulate the radiation interchange problem between real surfaces with as few idealizing assumptions as possible. However, some of the postulates on which the analysis is based are necessary in order to make the problem

mathematically tractable and it is therefore desirable to discuss them before proceeding with the detailed formulation. The following simplifying assumptions are employed in the analysis:

1. The geometric optics theory is valid for the analysis of radiant heat interchange. The two fundamental postulates of the theory are: 1) the various effects and quantities are additive, and 2) the directional change of radiation is negligible. The former assumption implies that the phenomena of diffraction, interference and coherence are excluded [22].
2. Planck's and Kirchhoff's laws are valid. This assumption implies that the body which is exchanging heat by radiation is at thermodynamic equilibrium defined by temperature T and that there is no change in the nature of the body.
3. The radiation characteristics of surfaces are independent of the polarization state of the incident intensity.
4. The medium separating the surfaces does not participate in the exchange of radiation, i.e., is non-radiating.
5. The index of refraction of the medium separating the surfaces is constant, i.e., is equal to unity.

That assumption 3 is not generally valid is well recognized [22] and has been examined in more detail by Edwards and Bevans [23]. No conceptual difficulties would be introduced by omitting assumptions 4 and 5; however, they have been retained in the present treatment for the sake of reducing the nonessential mathematical complications. Assumptions 1 and 2 are not expected to seriously impair the relevancy of the analysis for engineering applications.

For the purpose of defining the radiant energy quantities of interest consider some typical surface element, say dA, on an opaque surface specified by a position vector $\vec{r}$ as pictured in Fig. 1. The unit vector $\vec{\Omega}'$, i.e., the polar angle θ' and azimuth angle ϕ', denotes the direction of the incident pencil of rays and $d\Omega'$ the elementary solid angle around it. Similarly, the unit vector $\vec{\Omega}$ denotes the direction of the emitted and reflected pencil of rays and the elementary solid angle to which the rays are confined is $d\Omega$.

The local spectral radiant heat flux, $q(\vec{r},\lambda)$, can be expressed from the viewpoint of an observer just inside the body as

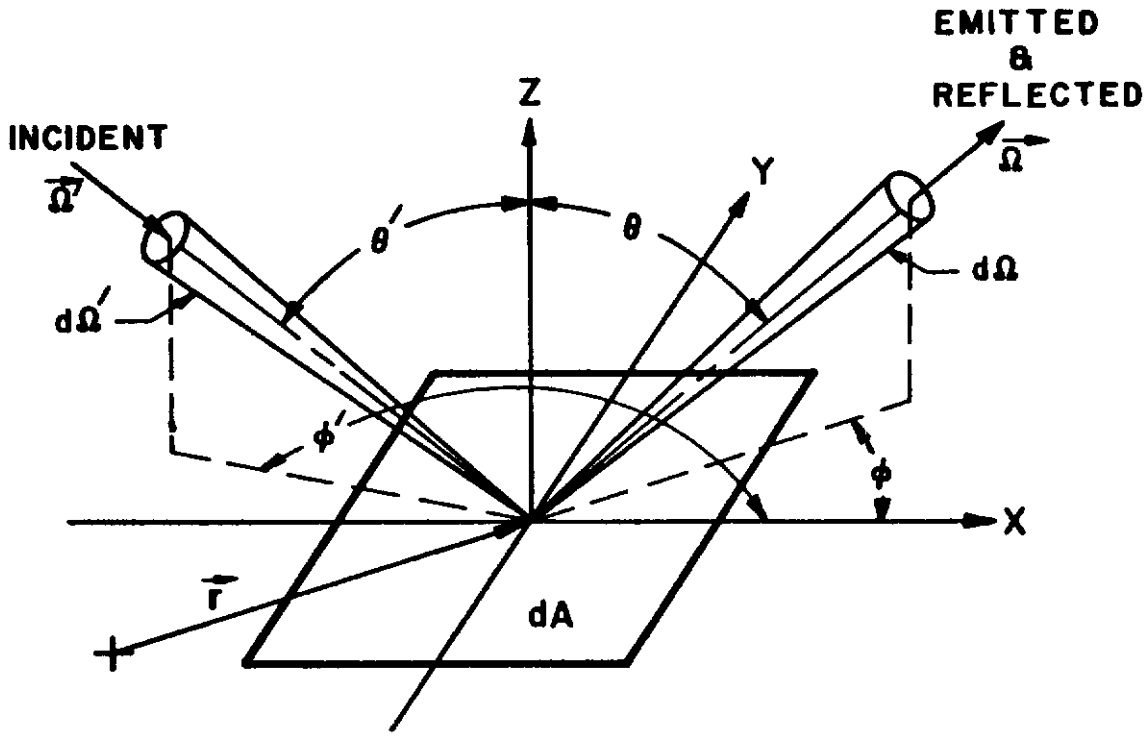

Figure 1

Geometry of Radiation Incident and Leaving a Differential Area

$$q(\vec{r},\lambda) = \epsilon(\vec{r},\lambda)E_b(\vec{r},\lambda) - \alpha(\vec{r},\lambda)G(\vec{r},\lambda) \qquad (3.1)$$

or from the viewpoint of an observer just outside of the body as

$$q(\vec{r},\lambda) = J(\vec{r},\lambda) - G(\vec{r},\lambda) \qquad (3.2)$$

The spectral irradiation (incident flux) $G(\vec{r},\lambda)$ is defined as

$$G(\vec{r},\lambda) = \int_{\Omega'} I'(\vec{r},\vec{\Omega}',\lambda)\cos\theta' d\Omega' \qquad (3.3)$$

and the spectral radiosity (leaving flux) is defined as

$$J(\vec{r},\lambda) = \int_{\Omega} I(\vec{r},\vec{\Omega},\lambda)\cos\theta d\Omega \qquad (3.4)$$

In Eq. (3.3) $I'(\vec{r},\vec{\Omega}',\lambda)$ denotes the spectral intensity of radiation incident on dA from the direction $\vec{\Omega}'$ and $I(\vec{r},\Omega,\lambda)$ denotes the spectral intensity of radiation leaving (emitted plus reflected) dA in the direction $\vec{\Omega}$. The total (integrated over the entire spectrum) local radiant heat flux is obtained by integrating $q(\vec{r},\lambda)$ over all wavelengths.

$$q(\vec{r}) = \int_0^\infty q(\vec{r},\lambda)d\lambda \qquad (3.5)$$

Examination of Eqs. (3.1) through (3.5) reveals that the evaluation of radiant heat flux reduces to finding the spectral intensity of radiation leaving or incident on a surface.

With the assumption of no diffraction, interference, coherence, and polarization effects the spectral intensity of radiation, $I_i(\vec{r}_i,\vec{\Omega}_i,\lambda)$, leaving the opaque differential element of area dA_i on surface i in the direction $\vec{\Omega}_i$, see Fig. 2, is

$$I_i(\vec{r}_i,\vec{\Omega}_i,\lambda) = \epsilon(\vec{r}_i,\vec{\Omega}_i,\lambda)I_b(\vec{r}_i,\lambda) + \int_{\Omega_i'} f_i(\vec{r}_i;\ \vec{\Omega}_i',\vec{\Omega}_i;\lambda)I_i'(\vec{r}_i,\vec{\Omega}_i',\lambda)\cos\theta_i' d\Omega_i' \qquad (3.6)$$

The first term in Eq. (3.6) represents the intensity of emitted radiation in the direction $\vec{\Omega}_i$ and the second the intensity of reflected radiation in the direction $\vec{\Omega}_i$ as a result of contributions due to the energy incident on the element of area dA_i from the surroundings. The reflection distribution function $f(\vec{r};\ \vec{\Omega}',\vec{\Omega};\lambda)$ can be interpreted as a probability function. The expression

$$f(\vec{r};\ \vec{\Omega}',\vec{\Omega};\ \lambda)\cos\theta' d\Omega'$$

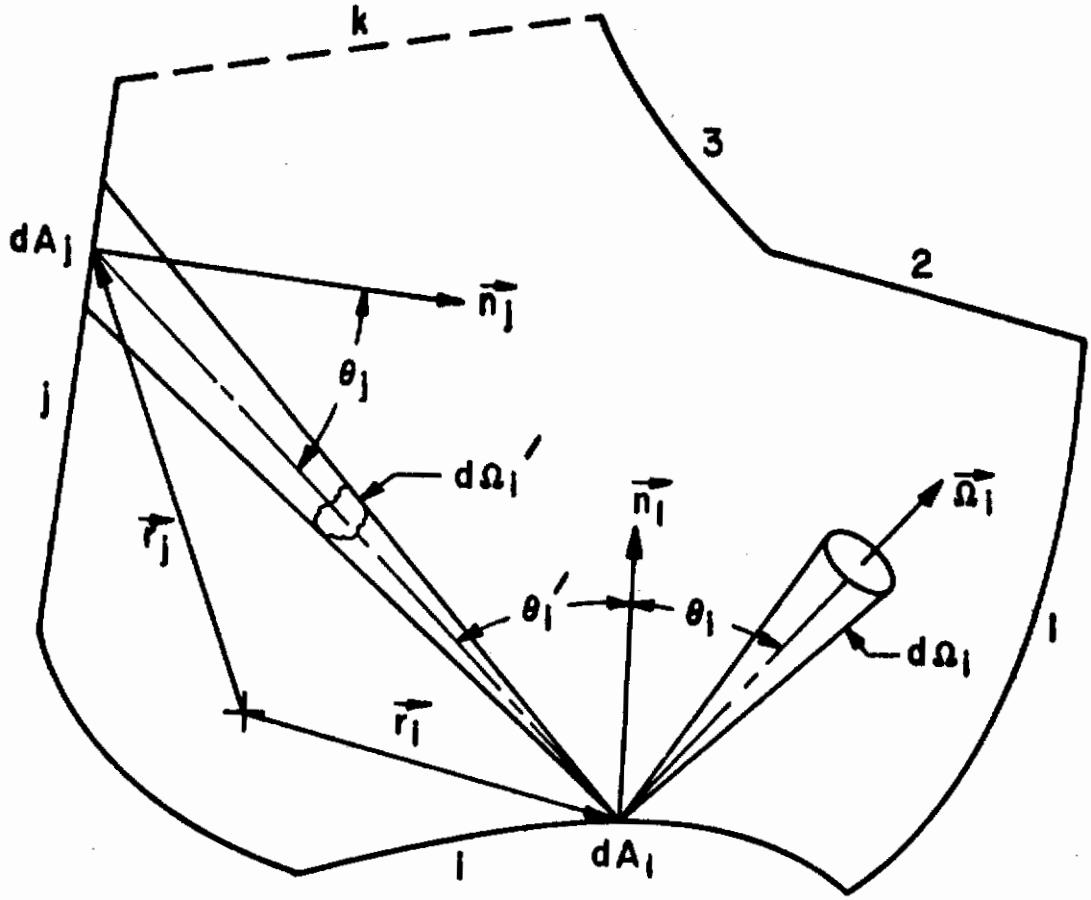

Figure 2

Geometry for Radiant Interchange in an Enclosure

represents the probability that an incoming bundle of rays $(\vec{\Omega}', d\Omega')$ will be reflected at a given point on the surface into the pencil rays $(\vec{\Omega}, d\Omega)$. It was first introduced by McNicholas [24] and employed by Polyak [12] in formulating the radiant interchange problem.

Since the intensity of radiation is constant along a path in a non-radiating medium having a constant index of refraction or in free space, the spectral intensity of radiation leaving the elementary area dA_j in the direction $\vec{\Omega}_j$, must be equal to the spectral intensity of radiation incident on the elementary area dA_i from direction $\vec{\Omega}_i'$, i.e.,

$$I_j(\vec{r}_j, \vec{\Omega}_j, \lambda) = I_i'(\vec{r}_i, \vec{\Omega}_i', \lambda) \tag{3.7}$$

We further note from Fig. 2 that the elementary solid angle $d\Omega_i'$ subtended by dA_j as viewed from dA_i is given by

$$d\Omega_i' = \cos\theta_j dA_j / |\vec{r}_i - \vec{r}_j|^2 \tag{3.8}$$

With the aid of Eqs. (3.7) and (3.8), Eq. (3.6) can be expressed as

$$I_i(\vec{r}_i, \theta_i, \phi_i, \lambda) = \epsilon_i(\vec{r}_i, \theta_i, \phi_i, \lambda) I_b(\vec{r}_i, \lambda) + \sum_{j=1}^{n} \int_{A_j} f_i(\vec{r}_i; \theta_i', \phi_i'; \theta_i, \phi_i; \lambda) I_j(\vec{r}_j, \theta_j, \phi_j, \lambda) K_{ij} dA_j \tag{3.9}$$

where the configuration kernel K_{ij} is defined as

$$K_{ij} = \cos\theta_i' \cos\theta_j / |\vec{r}_i - \vec{r}_j|^2 \tag{3.10}$$

Note that the angles involved in the sources of radiation (θ_j, ϕ_j) have now been referred to the source surfaces. The integration indicated in Eq. (3.9) extends only over those parts of surface j which are directly "visible" from dA_i. The summation over all surfaces j includes even the contributions from surface i itself if it is concave and is "visible" from dA_i.

Radiant energy may enter and leave the enclosure through the imaginary "surfaces"; however. the spectral intensity of radiation incident on a surface must be completely specified. Since the imaginary surface is perfectly transparent to radiation (it neither emits, absorbs, nor reflects), the radiation incident from some external source on the outside of surface k is equal to the spectral intensity of radiation leaving the surface

$$I_k'(\vec{r}_k,\ -\theta_k',\ -\phi_k',\lambda) = I_k(r_k,\theta_k,\phi_k,\lambda) \qquad (3.11)$$

Thus, any radiation which may enter the enclosure can be accounted for. For an enclosure consisting of m real surfaces, Eq. (3.9) contains m unknown functions I_1, I_2, ... I_m. Since the unknown appear under the integral sign, the m resulting equations are integral equations. Once the solution for I_i's has been determined from Eq. (3.9) for specified surface temperatures, the local radiant heat flux follows directly from Eq. (3.5). If, however, the local heat flux distribution is prescribed and it is necessary to calculate the temperature distribution the problem is much more difficult since an iterative procedure must be employed to solve Eqs. (3.5) and (3.9) simultaneously.

The preceding formulation of the problem is rigorous, theoretically exact, and straightforward; however, the exact solution of the governing equations is not feasible, and a numerical solution is in general too formidable and hardly an attractive prospect for engineering calculations. Thus, in order to make some progress it is desirable to select a favorable physical situation which retains the essential features of the analysis while avoiding the distractions of complex geometrical relationships. The physical system chosen for analysis is illustrated in Fig. 3. It consists of two finite width plates which extend indefinitely in the direction normal to the plane of the figure. The choice of this configuration was dictated by the following considerations: 1) the system has a simple geometrical character and with a proper choice of geometrical parameters approximates a large number of arrangements of practical engineering interest, 2) it encompasses open as well as closed systems and will thus permit a more critical examination of the influence of directional effects on radiation interchange, and 3) some heat transfer results are available from previous studies [6,14,25,26] for certain limiting situations.

For this geometry when both plates have surface temperatures and properties which are independent of the longitudinal coordinate, the integral Eqs. (3.9) reduce to a pair of equations

$$I_1(\xi_1,\xi_2,\eta_2,\lambda) = \epsilon_1(\xi_1,\xi_2,\eta_2,\lambda)I_{b1}(\xi_1,\lambda) +$$

$$\int_{-\infty}^{\infty}\int_0^1 f_1(\xi_1,\xi_2,\eta_2,\xi_2',\eta_2',\lambda)I_2(\xi_1,\xi_2',\eta_2',\lambda)K_{12}d\xi_2'd\eta_2' \qquad (3.12)$$

and

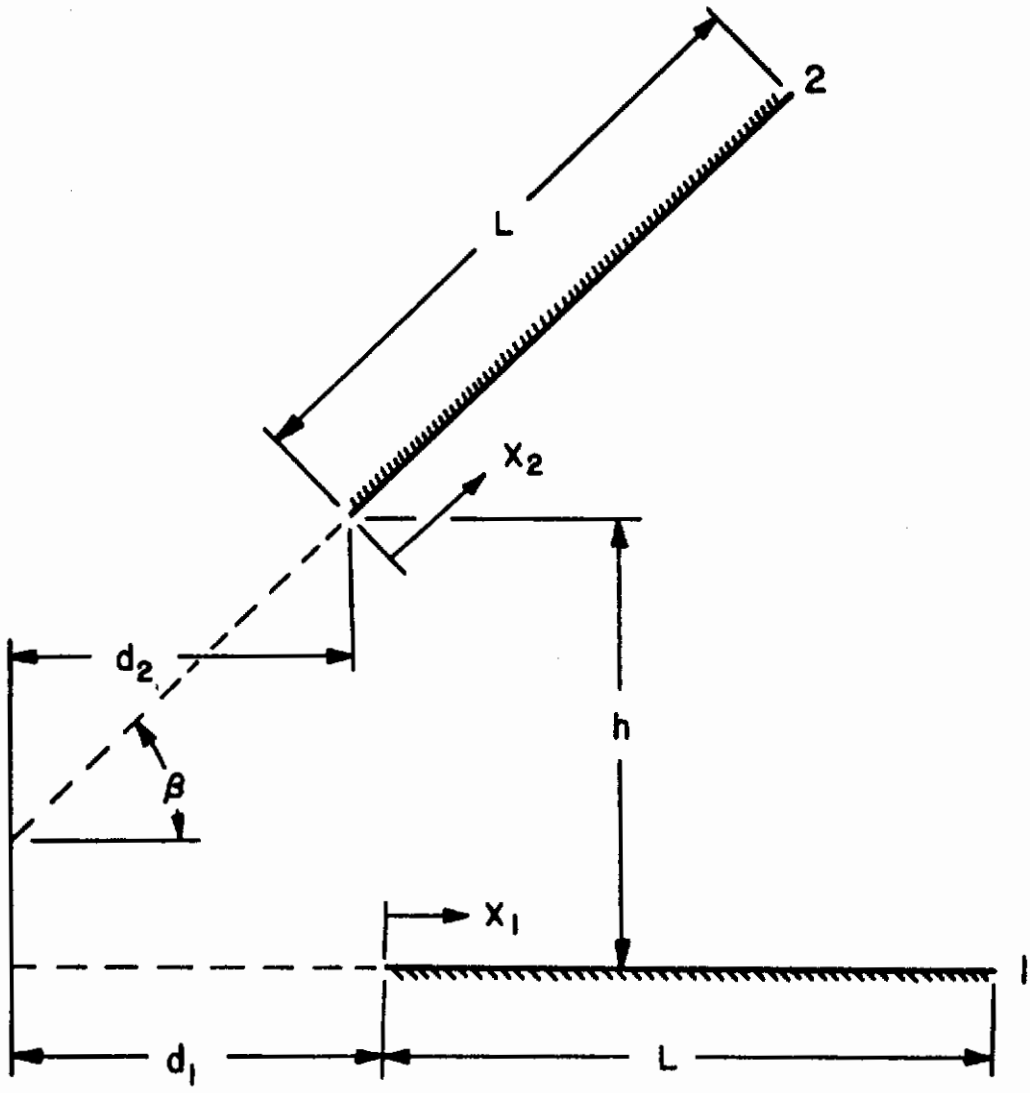

Figure 3

Infinitely Long Plate Configuration

$$I_2(\xi_2,\xi_1,\eta_1,\lambda) = \epsilon_2(\xi_2,\xi_1,\eta_1,\lambda)I_{b2}(\xi_2,\lambda) +$$

$$\int_{-\infty}^{\infty}\int_{0}^{1} f_2(\xi_2,\xi_1,\eta_1,\xi_1',\eta_1',\lambda)I_1(\xi_2,\xi_1',\eta_1',\lambda)K_{21}d\xi_1'd\eta_1' \quad (3.13)$$

The angles defining the directions of incidence, reflection and emission have been expressed in terms of the position coordinates. The mathematical details are given in Appendix A. It now remains only to adopt theoretical models for the radiation characteristics of the surfaces before proceeding with numerical solution of Eqs. (3.12) and (3.13).

3.2 Radiation Characteristics of Surfaces and Theoretical Models

In analyzing the interchange of radiant energy among surfaces, one needs an acceptable description of the emission, absorption and reflection characteristics, including the reflection distribution function, of the participating surfaces. For the present application, where an attempt is made to evaluate the importance of real surface effects, considerable detail is required in specifying the radiation properties. However, the intent here is not an accurate reproduction of radiation surface characteristics of any particular material by analytical expressions, but only a qualitatively correct functional form which represents the gross trends of the properties with direction and wavelength.

3.2.1 Reflection Distribution Function

A number of theoretical models for the distribution of reflected electromagnetic radiation from surfaces with different topographies have been proposed in the literature and are reviewed by Beckmann and Spizzichino [27]. However, most of these models are derived for electrical conductors having infinite conductivity and are usually modified in some approximate manner for application to real engineering materials. Houchens and Hering [28] have critically examined the Davies [29] and Beckmann [27] models. They have discarded the former in favor of the latter on the basis of two criteria. First, the Beckmann model has a firmer theoretical foundation and a wider range of applicability. Second, the Davies model violated the energy conservation requirement. Houchens and Hering have also found that the Beckmann model agrees reasonably well with the limited data available.

The basic postulates made by Beckmann in deriving the theoretical model for a rough surface are discussed in detail elsewhere [27,28] and need not be repeated here. The reflection distribution function for an infinite conductivity material, $f_\infty(\theta',\pi;\ \theta,\phi;\ \lambda)$, is conveniently expressed [27] as a sum of the coherently reflected energy, $f_{\infty,c}(\theta',\lambda)$, and the incoherently reflected energy, $f_{\infty,ic}(\theta',\pi;\ \theta,\phi,\lambda)$,

$$f_\infty(\theta',\pi;\ \theta,\phi;\ \lambda) = f_{\infty,c}(\theta';\ \lambda)U(\delta) + f_{\infty,ic}(\theta',\pi;\ \theta,\phi;\lambda) \quad (3.14)$$

where

$$f_{\infty,c}(\theta',\ \lambda) = \exp\left\{-[4\pi(\sigma_o/\lambda)\cos\theta']^2\right\} \quad (3.15)$$

$$f_{\infty,ic}(\theta',\pi;\ \theta,\phi;\ \lambda) = \frac{\pi\ (a_o/\lambda)^2}{\cos\theta\ \cos\theta'}\left[\frac{1+\cos\theta\cos\theta'-\sin\theta\sin\theta'\cos\phi}{\cos\theta+\cos\theta'}\right]^2 \exp\left\{-[2\pi(\sigma_o/\lambda)(\cos\theta+\cos\theta')]^2\right\}\sum_{m=1}^{\infty}\frac{[4\pi^2(\sigma_o/\lambda)^2(\cos\theta+\cos\theta')^2]^m}{m(m!)}$$

$$\exp\left\{-\frac{\pi^2}{m}\ (a_o/\lambda)^2[\sin^2\theta'+\sin^2\theta-2\sin\theta'\sin\theta\cos\phi]\right\} \quad (3.16)$$

and

$$U(\delta) = \delta(\theta' - \theta)\delta[\phi' - (\phi + \pi)]/\cos\theta' d\Omega' \quad (3.17)$$

In Eq. (3.17) $\delta(x)$ is the Dirac delta function and is defined as follows:

$$\delta(x-x') = \begin{cases} 0 & \text{if } x \neq x' \\ +\infty & \text{if } x = x' \end{cases} \quad \text{and} \quad \int_{-\infty}^{\infty}\delta(x-x')dx=1 \quad (3.18)$$

The reflection distribution function for engineering materials (having finite electrical conductivity) can be simply approximated by multiplying the reflection distribution function by the directional reflectivity $\rho(\theta',\lambda)$ of an actual material with an optically smooth surface such that [27,30]

$$f(\theta',\pi;\ \theta,\phi;\ \lambda) \simeq \rho(\theta',\lambda)f_\infty(\theta',\pi;\ \theta,\phi;\ \lambda) \quad (3.19)$$

In general this relation is not expected to correctly account for finite conductivity of materials; however, the difficulty of including this effect rigorously in the theory [27] partly justifies this approximation.

It is now of interest to show the relationship between the reflection distribution function and the directional radiation characteristics of the surface. The bidirectional reflectance $\rho(\theta',\phi';\ \theta,\phi,\lambda)$ [5] is related to the reflection distribution function by

$$\rho(\theta',\phi';\ \theta,\phi;\ \lambda) = f(\theta',\phi';\ \theta,\phi;\ \lambda)\cos\theta d\Omega \qquad (3.20)$$

But according to the Helhmoltz reciprocity principle [31] the distribution function is symmetrical with respect to the incidence and reflection angles, i.e.,

$$f(\theta',\phi';\ \theta,\phi;\ \lambda) = f(\theta,\phi;\ \theta',\phi';\ \lambda) \qquad (3.21)$$

This condition is a requisite of the 2nd Law of Thermodynamics and is rigorously valid only for phenomena at a surface which is in thermodynamic equilibrium with the surroundings. Integrating Eq. (3.20) over all reflected solid angles and making use of Eq. (3.21), yields

$$\rho(\theta',\phi',\lambda) = \int_{\Omega} f(\theta,\phi;\ \theta',\phi';\ \lambda)\cos\theta d\Omega \qquad (3.22)$$

This equation represents the spectral directional reflectance, i.e., the ratio of the reflected energy that is collected over the entire hemispherical space to the radiant energy contained in the incident beam $(\vec{\Omega}',d\Omega')$. Equation (3.22) may be utilized for finding the spectral directional absorptance of opaque materials through the relation

$$\alpha(\theta',\phi',\lambda) = 1 - \rho(\theta',\phi',\lambda) \qquad (3.23)$$

Consequently, making use of Kirchhoff's law

$$\epsilon(\theta',\phi',\lambda) = \alpha(\theta',\phi',\lambda) \qquad (3.24)$$

an equivalence is established between directional emittance and reflectance.

For two special cases the reflection distribution function reduces to very simple expressions. In the limiting case of perfectly diffuse reflection, the hemispherical reflectance $\rho(\lambda)$ is related to the reflection distribution function by

$$f(\theta',\pi;\ \theta,\phi;\ \lambda) = \rho(\lambda)/\pi \qquad (3.25)$$

In the other limiting case of perfectly specular reflection, the incident and reflected angles are related, i.e., $\theta' = \theta$ and $\phi' = \phi \pm \pi$. Thus, the reflection distribution function

for a perfectly specular reflection with the hemispherical reflectance $\rho(\lambda)$ reduces to

$$f(\theta',\pi;\ \theta,\phi;\ \lambda) = \rho(\lambda)U(\delta) \tag{3.26}$$

3.2.2 Directional Properties

A state of the art review of methods of predicting directional surface characteristics has recently been given by Sparrow and Cess [5]. Suffice it to say that the classical electromagnetic theory provides a prediction of spectral directional reflectivity of optically smooth and physically as well as chemically clean interfaces. The directional reflectivity for unpolarized incident radiation is expressed as the average of the reflectivities for radiation polarized perpendicular, $\rho_{\perp}(\theta',\lambda)$, and parallel, $\rho_{\parallel}(\theta',\lambda)$, to the plane of incidence

$$\rho(\theta',\lambda) = \tfrac{1}{2}[\rho_{\perp}(\theta',\lambda) + \rho_{\parallel}(\theta',\lambda)] \tag{3.27}$$

The directional reflectivities for the two components of polarization are given by Fresnel's equations in terms of the complex index of refraction, $\tilde{n}(\lambda) = n(\lambda) - ik(\lambda)$. The expressions are well known [5] and need not be repeated here. For an opaque material the spectral directional absorptivity is simply

$$\alpha(\theta',\lambda) = 1 - \rho(\theta',\lambda) \tag{3.28}$$

Furthermore, Kirchhoff's law, Eq. (3.24), permits one to infer spectral directional emissivity.

The theory and data agree only qualitatively; however, the directional trends predicted are reasonably correct. This provides at least a partial justification for using the electromagnetic theory to estimate dependence of properties on direction.

3.2.3 Theoretical Models for Radiation Surface Characteristics

In order to examine the validity of the commonly used simplified analyses, physically more realistic models have to be considered. For this purpose seven different models ranging from the diffuse model to the most sophisticated one for which the reflection distribution function is given by

Eq. (3.19) were adopted. In the following these models are briefly discussed.

Model A. This is the familiar diffuse model. The emissivity and reflectivity are considered to be independent of direction, and the radiation characteristics are assumed to be given by

$$\epsilon(\lambda) = 1 - \rho(\lambda) \tag{3.29}$$

and

$$f(\theta',\pi;\ \theta,\phi;\ \lambda) = \rho(\lambda)/\pi \tag{3.30}$$

This model has been studied most extensively and lends itself readily to analytical treatment. Some exact heat transfer results, based on this model, for the system considered here have already been reported [25].

Model B. This is the simple specular model. The surfaces are assumed to be diffuse emitters and specular reflectors. The emissivity and the reflectivity are independent of direction and are related by Eq. (3.29). The reflection distribution function is expressed as

$$f(\theta',\pi;\ \theta,\phi;\ \lambda) = \rho(\lambda)U(\delta) \tag{3.31}$$

The model was proposed recently [6,7] and some radiant heat transfer results are available [6,26].

Model C. This is the diffuse-specular model and is a combination of Models A and B. The surfaces are considered to be diffuse emitters and to have both a diffuse and a specular reflection component, such that

$$\rho(\lambda) = \rho^{s}(\lambda) + \rho^{d}(\lambda) \tag{3.32}$$

$$f(\theta',\pi;\ \theta,\phi;\ \lambda) = \rho^{s}(\lambda)U(\delta) + \rho^{d}(\lambda)/\pi \tag{3.33}$$

This approach suggested by Seban [9] is more realistic than the two previous models. It lends itself to analytical treatment and has been adopted by a number of investigators [5]. In this analysis the specular component of hemispherical reflectivity was calculated from the equation

$$\rho^{s}(\lambda) = \frac{1}{\pi}\int_0^{2\pi}\int_0^{\pi/2}\rho(\theta',\lambda)\exp\left\{-[4\pi(\sigma_o/\lambda)\cos\theta']^2\right\}\cos\theta'\sin\theta'\,d\theta'\,d\phi' \tag{3.34}$$

Model D. The reflectivity and emissivity are considered to be functions of direction, i.e.,

$$\epsilon(\theta',\lambda) = 1 - \rho(\theta',\lambda) \tag{3.35}$$

The radiant energy incident on the surface is assumed to be reflected diffusely; however, the fraction of energy in the incident bundle of rays which is reflected into the hemisphere depends on the incident direction such that the reflection distribution function is approximated by

$$f(\theta',\pi;\ \theta,\phi;\ \lambda) = \rho(\theta',\lambda)/\pi \tag{3.36}$$

The directional reflectivity for unpolarized radiation is predicted from Fresnel's equations.

Model E. In this model it is assumed that the surface is a specular reflector and that the emissivity and reflectivity depend on direction as given by Fresnel's equations. The reflection distribution function is approximated by

$$f(\theta',\pi;\ \theta,\phi;\ \lambda) = \rho(\theta',\lambda)U(\delta) \tag{3.37}$$

This idealization of radiation surface properties was used by Hering [14].

Model F. This is a combination of Models D and E and therefore a generalization of Model C which allows for the directional dependence of properties. The reflectivity and emissivity are considered to be given as a function of direction by Fresnel's equations. The fraction of diffusely or specularly reflected energy is also dependent on direction as given by the reflection distribution function

$$f(\theta',\pi;\ \theta,\phi;\ \lambda) = \rho(\theta',\lambda)\exp\left\{-[4\pi(\sigma_o/\lambda)\cos\theta']^2\right\}U(\delta) + \rho(\theta',\lambda)\left[1 - \exp\left\{-[4\pi(\sigma_o/\lambda)\cos\theta']^2\right\}\right]/\pi \tag{3.38}$$

Model G. The final and the most sophisticated model is based on Beckmann's expression for the reflection distribution function, Eq. (3.19). The directional reflectivity is predicted from Fresnel's equations and the directional emissivity calculated from Eq. (3.35).

3.3 Analytical Results and Discussion

Heat transfer results have been obtained for the parallel plate geometry for each of the seven theoretical models describing the radiation characteristics of surfaces. This arrangement is represented in Fig. 3 with $\beta = d_1 = d_2 = 0$. Furthermore, the results reported are restricted to the symmetrical situation. This was done by assuming that the radiation surface properties and temperatures are identical and uniform over both surfaces. This is arbitrary and the

assumption was introduced only for the purpose of reducing the number of independent parameters and thereby the computing effort. The nature of radiation interchange is, however, not affected by this choice and was considered to be a reasonable one. In view of the symmetry, $I_1(\xi_1,\xi_2,\eta_2\lambda) = I_2(\xi_2,\xi_1,\eta_1,\lambda)$, the problem reduces to the solution of a single integral Eq. (3.12) or Eq. (3.13) instead of a simultaneous solution of a pair of integral equations. The method of solution of the resulting integral equation is discussed in more detail in Appendix B.

When the directional and spectral dependence of radiation surface properties are considered many independent parameters are needed to describe the surface characteristics. Therefore, instead of arbitrarily choosing, say, the spectral hemispherical reflectance, and then calculating the optical constants and other parameters of interest the properties were predicted for an ideal engineering surface. The optical properties for this surface were assumed to be predicted by Drude's relation [32], with the electrical resistivity representative of a high alloy steel. For high alloy steels the theory predicts reasonably well the dependence of reflectance on wavelength but the agreement with experimental data is only qualitative and not quantitiative. It is recognized that for high electrical conductivity materials such as copper, gold, silver, etc. the optical properties predicted are no longer accurate and more sophisticated theories are needed [33, 34]. For the purpose of this study, the choice of the simple Drude relation to predict optical constants was considered reasonable. With the optical constants $n(\lambda)$ and $k(\lambda)$ known the spectral directional reflectivity was obtained from Fresnel's equations.

The numerical solutions were carried out for selected wavelengths in the range of general engineering interest λ=1,5,10,25. and 50μ. The values of the parameters σ_o and a_o characterizing the topographies of surface were chosen to include a complete range of values of optical roughness, σ_o/λ. The numerical calculations were performed for spacing to width ratios γ of 2.0,1.0,0.5, and 0.25. No attempt was made to obtain results for smaller values of γ because of an excessive use of computer time, particularly for models C,E, F and G when σ_o/λ was small and/or a_o/λ was large, and since an earlier study [17] indicated that the choice of the model in radiant heat transfer analysis is more critical for larger γ.

The local (spectral) heat flux $q(\xi,\lambda)$ was computed from Eq. (3.1) utilizing the solutions of the integral Eq. (3.13). The variation of $q(\xi,\lambda)$ along the surface is shown graphically in Fig. 4 with the wavelength (i.e., spectral hemispherical emissivity $\epsilon(\lambda)$) as a parameter*. The abscissa range extends only over half of the surface, since there is

*In Figs. 4,5,6, and 7 the letters A,B,...G refer to the theoretical models discussed in Section 3.2.3.

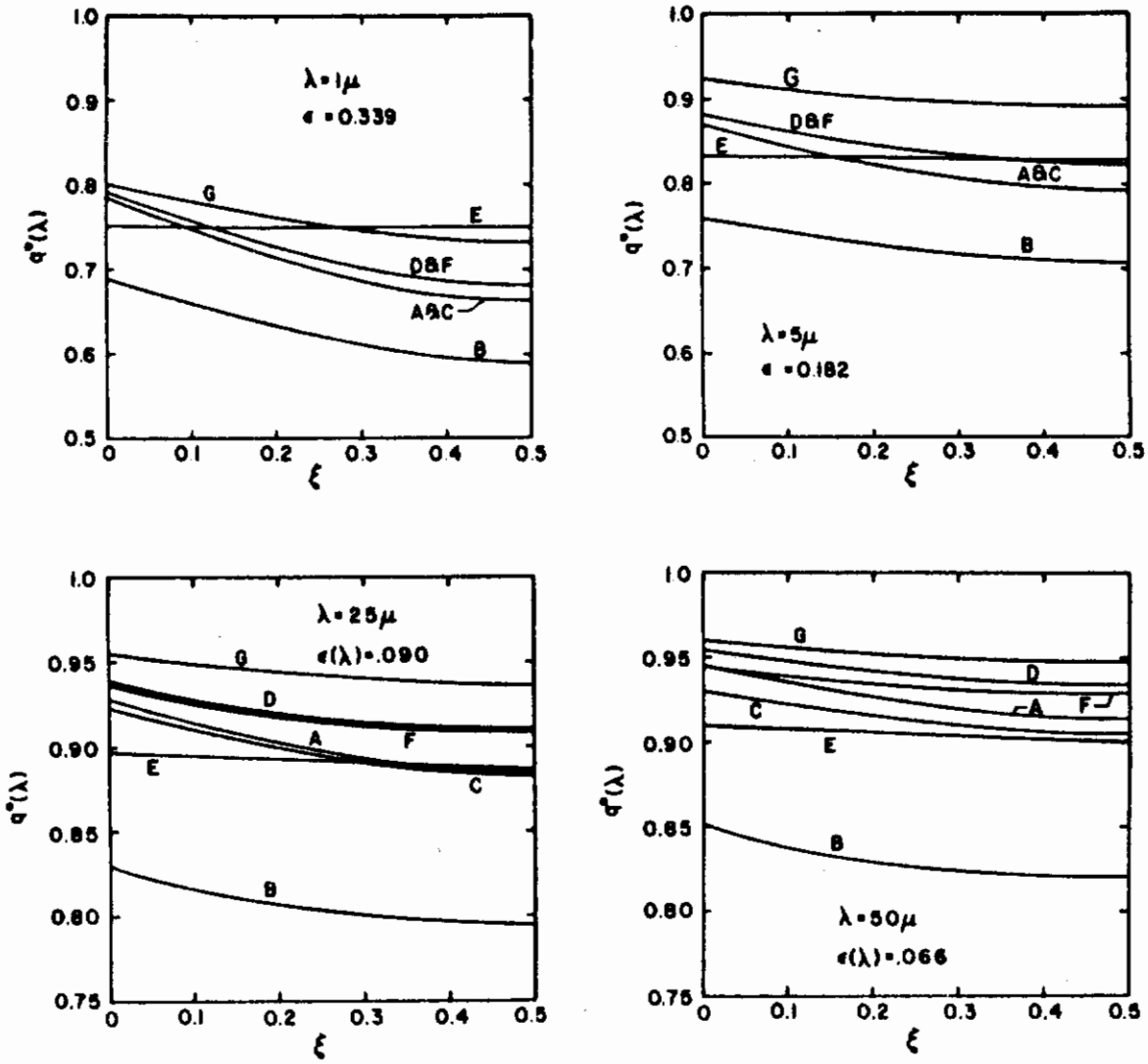

Figure 4

Effect of Wavelength on Local Heat Loss;
$\gamma = 0.5$, $\beta=\delta_1=\delta_2=0$, $\sigma_o=a_o = 5.0\mu$

symmetry about $\xi = 0.5$ for the parallel plate geometry. Heat transfer results for this geometry and diffuse (model A) surfaces have already been reported by Sparrow et al. [25] and for specular (model B) surfaces by Eckert and Sparrow [6]. Looking at the figure and taking note of the highly expended ordinate scale (since q is divided by ϵ), it is seen that the variation of the heat transfer along the plate is small for the relatively large spacing to width ratio $\gamma = h/L = 0.5$. This was expected on basis of the results reported in References 25 and 6. It is also observed that for the parameters considered the local heat loss $q(\xi,\lambda)$ is only slightly smaller than the emission $\epsilon(\lambda)\, E_b(\lambda)$ and that the predictions based on various models do not differ by more than 30 percent. Although q is generally the quantity of interest it does not appear to provide a critical comparison of the different models. Therefore, for the purpose of checking the validity of the models the results are reported on the basis of the local irradiation. It should be noted that this is the quantity which will actually be measured experimentally. The results of local irradiation calculations are presented in Figs. 5 through 7. The effect of wavelength is illustrated in Fig. 5 and the influence of the separation to width ratio in Fig. 6. The effect of optical roughness σ_o/λ and autocorrelation distance a_o/λ is illustrated in Fig. 7.

Several trends are apparent in Figs. 5 through 7. The first of these is that the models which assume reflection to be diffuse, either with or without directional effects, almost always predict a higher local heat transfer than those which assume specular reflection; that is, model A predicts a heat transfer rate greater than B and model D predicts a rate greater than E. This is due to the fact that for every diffuse reflection the radiation is reflected uniformly in all directions while for specular reflection only in one direction. Therefore, with each reflection more energy is lost from the system with diffuse reflection than with specular reflection. The second trend is that for direction dependent properties the heat loss is always greater than for constant properties. This is mainly due to the directional emissivity. Since metals characteristically have higher emissivities at directions far from the normal much of the emitted energy is lost directly from the system before any reflections occur thereby increasing the heat loss and decreasing the irradiation. This effect is evident in all three possible comparisons; D and A, E and B, and F and C. The third observation is that model G usually predicts lower irradiation, although the result is wavelength dependent. In some instances the local irradiation predicted on the basis of the specular model B is more than three times larger than

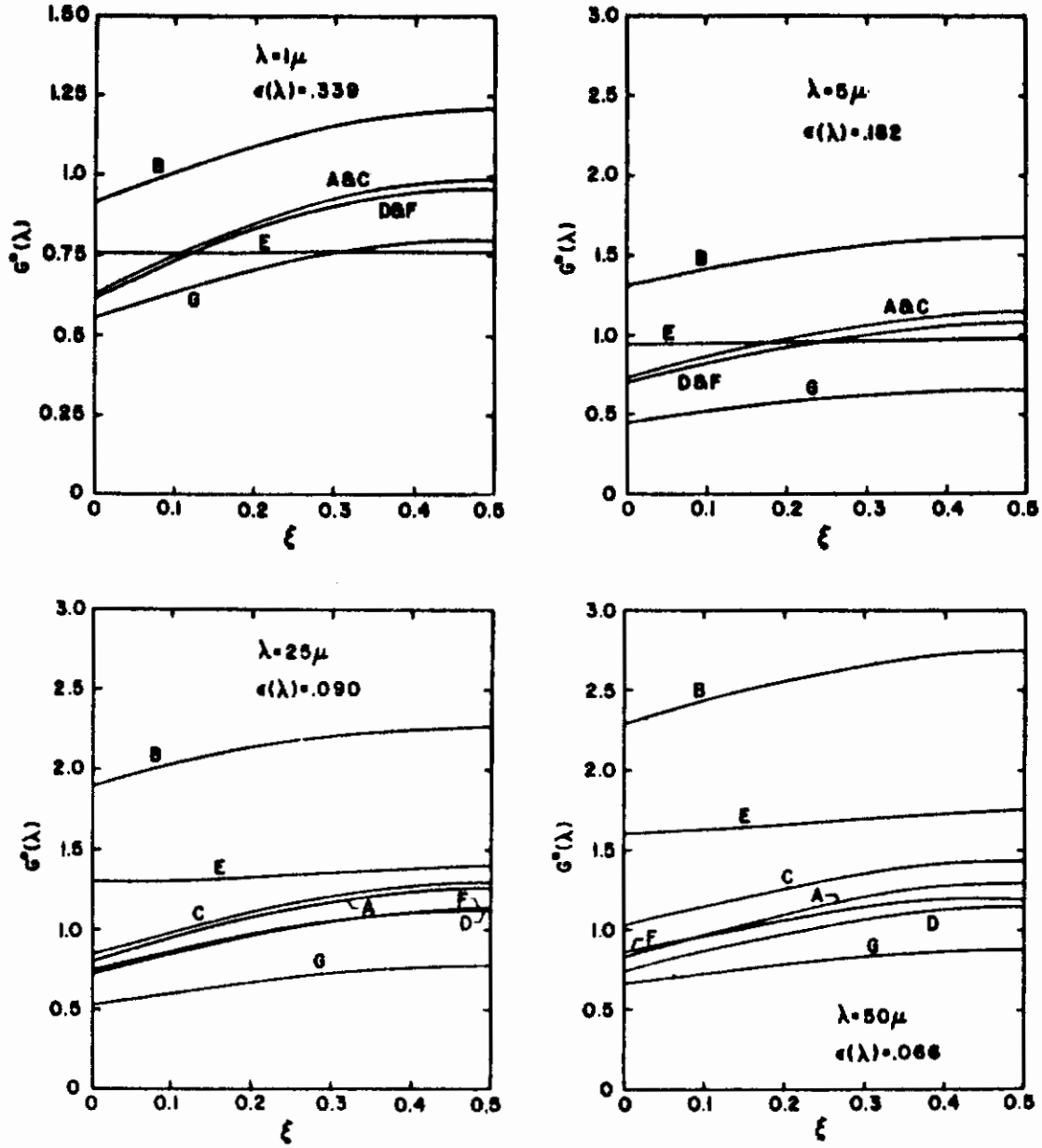

Figure 5

Effect of Wavelength on Local Irradiation;
$\gamma=0.5$. $\beta=\delta_1=\delta_2=0$, $\sigma_o=a_o=5.0\mu$

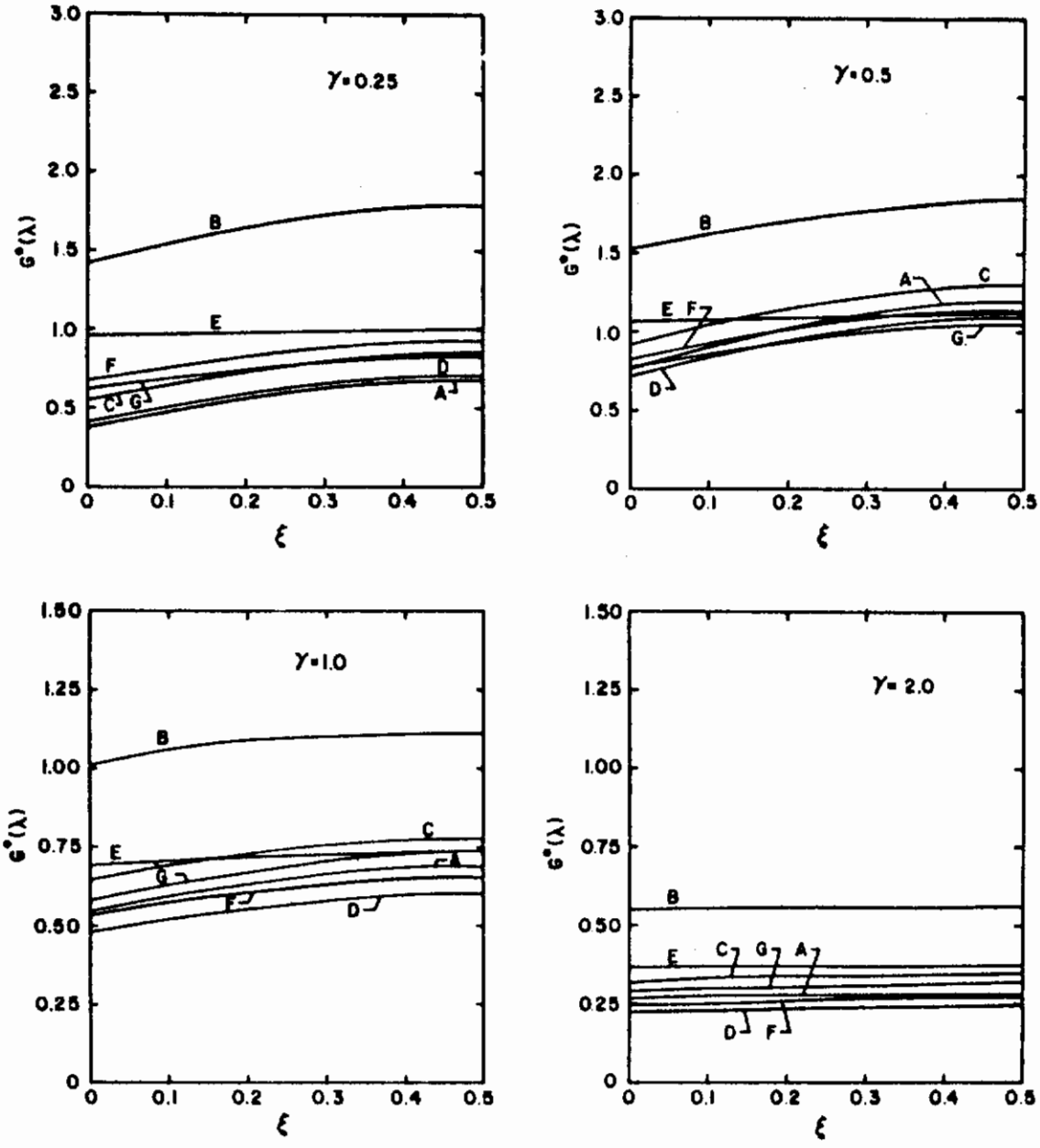

Figure 6

Effect of Spacing to Width Ratio γ on Local Irradiation; $\beta=\delta_1=\delta_2=0$, $\epsilon(\lambda) = 0.136$, $\lambda = 10.0\mu$, $\sigma_o=a_o= 5.0\mu$

that predicted on the basis of model G. It should be emphasized that these trends are indicated by the results presented; changing one or more parameters may alter these general trends completely.

As expected for surfaces approaching the optically smooth condition (case 2 in Fig. 7) the local irradiation predicted on the basis of models G and E are very close; however, the results based on the simple specular model B are about a factor of two higher. Thus, significant errors can result when model B is employed in radiant heat transfer calculations and the dependence of radiation surface characteristics on direction is ignored. The results presented in Figs. 5 through 7 show that even for very optically rough surfaces the predictions based on models G and A do not coincide. This was anticipated since the experimental data on the bidirectional reflectence has shown that the diffuse limit does not exist [5].

Model G while being the most detailed is also only approximate; there are however no exact solutions available with which all other simplified models could be compared. Based on the results obtained a few observations can be made. First, the choice of the model is not critical for predicting local radiant heat loss from the surface, at least for large and intermediate values of γ. The greatest percent difference between the predictions of the local heat loss occurs for small wavelengths (larger $\epsilon(\lambda)$). This of course is expected since for large values of σ_o/λ the surface is optically rough and therefore for given σ_o and a_o the difference between models B and G is the greatest. Second, the choice of the correct model is much more important in predicting radiation interchange between two surfaces at different temperatures than the local heat loss. This is due to the fact that the irradiation may differ by more than a factor of three based on the predictions of two distinct models. Third, it is clear from the results that under some conditions, see Fig. 6, the less detailed models such as C and F yield local irradiation $G^*(\xi,\lambda)$ close to that based on model G. The importance of these findings as they pertain to the design of thermal systems will be discussed in more detail in Chapter 5.

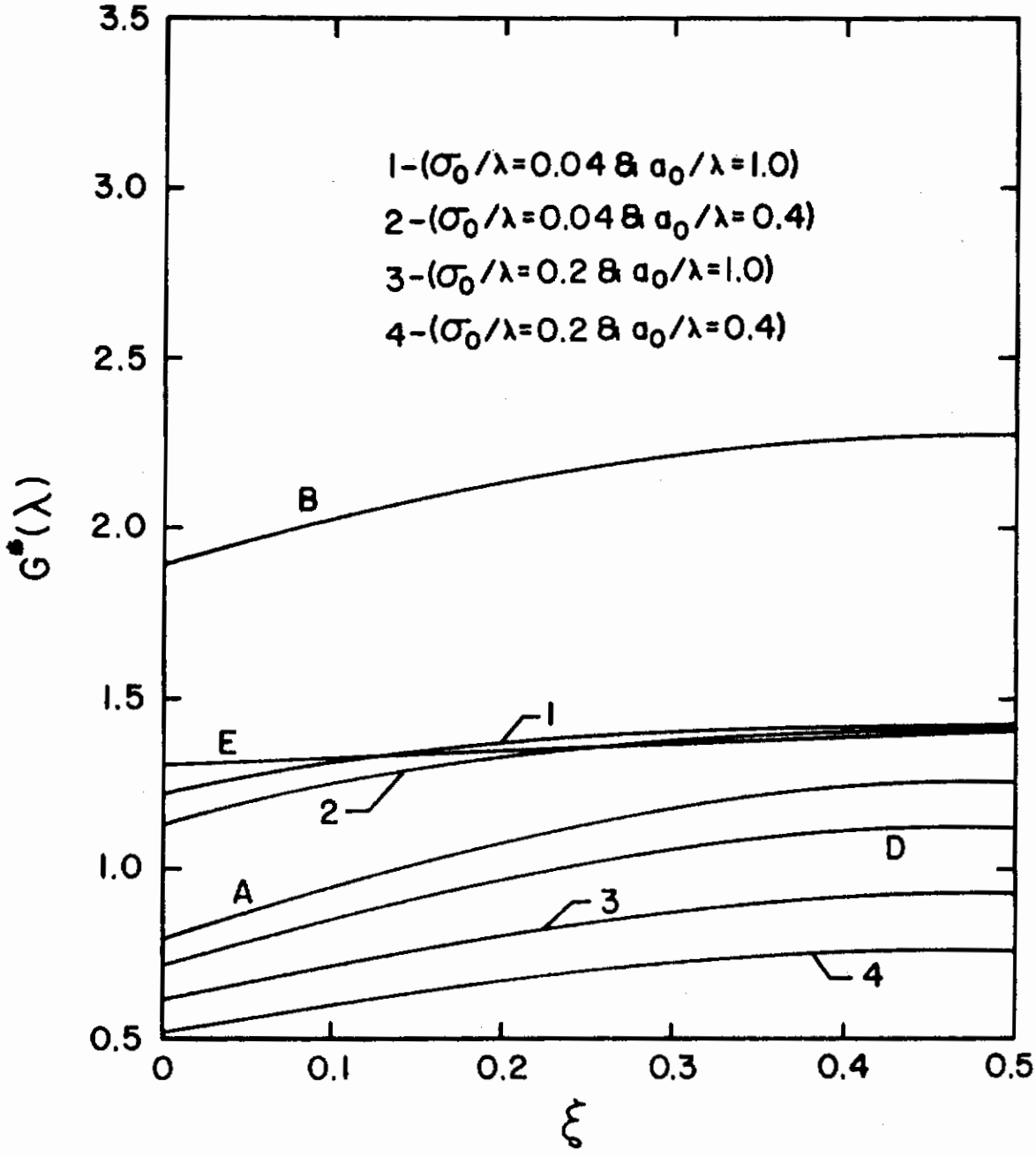

Figure 7

Effect of σ_0/λ and a_0/λ on Local Irradiation as Predicted by Model G; $\beta=\delta_1=\delta_2=0$, $\gamma = 0.5$, $\epsilon(\lambda) = 0.090$, $\lambda = 25.0\mu$

4. EXPERIMENTAL APPARATUS AND PROCEDURE

The objective of the experimental phase of the program was to evaluate different methods for predicting radiant interchange. Such an examination of the validity and accuracy of commonly employed models must of necessity use a simple physical system. In addition, the experimental system must be capable of providing a proper environment in which the effects of conduction, convection, extraneous radiation sources, and other losses can be carefully controlled or possibly eliminated. The experimental configuration must consist of simply arranged surfaces to permit a rigorous prediction of radiation heat transfer. The system design, test assembly, instrumentation, procedure, and calibration are discussed in this chapter.

Since the overall radiant heat transfer is not very sensitive to the model used for its prediction it is desirable to measure the local flux; the effects to be studied are much more pronounced locally than when averaged over the entire surface. There are, however, extreme experimental difficulties associated with a measurement of the net local radiant heat flux. Local irradiation (incident radiant flux) was instead measured in an attempt to experimentally evaluate the methods of radiant heat transfer analysis and accomplish the goals of the study. Various radiation detectors such as heat gauges and thermopiles are available which can measure the local irradiation. The other radiant energy quantities can be readily determined from the equations

$$q(\vec{r}) = \epsilon(\vec{r})E_b(\vec{r}) - \alpha(\vec{r})G(\vec{r}) \qquad (4.1)$$

and

$$q(\vec{r}) = J(\vec{r}) - G(\vec{r}) \qquad (4.2)$$

and thus provide a basis of comparison between analytical predictions and experimental data.

The configurations chosen for study consisted of two rectangular plates either parallel or perpendicular to each other. One side of the plate was long compared to the other and was effectively "infinite". These geometries were chosen for several reasons:

1. They represent configurations of practical interest since they are representative of spacecraft radiators, temperature control louvers, etc.

2. One independent parameter of many arising in the problem is eliminated by choosing relatively long surfaces.
3. A considerable amount of analytical results is available for these geometries, both from this study and the literature [6,14,25].
4. The configurations selected include both open and closed systems, thus facilitating a more complete evaluation of the analytical models.

The local irradiation measurements were made on a total (integrated over the entire spectrum) basis for several types of surfaces having different radiation characteristics so that the analytical predictions could be checked over a wide range of surface parameters. Since radiation properties vary appreciably with surface conditions, as the wide scatter of experimental data reported in the literature attests, the total hemispherical emissivities were also measured. Since the primary purpose of the experimental program was not a study of radiation properties, the details of these measurements are not included in this report but are given elsewhere [35].

4.1 General System Design

In order to make local irradiation measurements at a surface, the experimental system must be capable of providing the proper environment for these measurements by the elimination of convective heat transfer and of extraneous radiation influences from outside of the test surfaces. The external radiation sources were reduced by mounting the test assembly inside a black, liquid nitrogen cooled shroud which is described in the next section. The convective heat transfer was reduced to an insignificant fraction of the total heat transfer by placing the shroud within a vacuum system which was evacuated to a pressure 10^{-5} torr or lower during the testing.

The local irradiation measurements were made with thermopiles. This type of radiation detector was required since the measurements were on a total basis. Temperatures were measured with thermocouples.

The surfaces were arranged in the system in a manner that allowed a rapid interchange of the test surface as well as a change in the geometries. Details of the test assembly are discussed in Section 4.3. The test surfaces were heated to the desired temperature by electrical resistance heating. This method was chosen since it provided a ready means of controlling the surface temperatures and measuring the energy input to the system.

4.2 Environment Control Equipment

The enclosure, or shroud, necessary to provide the proper radiation environment for the test surfaces was constructed from a copper sheet bent into a cylindrical shape with both ends closed. This enclosure effectively eliminated radiation from outside the system. The inside of the shroud was coated with 3M Black Velvet Paint, which has a very high absorptivity, in order to reduce the effect of reflections. Also, to further reduce the reflected energy the test section was mounted in an off-center position. Portions of the shroud can be seen in Figs. 8 and 9. Copper tubing was soldered to the outside of the shroud to permit cooling of the shroud by liquid nitrogen thereby reducing its temperature and therefore the emission. It was estimated that for the most open configuration and the lowest surface temperatures considered, the radiation incident on a surface from outside of the test assembly was less than 2% of the total energy incident.

To achieve the desired vacuum conditions the complete shroud, containing the assembly with test surfaces, was placed inside an 18 inch diameter belljar. The belljar with its baseplate containing the necessary power, liquid nitrogen, and instrumentation feedthroughs was part of a complete Consolated Vacuum Corporation pumping system, model PSE. This four inch nominal size system, complete with liquid nitrogen cooled baffle, was capable of reducing the pressure within the belljar to the 10^{-6} - 10^{-7} torr range. The complete experimental system is shown in Fig. 8.

4.3 Test Assembly and Surface Specimens

The purpose of the test assembly was to provide a means of mounting the test surface specimens in several configurations and allow for rapid interchange of geometries and test surfaces. The test assembly consisted of a stainless steel framework to hold the test surfaces in the proper position. Mounting brackets on the end of the test surfaces were attached to the interchangeable end plates of the framework. By having several sets of end plates with holes into which the mounting brackets fitted, a rapid changing of geometries was accomplished. To keep the test surface properly aligned during the expansion caused by heating, springs were placed on the mounting brackets to maintain the test surfaces under tension.

A guard heater, which was constructed and attached in the same manner as the test surface.was mounted behind each specimen surface. The back side of the test surface was effectively insulated by adjusting the dissipation in the

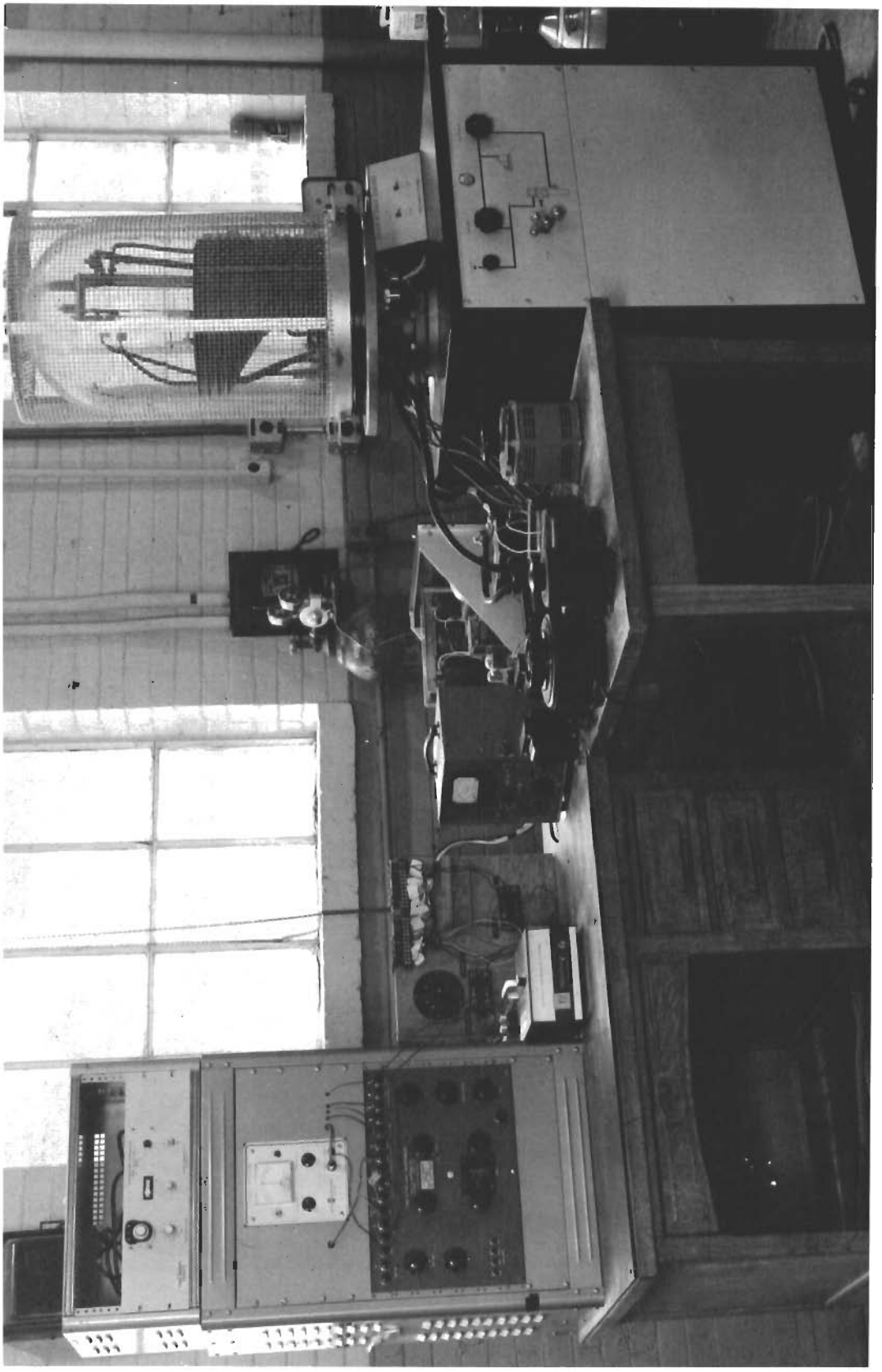

Figure 8
View of Complete Experimental System

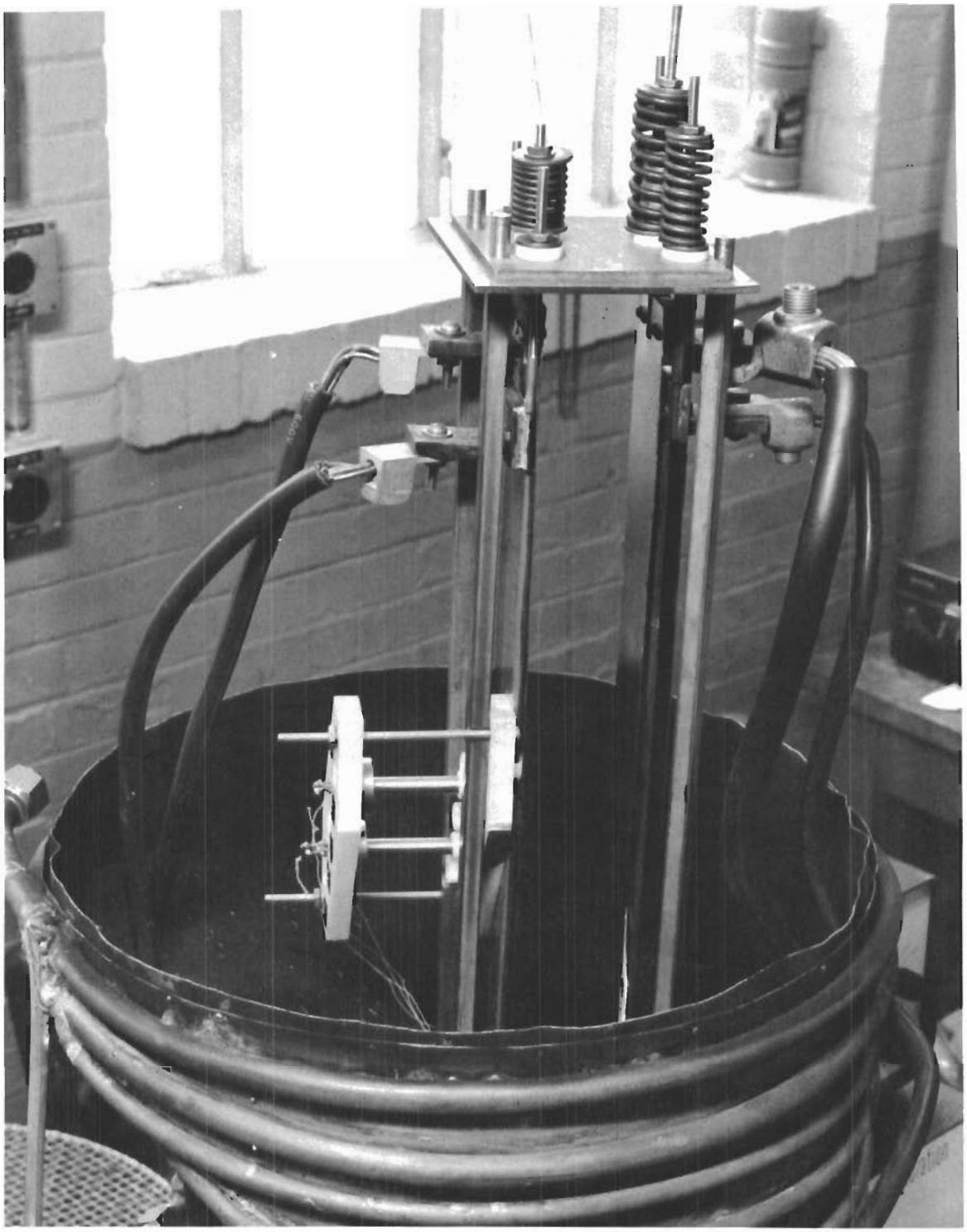

Figure 9
View of Test Assembly Mounted in the Lower Half of the Shroud

guard heater until the temperature difference between it and the test surface vanished.

The test surfaces were machined from type 303 stainless steel sheets 0.031 inch thick. This material was chosen for the following reasons: 1) a relatively low electrical conductivity was desirable since the test surfaces were heated to elevated temperatures electrically, 2) it is a common engineering material, and 3) extensive measurements of the directional reflectance are available in the literature [36]. The test surfaces were 2 inches wide by 22 inches long. The 22 inch length was the longest possible test surface that could be accomodated in the belljar. The 2 inch width was chosen so that the length to width would be slightly larger than 10. With these length to width and separation to width ratios, the view factor from a point at the center of one plate to the other plate was less than 1% different from what it would be were the other plate infinitely long. Also for the 22 inch long test surfaces the measured temperature distribution over three fourths of the length was practically constant and all end effects could be neglected.

Seven types of test surfaces were prepared as follows:

1. The "as received" type 303 selenium stainless steel was electropolished. The rms mechanical roughness was measured to be 0.28μ.
2. The stainless steel was sandblasted to a roughness of 2.9μ.
3. The "as received" stainless steel sheet was electroplated with gold. The resulting surface roughness was measured to be 0.075μ.
4. The stainless steel was sanded with Carborundum, type J135R medium emery cloth and then gold plated with a resulting roughness of 0.55μ.
5. The surfaces were coated to a thickness of approximately 0.007 inches with type 101-C10 3M Black Velvet Paint manufactured by Minnesota Mining and Manufacturing Company of St. Paul, Minnesota.
6. The surfaces were coated with Pyromark Black Paint to a thickness of approximately 0.005 inches. This paint is manufactured by the Tempil Corporation of New York, New York.
7. The surfaces were coated to a thickness of 0.004 inches with PV100 White Paint made by the Vita-Var Corporation of Orange, New Jersey.

The rms mechanical surface roughness of the metallic surfaces was measured with a Bendix Profilometer, model QB, which included a model LK tracer with a 25μ diameter point.

For the thermal flux measurements 3/32 inch diameter holes were drilled through the test plates to allow the incident radiation to pass through onto the thermopiles. This hole size was a compromise between the energy requirements for the thermopile, the effect of the hole on the radiative flux distribution of the system, and diffraction effects. The thermopiles were mounted in a Teflon fixture so that their receiving element would be approximately 1/64 of an inch behind the test surface hole.

Figure 10 shows an exploded view of the test section with test surfaces, guard plates, mounting brackets and plates, tension springs, mounted thermocouples, thermopiles and thermopile mounting fixture. The complete test assembly, ready for measurements, except for the top half of the shroud, is shown in Fig. 9.

The test plates were heated to the required temperature by passing an electrical current through them. This was accomplished by a system consisting of a voltage regulator, variable voltage transformers and 117 to 5 volt step-down transformers that allowed the power supplied to the test surfaces and guard heaters to be individually adjusted.

4.4 Instrumentation

For the measurement of local irradiation only two types of measurements were required: temperature and local incident flux. For temperature measurements chromel-alumel thermocouples were used. A precision grade of chromel and alumel wire, type 3G-178, manufactured by the Hoskins Manufacturing Company of Detroit, Michigan was employed. This wire specification has a guaranteed accuracy of $\pm$ 2°F or $\pm$ 3/8% whichever is greater. However, the wire was calibrated at the factory and a curve showing its deviation from the standard temperature-emf conversion table was supplied. This deviation curve was checked by using pure metallic freezing point samples supplied by the National Bureau of Standards and found to be accurate within 0.1°F at the freezing points of lead, tin and zinc. For the reference junction a Joseph Kaye and Company model 1150 automatic ice point thermoelectric refrigeration was employed. The thermocouple emf was measured using a Leeds and Northrup model K-3 potentiometer with its associated null detector, working voltage source and standard cell.

The irradiation was measured by placing thermopiles behind 3/32" diameter holes in the test surfaces. These thermopiles were manufactured by the Charles M. Reeder Company of Detroit, Michigan. They had a square receiving area 4 mm on a side and were of an uncompensated design.

Figure 10
View of Test Assembly, Components, Test Surfaces, Guard Plates, and Thermopiles

The thermopiles were windowless in order to eliminate selective absorption and reflection of incident radiation by the window material. The emf's produced by the thermopiles were measured by the K-3 potentiometer. The thermopiles were calibrated as an integral part of the experiment; the procedure is discussed in Section 4.5.

4.5 Experimental Procedure

The thermopiles were calibrated while mounted behind the test surface. This was accomplished by using two surfaces of known properties, so that the irradiation could be accurately calculated. Then a calibration curve of thermopile emf versus local irradiation could be drawn for the range of interest. The surfaces chosen were Black Velvet Paint for the surface behind which the thermopiles were mounted and Pyromark Black Paint for the other surface which was usually heated to a higher temperature. The Pyromark was chosen since it is a known diffuse emitter [37] and good absorber, while the 3M Black Velvet is a very good absorber. With these paints the system was considered to be composed of diffuse emitters and reflectors; therefore, model A of Chapter 3 was applicable and was employed to predict the local incident flux. Even if the surfaces were not diffuse reflectors the error introduced would be small since little energy would be reflected because of the high absorptivities of the paints.

The procedures followed in making the necessary calibration curves are:

1. The thermocouples were welded to the back side of both plates at the locations listed in Table 1; the thermopiles were mounted behind the Pyromark Black Paint test surface at locations also listed in Table 1.
2. The surfaces were mounted in the test assembly, enclosed within the shroud, and placed in the belljar which was then evacuated to a pressure of 10^{-5} torr or less.
3. Liquid nitrogen was pumped through the cooling coils of the shroud.
4. The two test surfaces were heated to the desired temperatures. The dissipation in the guard heaters was adjusted until the temperature difference was very small and the system was allowed to reach equilibrium. The 3M Black Velvet coated plate was heated to temperatures of 50°F, 75°F, and 100°F. These temperatures were selected as a suitable compromise between the

requirements for low temperatures, to keep the electrical energy input low and to maintain the thermopiles well within their operating range, and high temperatures to keep the opposite plate in the 700-800°F range. The temperature of the plate coated with 3M Velvet paint was varied so that the range of incident fluxes was the same as when the other test surfaces were employed.

5. The local irradiation was calculated assuming that both surfaces were gray, diffuse emitters, and diffuse reflectors using the procedure discussed in the next section.

6. Calibration curves were then drawn for the thermopiles at each temperature of the 3M Black Velvet test surface and for each geometry. Sample curves are shown in Fig. 11.

TABLE 1

Location of Thermopiles and Thermocouples

ξ	Thermopiles		Thermocouples	
	Parallel Plates ($\delta_1=\delta_2=\beta=0$)	Perpendicular Plates ($\gamma=\delta_1=0.25$. $\delta_2=0,\beta=90°$)	Parallel Plates ($\delta_1=\delta_2=\beta=0$)	Perpendicular Plates ($\gamma=\delta_2=0.25$. $\delta_2=0,\beta=90°$)
0.062	x		x	
0.125	x	x	x	x
0.250	x			
0.375	x	x	x	x
0.500	x	x	x	
0.625				
0.750		x		
0.875				x
0.937		x		x

The calibration procedure just described is a relative and not an absolute one. In this method the effects of thermopile mountings were accounted for, but possible errors may have arisen due to uncertainties in the radiation characteristics. As a check on the procedure an alternate absolute calibration was attempted. A black body cavity was constructed. It consisted of 1 inch diameter 18 inch long cylindrical tube which was heated electrically. The inside of the tube was coated with the Pyromark Black Paint. An apparent emittance of 0.99 was achieved with a 1/8 in. diameter hole drilled in the side of the tube. However, this procedure could only be used as a check of the other method since the distribution of the incident energy was different and therefore the effect of

the hole in front of the thermopile was not the same. Also the entire range of incident fluxes of interest could not be covered because the black body did not yield sufficient energy due to material limitations. A comparison of one of the thermopiles calibrated by both procedures is included in Fig. 11.

The actual measurement of the local incident flux proceeded in a manner similar to the determination of the calibration curves:

1. A set of test surfaces was instrumented and installed in the system at one particular geometry as described in the calibration procedure.
2. The system was evacuated and liquid nitrogen was circulated through the tubing surrounding the shroud. The test surfaces were heated to predetermined temperatures, the guard heaters were adjusted to the same temperatures, and the system allowed to reach equilibrium. The temperatures of the cold plate and the guard plate behind which the thermopiles were mounted was maintained at either the 50, 75, or 100°F levels as explained previously. The temperature of the hot plate was varied from 50°F to a high temperature in the 800°F range. The upper temperature was limited by the solder used in the test section and the fact that the radiation equilibrium temperature of the cold plate could not exceed 100°F.
3. The thermocouple and thermopile emf's were recorded and the procedure was repeated for a new test condition and geometry.

4.6 Data Reduction Procedure

The standard emf-temperature conversion table for chromel-alumel thermocouples was employed using a second order interpolation procedure to convert the thermocouple emf's to surface temperature. In this procedure the deviation from the standard conversion table as reported by the manufacturer of this wire was also taken into account. The temperature was measured at the rear of the test plate, and assumed to be the surface temperature since the difference was always less than 0.25°F. The emittance is not known with sufficient accuracy to warrant the correction for the temperature drop across the plate.

The conversion of thermopile emf to incident flux was straightforward. From the appropriate calibration curve for the proper thermopile, cold plate temperature, and geometry, the incident flux was found from the measured emf by a second order interpolation procedure.

The data reduction procedures used to calculate surface temperatures necessary for the preparation of the calibration curves were more involved because the surfaces were coated with paints. Since the paints have a low thermal conductivity the temperature difference across the paint film was calculated from a knowledge of the heat loss or gain, the film thickness, and an estimate of the thermal conductivity of the paint films. This temperature difference amounted to as much as 8°F for the 3M Black Velvet Paint at high local heat transfer rates.

After the surface temperatures were determined the local irradiation was calculated using the assumptions of the diffuse emission and reflection, model A. It can be shown that under the above assumptions the integral equations (3.12) and (3.13) for the total radiosity (see Fig. 3) becomes

$$J_1(\xi_1) = \epsilon_1(\xi_1)\sigma T_1^4(\xi_1) +$$

$$\frac{\rho_1(\xi_1)}{2} \int_0^1 J_2(\xi_2) \left\{ \frac{\kappa_3[\kappa_3\cos\beta + (\kappa_1-\kappa_2)\sin\beta]}{[(\kappa_1-\kappa_2)^2 + \kappa_3^2]^{3/2}} \right\} d\xi_2 \quad (4.4)$$

and

$$J_2(\xi_2) = \epsilon_2(\xi_2)\sigma T_2^4(\xi_2) +$$

$$\frac{\rho_2(\xi_2)}{2} \int_0^1 J_1(\xi_1) \left\{ \frac{\kappa_3[\kappa_3\cos\beta + (\kappa_1-\kappa_2)\sin\beta]}{[(\kappa_1-\kappa_2)^2 + \kappa_3^2]^{3/2}} \right\} d\xi_1 \quad (4.5)$$

where

$$\kappa_1 = \delta_1 + \xi_1$$

$$\kappa_2 = \delta_2 + \xi_2 \cos\beta$$

$$\kappa_3 = \gamma + \xi_2 \sin\beta$$

These equations were solved using the same method as discussed in Appendix B, except that 48 Gaussian integration points were used to increase the accuracy. Once the incident flux and thermopile emf were known for each thermopile, geometry, and temperature the calibration curves could easily be drawn. Examples of such calibration curves are illustrated in Fig. 11.

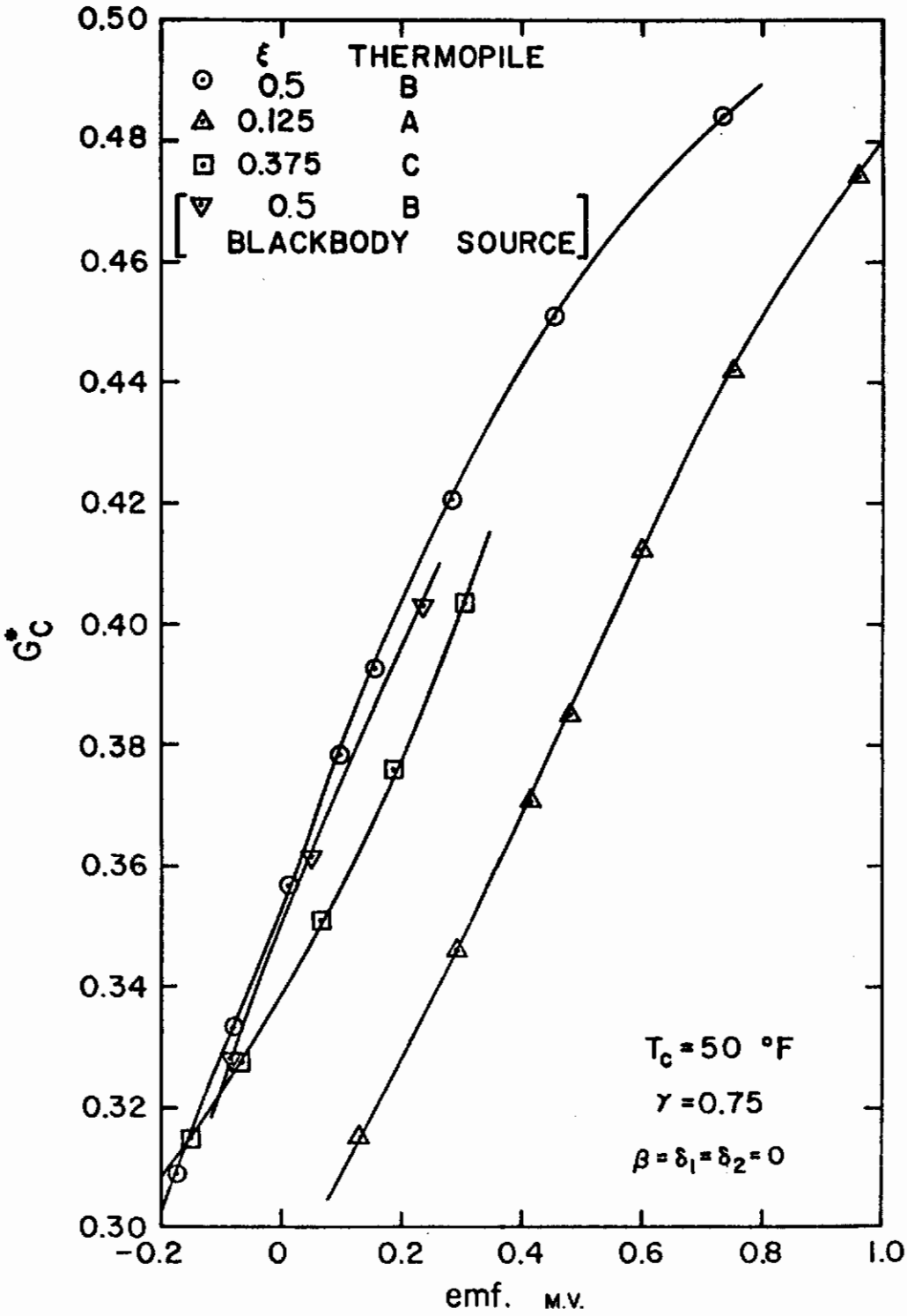

Figure 11

Typical Thermopile Calibration Curves

4.7 Presentation of Experimental Data

All of the experimental data are tabulated in Appendix D. Since the emissivity of the surfaces is dependent on temperature a unique way of presenting the results which would collapse all of the data could not be found. Therefore, the data are tabulated in terms of the local dimensionless irradiation, i.e., (the ratio of the local irradiation at the cold plate to the emissive power of the cold plate), $G_c^* = G_c/\epsilon_c \sigma T_c^4$. This of course is arbitrary and a number of other choices are possible; however, this particular dimensionalization is usetul since it expands the scale of G_c^* and facilitates the comparison between experimental data and analytical predictions.

For the parallel plate configuration ($\beta=\delta_1=\delta_2=0$) results were obtained with $\gamma=0.75$, 0.333, and 0.125. The value of $\gamma=0.125$ was the smallest possible due to the interference of test surfaces with the mountings of the test assembly. In the adjacent plate configuration results were obtained at $\beta = 90°$ with $\delta_1=\gamma=0.25$ and $\delta_2=0$. The particular value of the included angle was chosen because all the energy that is reflected specularly would immediately be lost from the system, thus allowing a critical comparison of experiment with analysis. Interference of the mounting brackets and guard plates did not permit the plates to have a common edge.

Data were taken for three sets of surface temperatures and for each of the five surface conditions. The temperature of the cold plate was maintained at either 50, 75, or 100°F as described in Section 4.5. The hot plate was kept at either 50°F, an intermediate temperature range of 200-300°F, or a high temperature range of 600-900°F depending on the geometry as also discussed in Section 4.5. The surface temperatures for each geometry and material are listed in Appendix D.

5. COMPARISON OF EXPERIMENTAL DATA WITH ANALYSES

In this chapter the experimental data are compared with analytical predictions based on several simplified models for radiation characteristics of surfaces. The purpose of these comparisons is to examine the validity of the commonly used simplified methods of radiant heat transfer analysis. Only some representative data are presented graphically with the remaining data tabulated in Appendix D. Some computational details needed to predict the local irradiation are presented in Section 5.1. In Section 5.2 the comparison between experiment and analysis is presented and discussed.

5.1 Details of Calculations

The diffuse, specular, and specular-diffuse constant property models (A, B and C) result in the simplest computational procedure; therefore, the comparision between data and predictions are primarily based on these models. In all the calculations the surfaces were assumed to be gray. To demonstrate the superiority of the directional dependent property models D, E, F and G over constant property models one selected comparison was made. A more extensive comparison between experiment and analysis was impractical and beyond the scope of this study.

For the diffuse, specular and specular-diffuse constant property models the analysis of radiant heat transfer based on the gray property assumption is well known [5,6,25]. It was found that the more general procedure discussed in Chapter 3 for solving radiation interchange problems with nonelementary emission and reflection from surfaces was time consuming on the digital computer and hence the radiosity method [5,6,26] was adopted for calculating the radiant heat transfer quantities of interest.

In the calculations based on the diffuse and specular models the experimentally determined values of total hemispherical emissivity ϵ [35] were used and the total hemispherical reflectivity was evaluated from $\rho = 1 - \epsilon$. For the specular-diffuse model the specular component of hemispherical reflectivity was estimated from Eq. (3.34) with the optical roughness σ_o replaced by the root mean square mechanical roughness σ_m. This is only approximate and it is recognized that a difference between σ_o and σ_m exists as the data of Birkebak and Eckert [38] indicate. Since the results were calculated on the gray basis the wavelength λ was replaced in Eq. (3.34) by a mean wavelength λ_m. The latter was evaluated at the peak of the spectral blackbody emissive power curve corresponding to the particular surface temperature. This is also somewhat

arbitrary but in view of the fact that $\sigma_m < \sigma_o$ and $\lambda_{max} < \lambda_m$ the ratio σ_m/λ_{max} is expected to be a reasonable approximation for σ_o/λ_m.

For the more sophisticated models D, E, F, and G, the optical constants were evaluated from the simple Drude theory [32]. The directional reflectivity was calculated from Fresnel's equations and then multiplied by a constant correction factor so that the resulting hemispherical reflectivity would be equal to the measured value. The irradiation was then evaluated following the precedure presented in Chapter 3.

5.2 Results and Discussion

In Fig. 12 the analytical predictions are compared with experimental data on sandblasted type 303 stainless steel for the parallel plate geometry.* The directional reflectivity for sandblasted stainless steel of this type has been measured by Edwards and Catton [36] and the results show that for angles of incidence θ' from 0 to 75° the directional reflectivity is practically constant. The recent bidirectional reflectance measurements by Love and Francis [39] on a similar type 302 sandblasted stainless steel showed that it is almost diffuse. This, in view of the fact that σ_m/λ_m was at least 0.3 or greater for the surface, the comparison of data with the predictions based on the diffuse model appears to be appropriate. Since the surface is very rough the specular-diffuse model would predict the same irradiation values. On the graph for $\gamma = 0.75$ the squares and circles represent data taken with different sets of thermopiles three months apart. This provides an indication of the reproducibility of data. The experimental points are generally higher than predictions, but the maximum difference is less than 5 percent. Results presented in Fig. 13 show that the maximum deviation between data and predictions increases to approximately 15 percent as the temperature level increases. Since the local heat flux at the cold surface is given by

$$q_c^*(\xi) = q_c(\xi)/\epsilon_c \sigma T_c^4 = 1 - \alpha_c G_c^*(\xi) \qquad (5.1)$$

this finding implies that the analysis would predict too high a heat flux and that the discrepancy would increase with an increase in the temperature difference between the two surfaces.

Comparisons between data and predictions for polished stainless steel in the parallel plate geometry are shown in Figs. 14 and 15. The effect of temperature level with $\gamma = 0.125$ is illustrated in Fig. 14. Since polished stainless steel is neither purely diffuse nor a purely specular reflector, the analytical results are included for the diffuse, specular,

*In Figs. 12 through 20 the circle with a dot in the center represents experimental data.

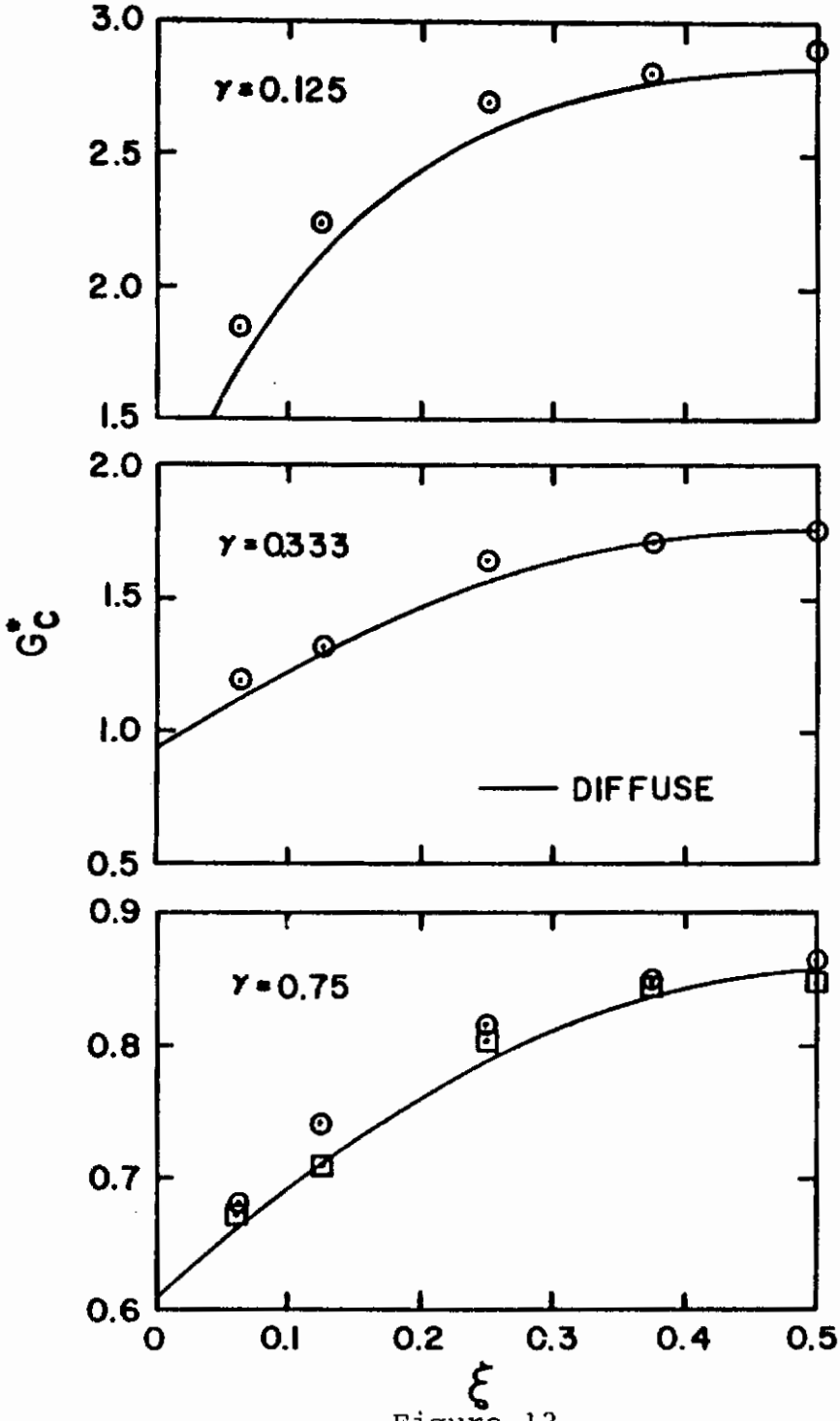

Figure 12

Comparison Between Experiment and Analysis for Sandblasted Stainless Steel; $\beta=\delta_1=\delta_2=0$, $T_h = T_c = 50^{\circ}F$

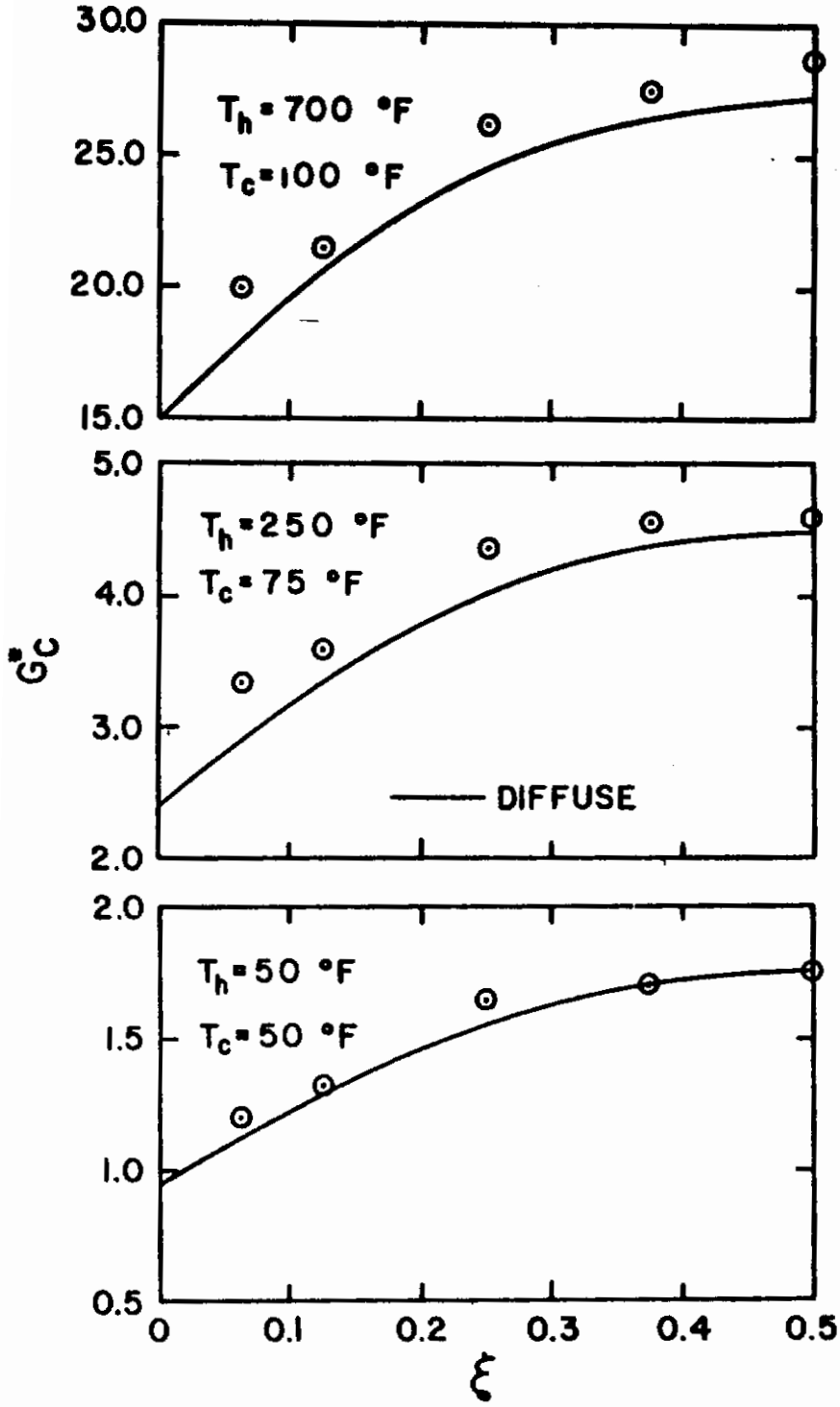

Figure 13

Comparison Between Experiment and Analysis for Sandblased Stainless Steel; $\beta=\delta_1=\delta_2=0$, $\gamma = 0.333$

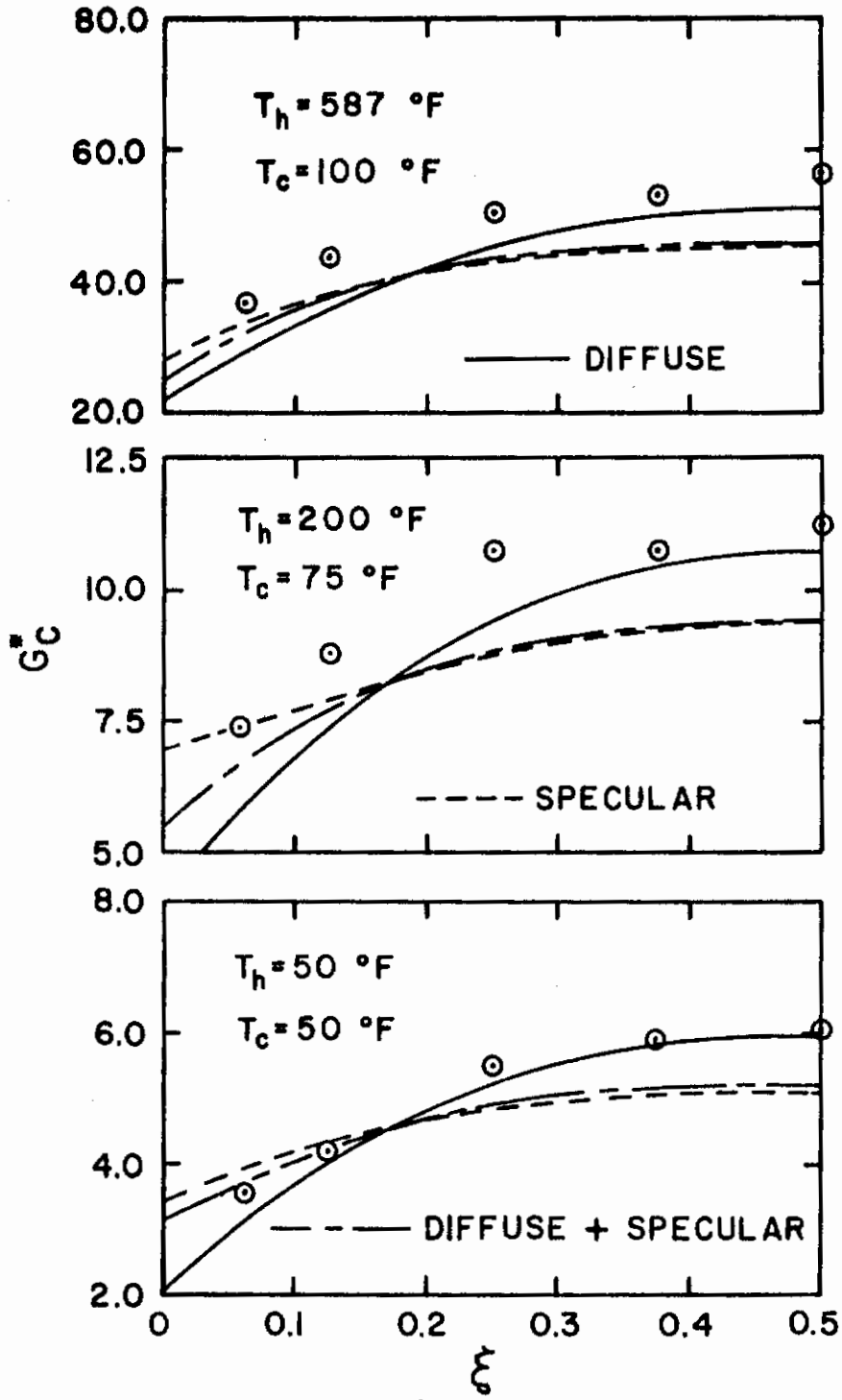

Figure 14

Comparison Between Experiment and Analysis for Polished Stainless Steel; $\beta=\delta_1=\delta_2=0$, $\gamma = 0.125$

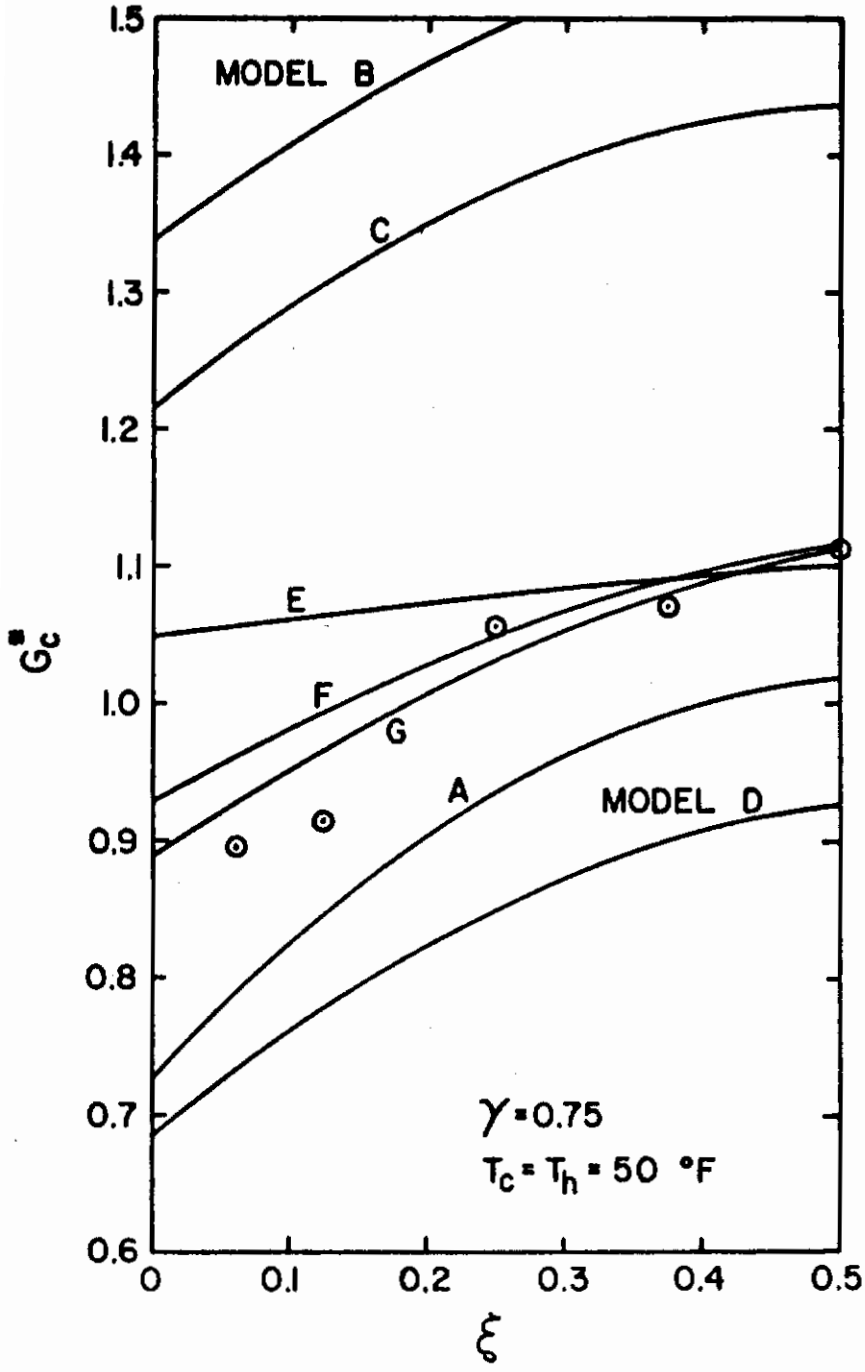

Figure 15
Comparison Between Experiment and All Analytical Models for Polished Stainless Steel; $\beta=\delta_1=\delta_2=0$

and diffuse-specular constant property models. The reason the predictions for G_c^* based on the latter two models are close is that the estimated value of ρ^s/ρ is greater than 0.9. Again the difference between the experiment and diffuse analysis is less than 20 percent. The importance of accounting for the variation of radiation characteristics with direction is illustrated in Fig. 15 where the predictions based on all seven models are compared with experimental data for polished stainless steel. Since $(\sigma_m/\lambda_{max})\approx 0.03$ and it is estimated that $(\rho^s/\rho)\approx 0.95$, it is expected that the polished stainless steel will reflect practically specularly. The results show that model G fits the data better than any other model and that model F is also in very good agreement with the experiment. This indicates that the small diffuse component of reflectivity is still important even for a surface this smooth. The local irradiation predicted by the simple specular model B is about 50 percent higher than experiment. The importance of taking into account the variation of radiation surface characteristics with direction particularly for specularly reflecting surfaces is emphasized by the differences in values predicted by models B and E.

A comparison between analysis and experiment for a rough gold electroplated surface with the spacing to width ratio as a parameter is shown in Fig. 16. Since σ_m/λ_{max} is between 0.05 and 0.1 for the temperature conditions corresponding to this figure the surfaces have a large specular component of hemispherical reflectance, i.e., approximately $\rho^s/\rho \approx 0.75$ to 0.38. Again the results show that the data agree best with the simple diffuse model. There is also good agreement between data and analysis based on model C, except for $\gamma=0.125$. For the two larger spacing to width ratios, model B predicts considerably higher values for G_c^* than obtained experimentally. At $\gamma=0.75$ the predictions based on model B are off the scale of the graph with $G_c^*\approx 37$.

For the smooth electroplated gold surface the ratio $(\sigma_m/\lambda_{max}) \approx 0.007$ which indicates that it should be a good specular reflector. Upon visual observation the surface appeared mirror-like in the visible part of the spectrum; therefore it should definitely be specular in the infrared part of the spectrum. As seen from Fig. 17 the agreement between the specular model B and experiment is reasonably good for a small spacing to width ratio, $\gamma = 0.125$. For $\gamma = 0.75$ the curve predicted by model B is off the scale of the graph with an average irradiation $G_c^*\approx 2$. The results for the diffuse-specular model C coincide with those of model B and separate curves could not be drawn. Surprisingly, the predictions based on the diffuse model are in best agreement with the data. The experimental results are a maximum of 10 percent higher than the calculations.

Typical results obtained with the PV 100 white paint are

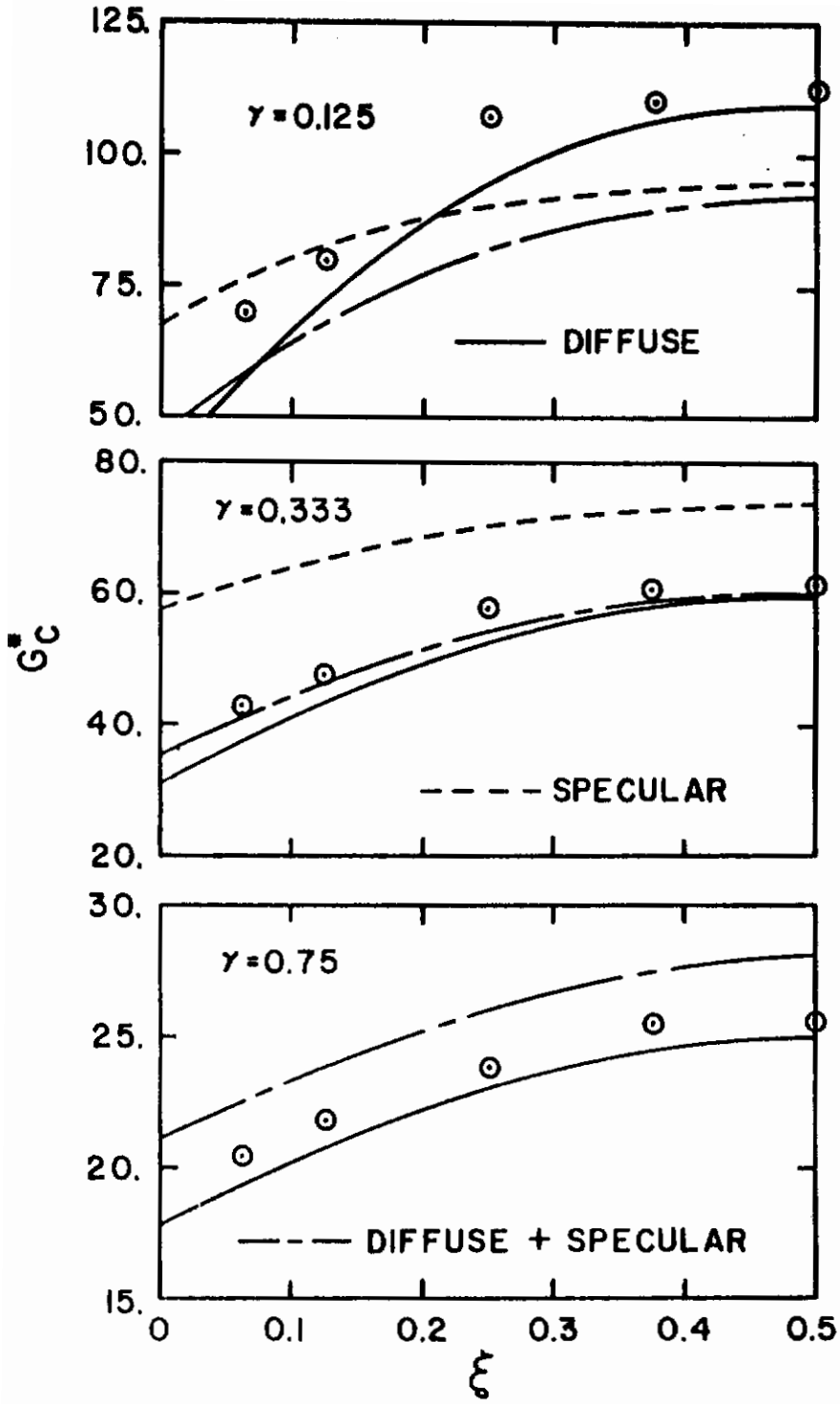

Figure 16

Comparison Between Experiment and Analysis for Rough Electroplated Gold; $\beta=\delta_1=\delta_2=0$, $T_h = 700^{\circ}F$, $T_c = 100^{\circ}F$

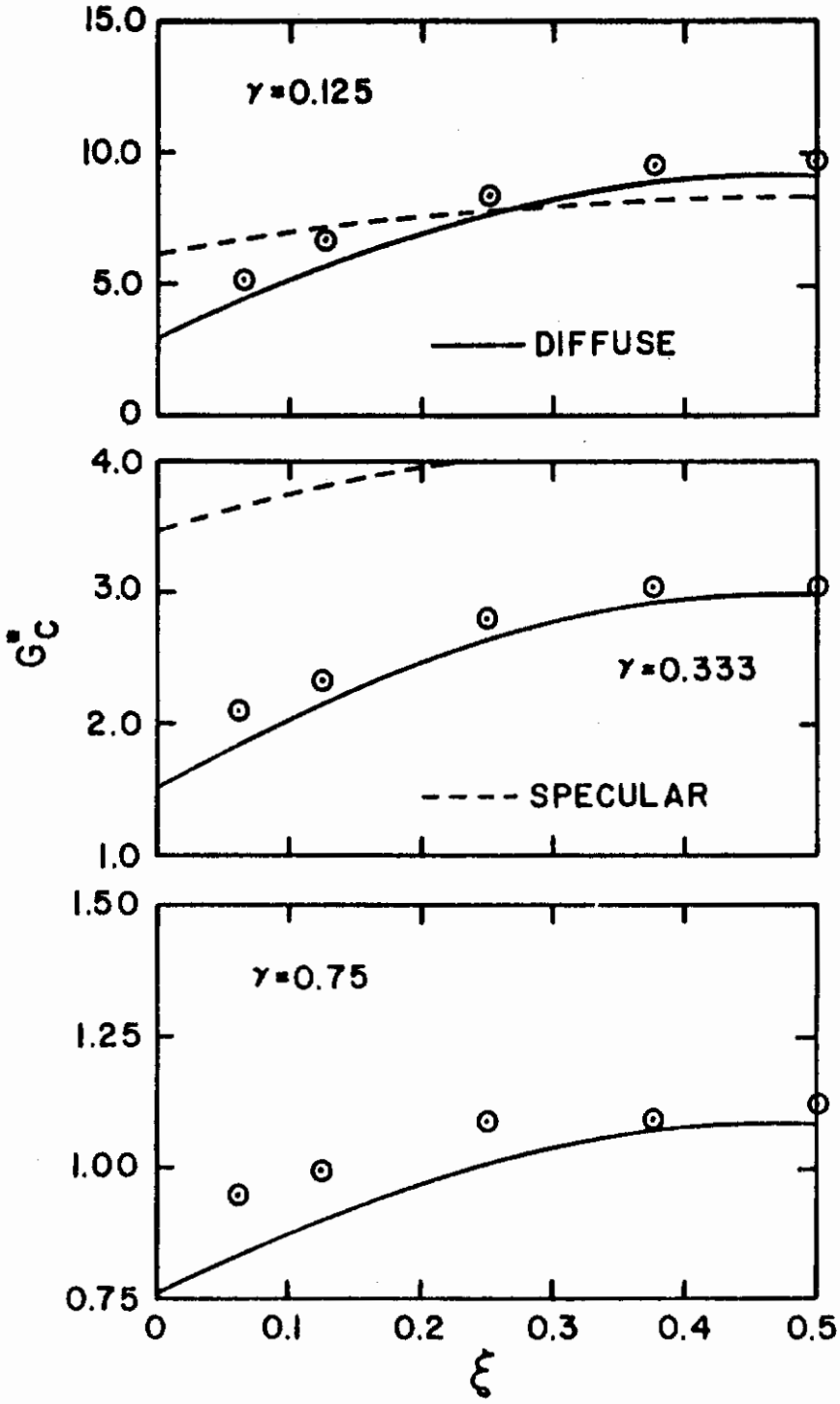

Figure 17

Comparison Between Experiment and Analysis for Smooth Electroplated Gold; $\beta=\delta_1=\delta_2=0$, $T_h=T_c=50^{\circ}F$

compared with the predictions based on the diffuse model in Fig. 18. The maximum difference between the data and the analysis is less than 10 percent. The good agreement is due to the fact that the paint is a good emitter, $\epsilon \approx 0.85$; therefore, almost all of the energy incident on the cold plate is the result of emission from the other plate. Since the paint is a dielectric material its emissivity is expected to be independent of the angle of emission except at oblique angles, $\theta > 60°$. This probably accounts for the good agreement between experiment and analysis based on the diffuse model.

As the results presented in Fig. 19 show the data for sandblasted stainless steel agree within a maximum of 10 percent with the predictions based on the diffuse model for the plates arranged perpendicularly to each other. An equally good agreement has been obtained also for polished stainless steel, and rough and smooth electroplated gold as illustrated in Fig. 20. For these surfaces the estimated ratios of the specular component of reflectivity to the hemispherical reflectivity ρ_s/ρ range from 0.4 to over 0.99 and yet the simple diffuse analysis predicts irradiation values in good agreement with the data. The values of G_c^* predicted on the basis of the specular and diffuse-specular models are off the scale of the graphs. The results for rough gold based on the latter model are closest to the data yet range from $G_c^* \approx 4$ to about 2 over the width of the plate. The results shown in Fig. 20 clearly indicate the importance of directional effects for approaching the optically smooth condition. The reason for poorer agreement between data and predictions at larger values of ξ is clear. This is due to the dependence of emissivity on direction since for surfaces having a large specular reflectivity component the irradiation is largely due to radiant energy emitted directly from the opposite surface.

The testing procedure and the equipment were such that reproducible data could be obtained. In almost all comparisons the data is within the experimental accuracy of the predictions based on the diffuse analysis. The agreement is particularly good in situations where both of the surfaces are at the same temperature. The predictions of the other analytical models, especially the simple specular model, do not fall within the limits of the estimated accuracy of the measurements.

An examination of the results presented for metallic surfaces quickly shows one consistent trend except when the temperatures of both plates are identical. In all cases the measured irradiation exceeded the value predicted by the diffuse analysis. No consistent trend is apparent between the specular or the duffuse-specular analysis and the data. In the experiments performed on a total basis it is difficult

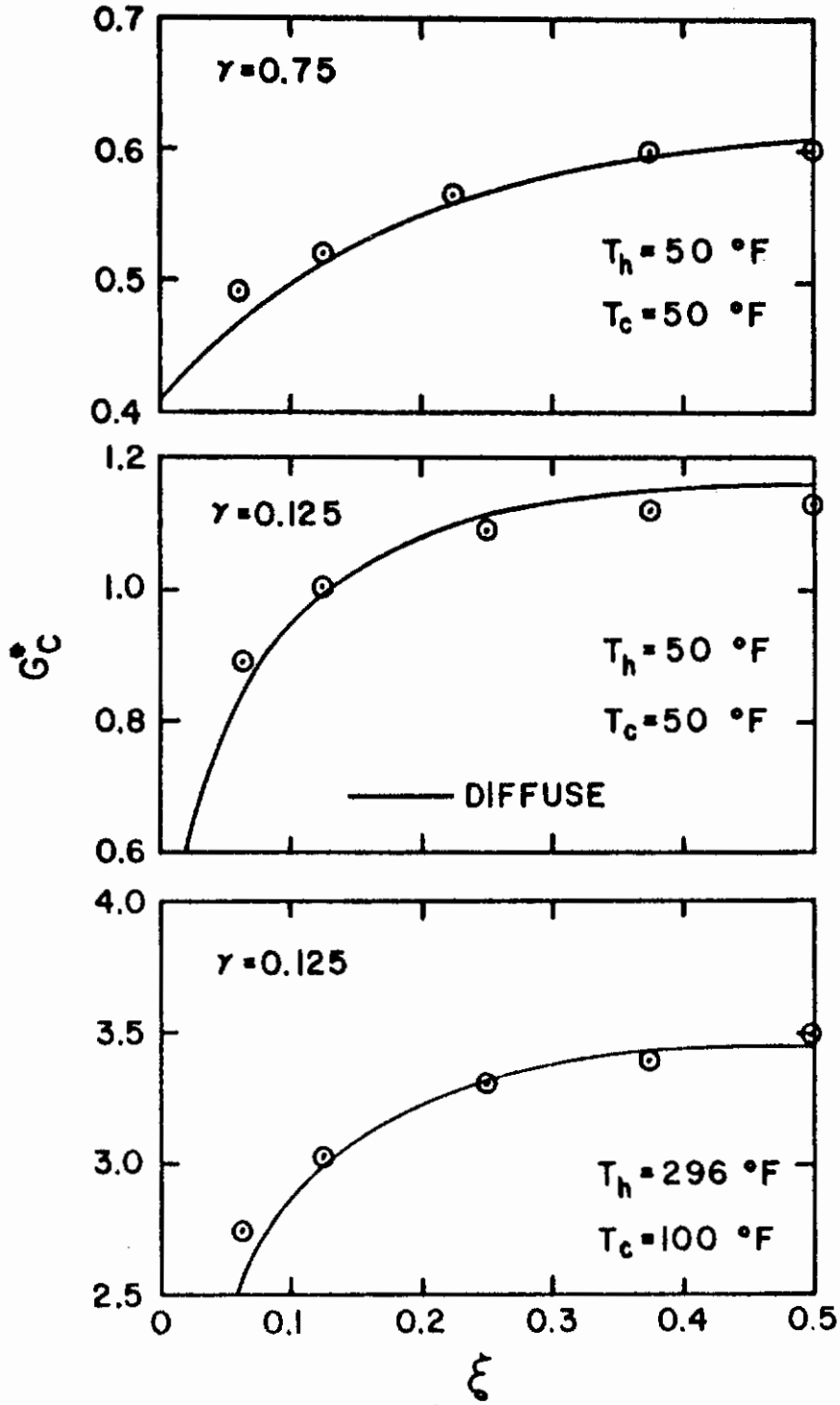

Figure 18

Comparison Between Experiment and Analysis for PV 100 White Paint; $\beta=\delta_1=\delta_2=0$

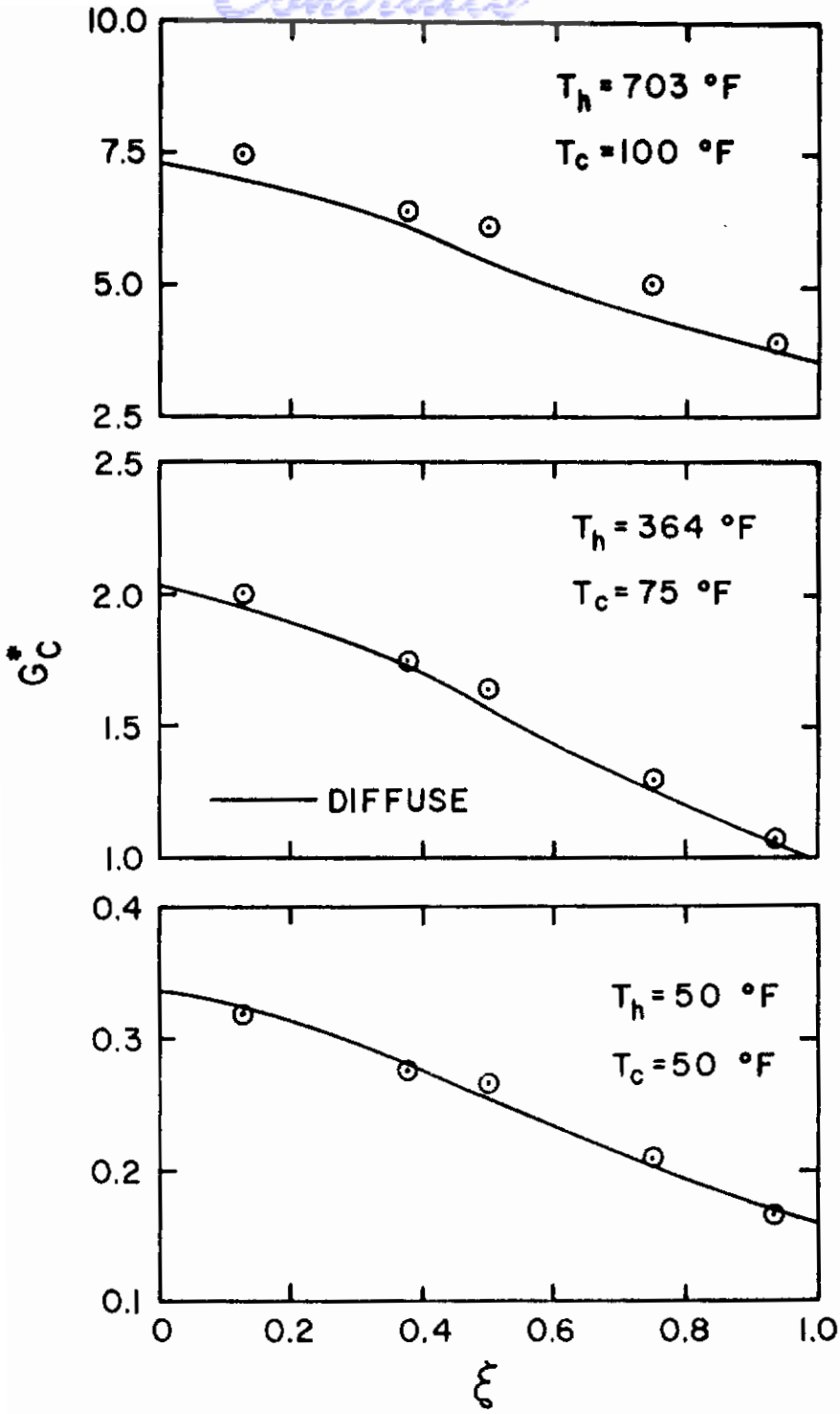

Figure 19

Comparison Between Experiment and Analysis for Sandblasted Stainless Steel; $\beta=90^{\circ}$. $\gamma=\delta_1=0.25$ and $\delta_2=0$

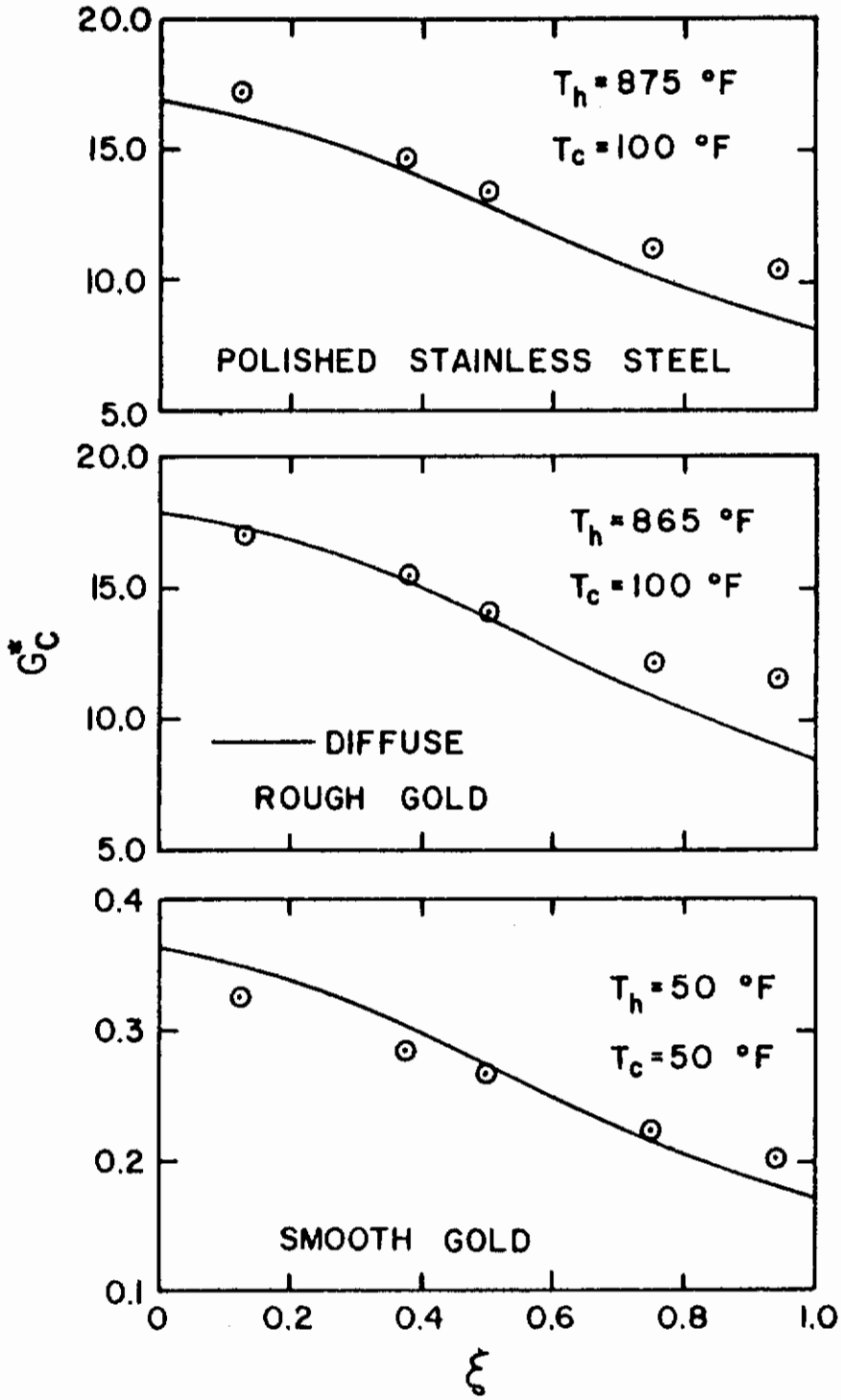

Figure 20
Comparison Between Experiment and Analysis for Different Materials; $\beta=90^{\circ}$, $\gamma = \delta_1 = 0.25$ and $\delta_2 = 0$

to separate the directional from the spectral effects. For example, it is believed that the increasing temperature difference, see Fig. 14, is due to directional effects rather than spectral effects. Following the procedures discussed in [40] calculations performed on a semigray and band model basis (the results are not included here) have yielded larger discrepancies between data and predictions than those based on a simple gray analysis. However, this may have been due to the inconsistency between analysis and construction of the calibration curves. The latter of course were calculated on the gray basis since the black paints used were approximately gray. For the other three metallic surfaces, polished stainless steel, rough gold, and smooth gold, the increase in the discrepancy between data and the diffuse analysis with increasing temperature difference, may be due to spectral as well as directional effects since the range of σ_m/λ_{max} for these surfaces is such that ρ^s/ρ changes considerably with plate temperature. The arguments presented here regarding directional and spectral effects are not conclusive. The real cause of this discrepancy remains to be determined by future experiments and analysis performed on the spectral basis.

While the results presented in Figs. 12 through 20 are on the basis of local irradiation, similar comparisons could be made on the local heat flux basis. The discrepancy between experiment and analysis would be smaller, see Eq. (5.1), particularly for metallic surfaces because of their lower absorptivity, i.e., emissivity under a gray assumption.

The conclusions reached in this study agree with those arrived at by Bevans et al.[18]; namely, that the diffuse-specular model is a more realistic approximation of the radiation characteristics of surfaces but that the dependence of the specular component of reflectivity on direction must be accounted for in the analysis. It is interesting to note that this conclusion was reached on the basis of different data. The experiments and analysis of Reference 18 were performed for different materials and on an overall rather than local heat transfer basis.

6. ANALYSIS OF RADIANT HEAT TRANSFER BY MONTE CARLO METHOD

The purpose of this chapter is to estimate what level of detail is important in the prediction of the overall radiant heat transfer and the heat interchange rates as well as the local radiant heat flux using the Monte Carlo method. The radiation exchange problem as formulated in Chapter 3 is rigorous; however, the solution of a system of simultaneous integral equations governing radiation interchange in complex enclosures with direction and wavelength dependent surface properties is impractical for engineering calculations. Because of the mathematical difficulties in solving equations for the intensity of radiation leaving a surface in the case of a non-elementary distribution of emitted and reflected radiation the problem has been solved by a statistical method known as the Monte Carlo Method.

The basis of the method is briefly discussed in Section 6.1 and some of the computational details are given in Section 6.2. The accuracy of this computational procedure is estimated and the results based on several models are compared and discussed in Section 6.3.

6.1 Monte Carlo Method

The Monte Carlo method is in essence a statistical method which can be simply interpreted in terms of physical processes. The method takes the Lagrangian point of view by considering individual histories of "energy bundles" or photons from the point of emission to point of absorption or escape from the system. The integral equation formulation of radiation interchange among surfaces, on the other hand, takes the Eulerian point of view by focussing attention on the directional distribution of intensity of radiation incident or leaving a particular location. The method is conceptually very simple and can be extended to very general situations. It has been applied to radiation interchange problems by a number of investigators [15,16,41], to mention just a few. A more complete bibliography is given by Toor [17]. The details pertinent to the Monte Carlo method are well known [15] and need not be repeated here. For definiteness only the basic concepts and definitions relating to the present problem will be introduced.

The energy emitted by a surface is divided into a number of equal energy parts called "energy bundles". Application of the Monte Carlo method consists of emitting these energy bundles in directions from a surface (or an

elementary area) proportional to the actual energy emitted from the surface locations in those directions. These energy bundles then play the game of chance according to the actual deterministic and random features of the physical processes step by step [42]. In other words, the energy bundles are followed and the events in their life history are noted until the energy bundle is absorbed or escapes from the system. The directions of the energy bundles are modified by the surfaces of the system according to the actual reflection, transmission, polarization, etc. characteristics. After tracing the histories of a sufficiently large number of bundles and summing (or averaging) the events one can determine what fraction of the emitted energy has been absorbed and reflected at each surface or has escaped from the system through an opening. The basic simplifying assumptions are identical to those made in Section 3.1 and need not be repeated.

Consider radiation interchange in an enclosure consisting of any number of real or imaginary surfaces and direct attention to the emission of radiation from an elementary area dA_i located at a point denoted by the position vector $\vec{r}$. According to the definition of the emissive power the amount of radiant energy emitted from dA_i is

$$E_i(\vec{r}_i)dA_i = \left[\int_0^{\infty} \int_{\Omega_i} \epsilon_i(\vec{r}_i,\vec{\Omega}_i,\lambda) \quad I_b(\vec{r}_i,\lambda) \cos\theta_i d\Omega_i d\lambda \right] dA_i \qquad (6.1)$$

If this emitted energy is subdivided into N_i individual "energy bundles" or "energy packets", then the energy per bundle is given by

$$e_i = E_i dA_i / N_i \qquad (6.2)$$

If out of the total number of (N_i) energy bundles emitted $N_{di\to j}$ are eventually absorbed at surface j directly or after interreflections, the absorption factor $\mathcal{F}'_{di-j}$ can be expressed as

$$\mathcal{F}'_{di-j} = \lim_{N_i \to \infty} (N_{di\to j}/N_i) \qquad (6.3)$$

The factor $\mathcal{F}'_{di-j}$ is a generalization of the absorption factor introduced by Gebhart [43]. The absorption factor between two finite surfaces is defined in an analogous manner,

$$\mathcal{F}'_{ij} = \lim_{N_i \to \infty} (N_{i\to j}/N_i) \qquad (6.4)$$

where N_{ij} represents the number of energy bundles emitted by a finite surface i which are eventually absorbed at surface j. The absorption factors $\mathcal{F}'_{ij}$ are simply related

to the Hottel's radiation exchange factors $\mathcal{F}_{ij}$ by [1]

$$\mathcal{F}_{ij} = \epsilon_i \mathcal{F}'_{ij} \tag{6.5}$$

where ϵ_i is the total hemispherical emissivity of surface i. The absorption factors arise more naturally in the calculations than the radiation exchange factors and therefore the results are presented in terms of the former.

For tracing the histories of N_i energy bundles each has to be emitted from the positions $(\vec{r}_i)$ on surface i and in directions $\vec{\Omega}_i$ in such a manner that these N_i energy bundles are representative of the actual energy emitted from the surface i. Also the wavelength labels attached to energy bundles should represent the actual energy emitted in those wavelength intervals and in these directions. This can be done by forming a cumulative distribution function for given emission characteristics of the surface. For example, if the energy emitted from an isotropic surface i is uniform then the polar angle of emission θ_i is given by

$$R_{\theta_i} = \frac{\int_0^{\theta_i} \int_0^{\infty} \epsilon_i(\theta_i,\lambda) I_{bi}(\lambda) \cos\theta_i \sin\theta_i \, d\lambda d\theta_i}{\int_0^{\pi/2} \int_0^{\infty} \epsilon_i(\theta_i,\lambda) I_{bi}(\lambda) \cos\theta_i \sin\theta_i \, d\lambda d\theta_i} \tag{6.6}$$

where R_{θ_i} is a random number between 0 and 1. Formation of other cumulative distribution functions needed in the calculations is discussed in detail by Toor [17] and expressions for some limiting cases have also been given [15,41].

After the energy bundle is emitted from some point on surface in some direction its point and angle of incidence on surface k (say) is determined. The decision whether this energy bundle is absorbed, transmitted or reflected is made by generating a random number R in the range 0 to 1. If

$R<\alpha$	the bundle is absorbed
$\alpha<R<\alpha+\tau$	the bundle is transmitted
$\alpha+\tau<R<\alpha+\tau+\rho^s$	the bundle is reflected specularly

and if

$\alpha+\tau+\rho^s<R<\alpha+\tau+\rho^s+\rho^d$ the bundle is reflected diffusely.

If the bundle is absorbed then the energy is added to the account of the particular surface or subdivision if local values are desired. If it is reflected the direction of the reflected bundle is determined from the reflection

characteristics of the surface at that point. For example, the polar angle of the reflected energy bundle is given by

$$R_{\theta_i}(\theta_i',\phi_i',\lambda)=\frac{\int_0^{\theta_i}\int_0^{2\pi} f_i(\theta_i',\phi_i',\theta_i,\phi_i,\lambda)\cos\theta_i\sin\theta_i\,d\phi_i\,d\theta_i}{\int_0^{\pi/2}\int_0^{2\pi} f_i(\theta_i',\phi_i',\theta_i,\phi_i,\lambda)\cos\theta_i\sin\theta_i\,d\phi_i\,d\theta_i} \quad (6.7)$$

and corresponding to this value of θ_i the azimuthal angle ϕ_i of reflected energy bundle is calculated in the same way. The cumulative distribution functions for the limiting cases of diffuse and specular reflection are given by Howell [15] and Toor [17]. After determining the direction of the reflection, the energy bundle is again followed till it is absorbed at the surface or leaves the enclosure. A general computer flow chart for calculation procedure is shown in Fig. 21.

6.2 Method of Solution

In the solution of a radiant interchange problem by the Monte Carlo method good quality random numbers are required. The speed of generation and cycle are also of considerable importance. The methods for generating random numbers vary from using noise of electron tubes, radiation of radioactive substances, etc., to generation by arithmetical algorithms on digitial computers. The numbers generated by arithmetical processes are not generated in a truly random fashion but pass some criterion of randomness and are called pseudo-random numbers. The choice of a random number generator depends upon the particular problem and the computer used. A detailed discussion is given by Taussky and Todd in [42]. The present problem was solved on an IBM 7094 computer, and the multiplicative congruential generator was used. It generates the random number sequence by taking the lower order 36 bits of the products $x_i x5^{15}$ where x_i is the previous random number and $x_0=1$. The output is a number between 0 and 1.

Since it is not possible to trace an infinite number of energy bundles, see Eq. (6.3), the number of energy bundles to be emitted has also to be decided. This depends upon the accuracy needed and the availability of computer time. The accuracy of the Monte Carlo method depends upon the sample size and can best be explained by a simple example. Let the exact value of $\mathcal{F}_{ij}'$ be p and p' be the value

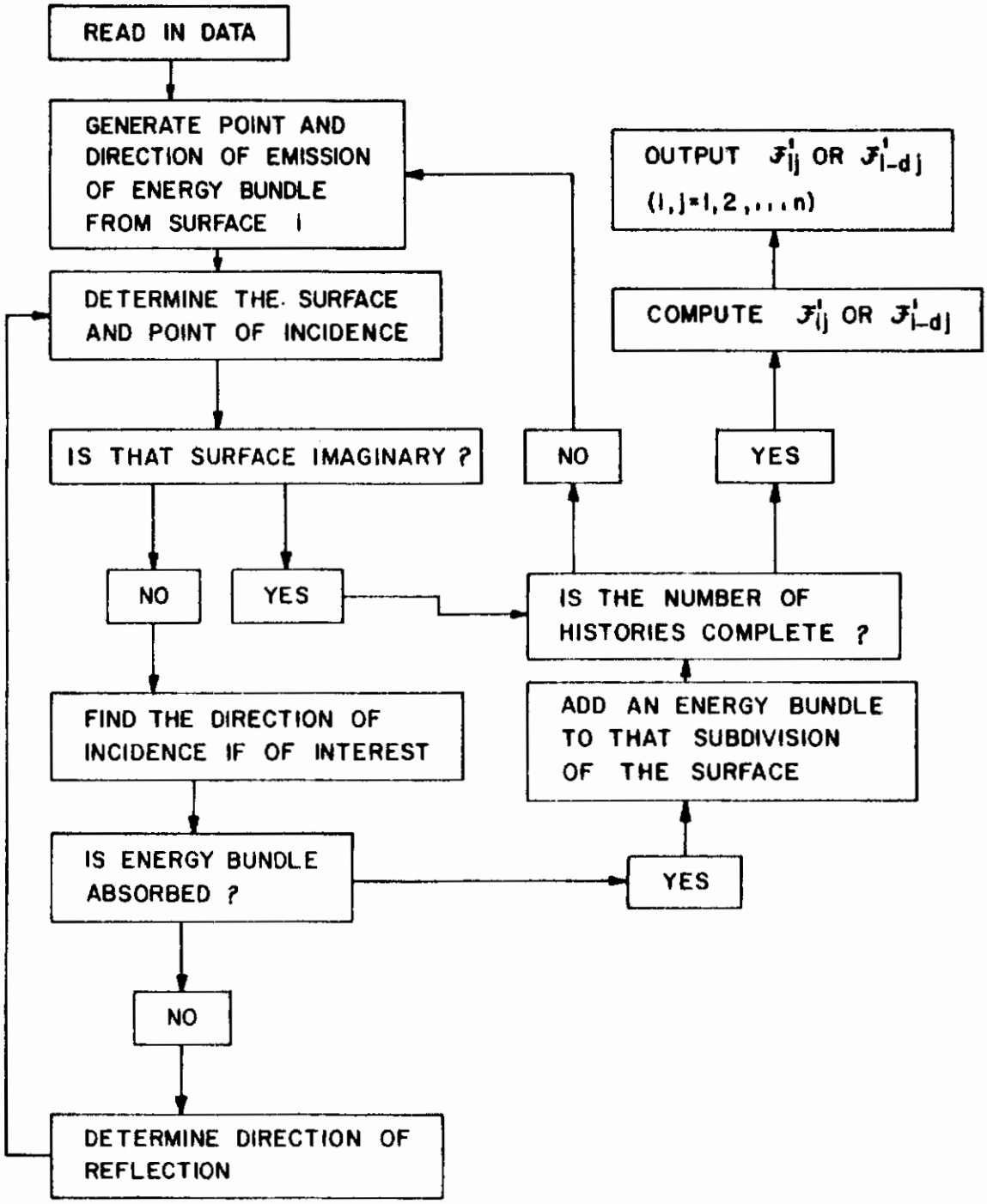

Figure 21

General Flow Chart for Calculation of $\mathcal{F}'_{ij}$ or $\mathcal{F}'_{i-dj}$

we predict after tracing N energy bundles by the Monte Carlo method. Then for sufficiently large N the probability P that p' lies within r % of p is [44]

$$P \simeq \mathrm{erf}(\zeta) \tag{6.8}$$

where

$$\zeta = (r/100)\,[Np/2(1-p)]^{\frac{1}{2}} \tag{6.9}$$

As $N \to \infty$ Eq. (6.8) becomes exact since the error function (erf) increases monotonically with ζ. The value of P can be increased by increasing ζ. It may be noted that ζ is proportional to $N^{\frac{1}{2}}$ and is minimum for p=0. It becomes clear from the above that for the same accuracy N should be large when p is small while N should be small when p is near unity. Since the computer time is directly proportional to the number of energy bundles traced, i.e., N, Monte Carlo is expected to be very time consuming for small values of p. In the above discussion it has been assumed that the exact value of p is known, which is not the case; however, for large N, p and p' are approximately equal and one can predict a sufficiently accurate value of p by substituting p' for p. A number of shortcut methods to increase the accuracy of the Monte Carlo method without increasing the computer time have been suggested by Toor [17].

In the calculations the surfaces were considered as gray and the emission from the surface was taken to be uniform. For constant property models simple analytical relations exist between the cumulative distribution functions for azimuthal as well as the polar angles for emission and reflection [15]. For direction dependent property models, the values of θ vs R_θ for determining the direction of emission were stored in a form of a table in the memory of the computer and the values of θ were obtained by interpolation. For determining the direction of energy bundles reflected bidirectionally using the cumulative distribution function given by Eq. (6.7) for example, the values of θ vs $R_\theta(\theta',\phi',\lambda)$ and ϕ vs $R_\phi(\theta',\phi',\theta,\lambda)$ were calculated and stored in the computer memory at 5° step increments of the angle of incidence θ'. From this table the direction of the reflected energy bundle, corresponding to a given direction of incidence (θ',ϕ'), was obtained by interpolation.

Once the absorption factors $\mathcal{F}'_{i-j}$ and $\mathcal{F}'_{di-j}$ have been determined the overall heat transfer rate at a surface, the overall net radiant interchange between two surfaces, and the local radiant heat flux can be computed immediately. Recalling that the overall radiant heat transfer rate from surface i can in general be expressed as the difference between energies emitted and absorbed at a surface, one

can write

$$Q_i = A_i \epsilon_i (\sigma T_i^4 - \sum_{j=1}^{n} \mathcal{J}'_{ij} \sigma T_j^4) \tag{6.10}$$

if use is made of reciprocity condition

$$A_i \epsilon_i \mathcal{J}'_{ij} = A_j \epsilon_j \mathcal{J}'_{ji} \tag{6.11}$$

and if there is no radiation falling on the system from some external source. The net radiant interchange between two surfaces i and j is given in terms of the absorption factors $\mathcal{J}'_{ij}$ as

$$Q_{i \rightleftarrows j} = A_i \mathcal{J}'_{ij} \epsilon_i (\sigma T_i^4 - \sigma T_j^4) \tag{6.12}$$

The local radiant heat flux at i can be expressed analogously to that by Eq. (6.10), and we can write

$$q_i = dQ_i / dA_i = \epsilon_i (\sigma T_i^4 - \sum_{j=1}^{n} \mathcal{J}'_{di-j} \sigma T_j^4) \tag{6.13}$$

where in writing Eq. (6.13) use was made of the reciprocity condition

$$\epsilon_i dA_i \mathcal{J}'_{di-j} = \epsilon_j A_j \mathcal{J}'_{j-di} \tag{6.14}$$

various special cases follow immediately from Eqs. (6.10) and (6.13). For example, when there are only two surfaces in the system and both are at the same temperature the local radiant heat loss, Eq. (6.13), reduces to

$$q_i / \epsilon_i \sigma T_i^4 = 1 - \mathcal{J}'_{di-i} - \mathcal{J}'_{di-j} \tag{6.15}$$

6.3 Results and Discussion

6.3.1 Independent Parameters

Radiation heat exchange between surfaces depends on the geometry of the system, the radiation characteristics of surfaces and on the boundary conditions prescribed. There is, of course, an infinite number of combinations of the various independent parameters, and so it is necessary to be selective. The systems and parameters chosen as well as the reason for the particular choices are given in the following paragraphs.

The geometrical arrangements selected for study are illustrated in Fig. 22, and are henceforth referred to as Configuration 1, Configuration 2, etc. The choice of these simple configurations was dictated by the fact that such simply arranged surfaces arise in engineering systems. The systems chosen cover a complete range of configurations and as such permit a critical examination of the influence of directional characteristics of surfaces on radiation interchange.

The hemispherical emissivities adopted for the calculations were 0.9, 0.5 and 0.1. The reason for choosing these values were twofold. First, they encompass a wide range of materials including poor as well as good electrical conductors. Second, these values were taken to facilitate direct comparison of the present results with those reported in References 6, 14 and 25. The directional reflectivities and emissivities for a specularly reflecting surface were calculated from Fresnel's equations. The complex index of refraction, $\tilde{n} = n - ik$, that is, the index of refraction n and the index of absorption k corresponding to these hemispherical emissivities are as follows:

ϵ	n	k
0.9	1.5565	0
0.5	6.1038	0
0.1	23.4520	23.4520

These constants are identical to those used by Hering [14] and were adopted in the present study to facilitate comparison. The justification for choosing these particular values is given by Hering. Furthermore, it should be remarked that the intent here has not been an accurate reproduction of directional radiation properties for a particular material, but only a qualitatively correct functional form which represents the gross trends of the characteristics with direction.

Results have been obtained for the following models:

I. Constant (direction independent) properties, CP.
   1. Diffuse emission and reflection with uniform radiosity, D* (the results reported for this model were obtained analytically)
   2. Diffuse emission and reflection, D (model A)
   3. Diffuse emission and specular reflection, S (model B)

II. Direction dependent properties, DP.
   1. Directional emission and specular reflection with the reflectivity given by Fresnel's equations, S (model E)
   2. Directional emission and bidirectional reflection with the directional reflectivity given by Fresnel's

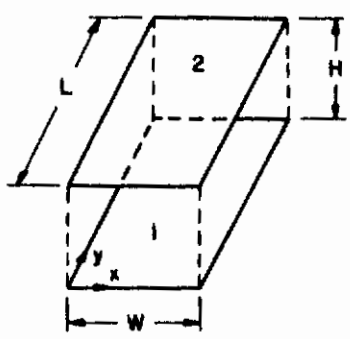

CONFIGURATION - 1

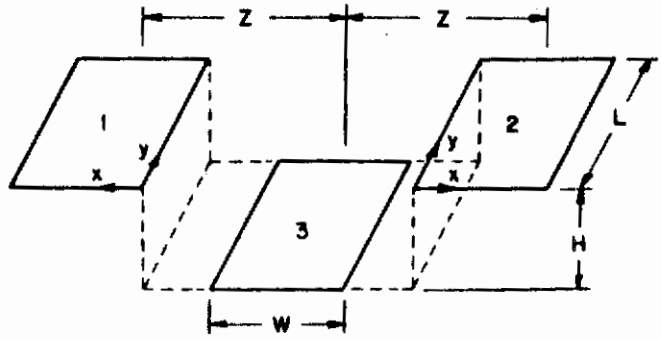

CONFIGURATION - 2

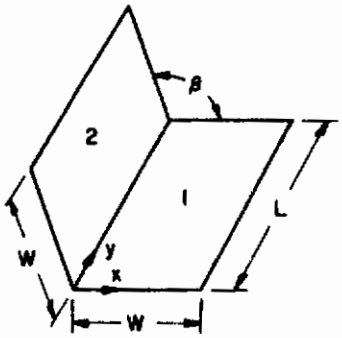

CONFIGURATION - 3

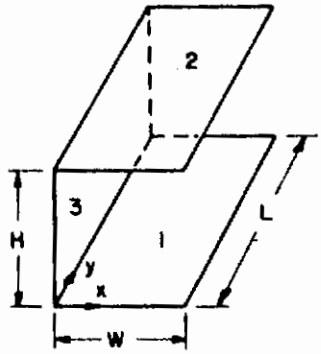

CONFIGURATION - 4

Figure 22

Configurations Analyzed

equations and the reflection distribution function by Eq. (3.19), BP (σ_o/λ;a_o/λ) (model G)

The reason the diffuse emission, reflection and uniform radiosity model (denoted for the sake of brevity by D*) was also considered is that all of the zonal methods of radiant heat transfer analysis such as the radiosity, Hottel, Gebhart, and Oppenheim electric analog methods are based on this model [1].

6.3.2 Comparison of Monte Carlo with Exact Results

The accuracy of the Monte Carlo method can be estimated and the validity of its use in radiant heat exchange calculations established by comparing the overall and the local radiant heat loss predictions with those reported previously which were based on exact numerical solutions. A comparison of the overall heat loss from surface 1 and 2 for Configuration 3 is given in Table 2. The exact results of Sparrow et al. [25] based on the diffuse model and the results of Hering [14] based on the specular model with constant (CP) and dependent properties (DP) are compared with Monte Carlo calculations in Table 2. Inspection of the table reveals generally good agreement up to two significant figures. It should be remarked in passing that the exact results of Sparrow et al. [25] and of Hering [14] were obtained for infinitely long plates, but the Monte Carlo calculations were based on length to width ratios L/W=5,000. These ratios are sufficiently large to accurately approximate the infinitely long plates. An equally good agreement has been obtained for Configuration 1 with diffuse surfaces [17]. These findings give some confidence in the Monte Carlo method and establish its utility in overall radiant interchange calculations.

A comparison between the exact analytical predictions of Hering [45] and the approximate results based on the Monte Carlo method for the local heat loss are given in Fig. 23. This is a more severe test of the accuracy of the Monte Carlo method than has been provided by the comparison of the overall heat losses from the surface. The Monte Carlo results are somewhat scattered but clearly reveal the main trends. The largest difference between the results occur near the apex. The local heat flux predicted is a maximum of 3 percent higher than the exact result. This small discrepancy establishes the utility and validity of the Monte Carlo in local radiant heat transfer calculations.

Although the Monte Carlo results given in Table 2 and in Fig. 23 agree well with the exact solutions there is no assurance of a comparable degree of accuracy for other configurations or for a different functional dependence of

TABLE 2

Comparison of Overall Heat Loss From Surface 1 (or 2) for Configuration 3 with Infinitely Long Plates, $T_1 = T_2 = T$ and $\epsilon_1 = \epsilon_2 = \epsilon$.

Model		$Q/W\sigma T^4$					
	ϵ	0.9		0.5		0.1	
	$\beta°$	Monte Carlo	Exact	Monte Carlo	Exact	Monte Carlo	Exact
Specular DP Ref. [14]	45	.376	.377	.302	.304	.0895	.0895
	60	.489	.490	.356	.356	.0930	.0930
	90	.681	.677	.426	.425	.0966	.0965
	135	.861	.858	.480	.479	.0983	.0983
Specular CP Ref. [14]	45	.376	.376	.302	.304	.0907	.0906
	60	.484	.484	.359	.358	.0940	.0938
	90	.662	.663	.427	.427	.0971	.0971
	135	.837	.838	.480	.481	.0993	.0992
Diffuse Ref. [25]	45	.363	.365	.269	.268	.0836	.0838
	60	.471	.471	.328	.327	.0896	.0899
	90	.658	.658	.412	.412	.0958	.0958
	135	.836	.836	.479	.480	.0992	.0992

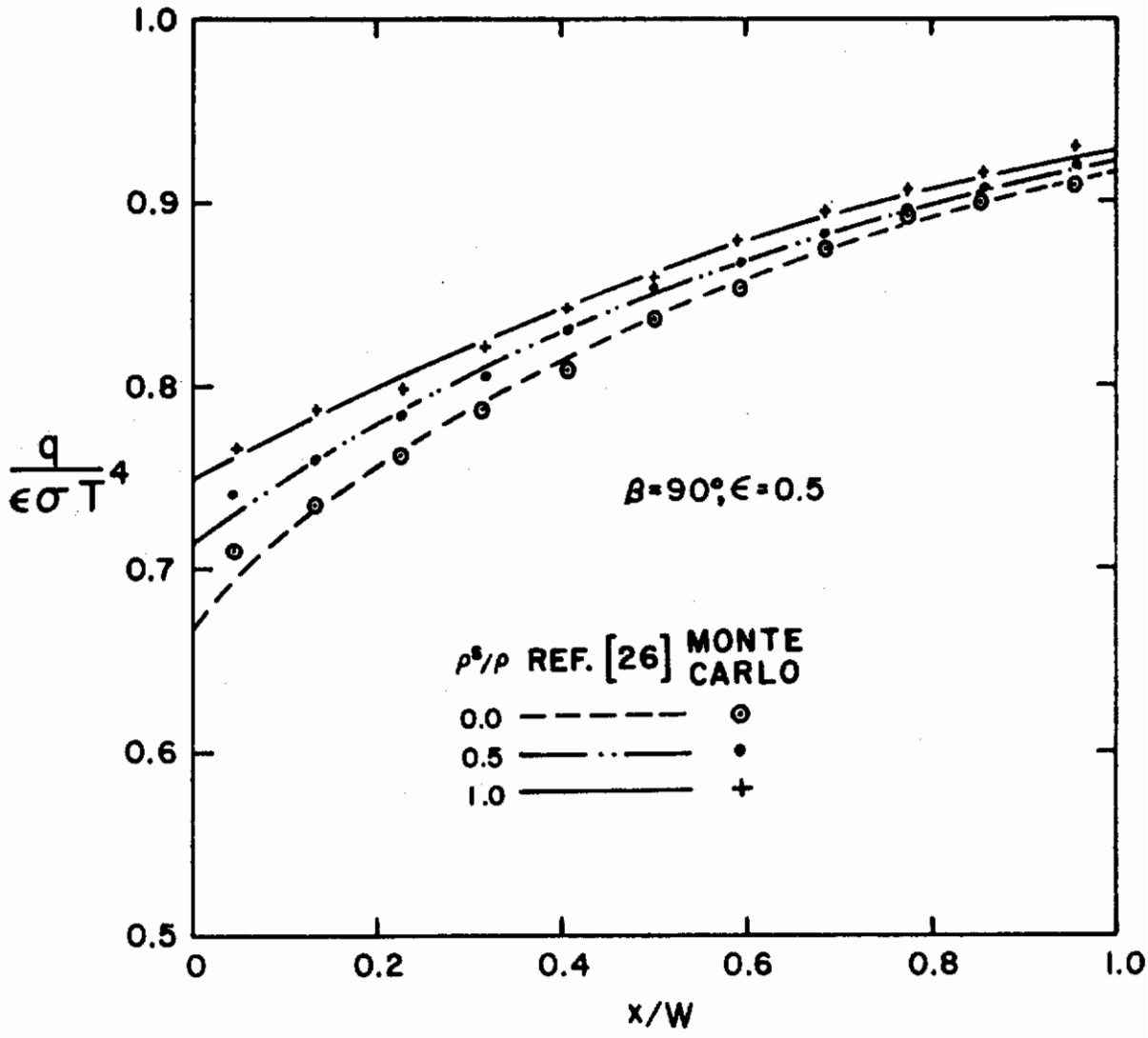

Figure 23

Comparison of Monte Carlo and Analytical [26] Results for Local Heat Loss for Configuration 3; Identical Surfaces, $\epsilon_1 = \epsilon_2 = \epsilon$, $T_1 = T_2 = T$, $L/W = 5000.0$

characteristics on direction. It is clear from Eq. (6.10) that if $\mathcal{F}'_{ii} + \mathcal{F}'_{ij}$ is small compared to unity, errors in the absorption factors are masked when the results are presented in terms of the overall heat loss and it is then that there is greater probability of a larger percent error in the absorption factors. It should be kept in mind that the Monte Carlo results are approximate and larger $\mathcal{F}'_{ij}$ carry greater weight of confidence.

The Monte Carlo method yields results of acceptable engineering accuracy. Although the computer time taken to solve a problem for a specific configuration depends on the number of trials (probability of accuracy desired), the radiation characteristics, the computer program, etc., an idea of the computer time used can be obtained from the example given below. The calculation of the local absorption factors needed to predict the local heat loss results presented in Fig. 23 took about 3.5 minutes for the diffuse model and about 2.5 minutes for the specular model on the IBM 7094 computer. In both cases 50,000 histories of energy bundles were traced. The method is more efficient for calculating overall absorption factors or heat transfer and considerably less efficient for predicting local values. For example, only 5,000 histories of energy bundles were traced (for a given value of ϵ and β) to predict the overall heat loss results presented in Table 2.

6.3.3 Overall Radiant Heat Loss and Radiant Heat Interchange

The absorption factors $\mathcal{F}'_{i2}$ and $\mathcal{F}'_{i1}$ for the four configurations studied are tabulated in the Appendix E in Tables E-1 through E-7. The results obtained encompass a large number of situations and include the "open" and "closed" systems. In the broad sense, the word "open" refers to such a system for which the ratio of the overall heat loss to emission is approximately equal to unity, i.e., $Q_i/A_i\epsilon_i\sigma T_i^4 \approx 1$. The word "closed" refers to a system for which this ratio is much smaller than one. The absorption factors for Configuration 4 when surface 3 is adiabatic and a perfectly specular reflector would be identical to those given for Configuration 1 in Tables E-1 and E-2 with values of H/W and L/W twice as large as in Configuration 1. For this reason the results are not included.

In brief, from the examination of the tabulated absorption factors the following conclusions may be drawn.

1. The comparison of the results for the diffuse models with uniform (D*) and nonuniform radiosities (D) show exceptionally good agreement. A similar finding has already been noted by Sparrow et al. [25].

2. The greatest difference between the results for the diffuse (D) and specular (S) constant property models occurs for "open" systems when the surfaces are highly reflecting, $\epsilon = 0.1$. In some instances $\mathcal{J}'_{12}$ based on the specular model may be greater by a factor of 5 than those based on the diffuse model.

3. The absorption factors for the specular model (S) based on the constant property (CP) analysis are generally in very good agreement with those from a directional property (DP) analysis. The difference between the two sets of results is smallest for highly absorbing surfaces ($\epsilon = 0.9$) and is greatest for highly reflecting surfaces ($\epsilon = 0.1$). The difference between CP and DP results is smallest for a "closed" configuration and increases as the system becomes more "open". For some cases (see Table E-1, $\epsilon = 0.1$) the two sets of results differ by more than a factor of two.

4. No general conclusions can be drawn regarding the absorption factors based on the Beckmann model for the reflection distribution function. Only for Configuration 2 (Table E-3) do the results for $\mathcal{J}'_{12}$ fall between the limiting diffuse and specular models. The greatest difference between the results based on BP and the other models occurs again for $\epsilon = 0.1$ and open systems.

5. For closed and intermediate systems the overall heat loss from a surface is not very sensitive to the choice of the model for the reflection characteristics as can be seen from the tabulated results. For example, since the average beam of radiation emitted from a surface, which is a part of a closed system, undergoes, say, more than 10 reflections for a surface having $\epsilon = 0.1$, its direction is practically random. In this case the probability that the beam will be absorbed by the surface is proportional to the absorptivity of the surface and is independent of the character of the reflections.

6. For open systems with highly reflecting surfaces the overall heat transfer is much more sensitive to the nature of reflections since even for $\epsilon = 0.1$ the beam undergoes few if any reflections at all. It is clear from Eq. (6.10) and the tabulated results that the largest difference between the overall heat transfer predictions at surface i based on the various models occurs for open systems having highly reflecting surfaces when the temperature of surface j is larger than that of surface i.

7. The choice of the model and the detailed radiation characteristics are very critical for predicting overall radiant interchange in very open systems having highly reflecting surfaces. The prediction of radiant heat interchange

among two surfaces based on any two models may differ by a factor of several or even many orders of magnitude.

6.3.4 Local Radiant Heat Loss

Recall that the local radiant heat flux can be readily evaluated once the local absorption factors $\mathcal{J}'_{di-j}$ or $\mathcal{J}'_{j-di}$ are known, see Eq. (6.13). The results presented in this report are in terms of the factor $\mathcal{J}''_{j-di}$ instead of $\mathcal{J}'_{j-di}$

$$\mathcal{J}''_{j-di} = \mathcal{J}'_{j-di} \, (A_j/dA_i) \qquad (6.16)$$

This is advantageous since now $\mathcal{J}''_{j-di}$ is independent of the size of the elementary area used in the numerical calculations. It should be noted that the results for $\mathcal{J}''_{j-di}$ presented are not truly local but represent values averaged over a finite area ΔA_i. The surface was divided into 10 strips or into i x j rectangular zones for infinitely long and finite surface, respectively. The calculated points have been omitted from the figures for the sake of clarity but some representative results are given by Toor [17]. Since there was some scatter in the calculated results the lines drawn through the points represent smoothed values.

For the purpose of estimating the detail required in describing the radiation characteristics of surfaces when predicting the radiant heat flux the local absorption factors were calculated for a range of parameters and all four configurations considered. Since it is expected that the greatest difference between the various models would occur when the reflectivity is high, most of the results presented are for this case, $\epsilon = 0.1$. Some representative results for the local heat loss are presented in Figs. 24, 27, 30, and 33 and the corresponding absorption factors needed to calculate the former in Figs. 25-26, 28-29, 31-32, and 34-35, respectively. The local radiant heat loss and absorption factors for Configuration 4 when surface 3 is adiabatic and a perfectly specular reflector would be identical to those given in Figs. 24 and 25-26, respectively, for values of H/W and L/W twice as large; however, due consideration should be given to the coordinate system of the two configurations.

Results presented in the figures show that in some instances, see Fig. 29, the local absorption factors may vary by more than an order of magnitude from one edge of a surface to another. Whether this large variation in the local absorption factors along a surface is important depends on whether one is interested in the local heat loss or the local radiation

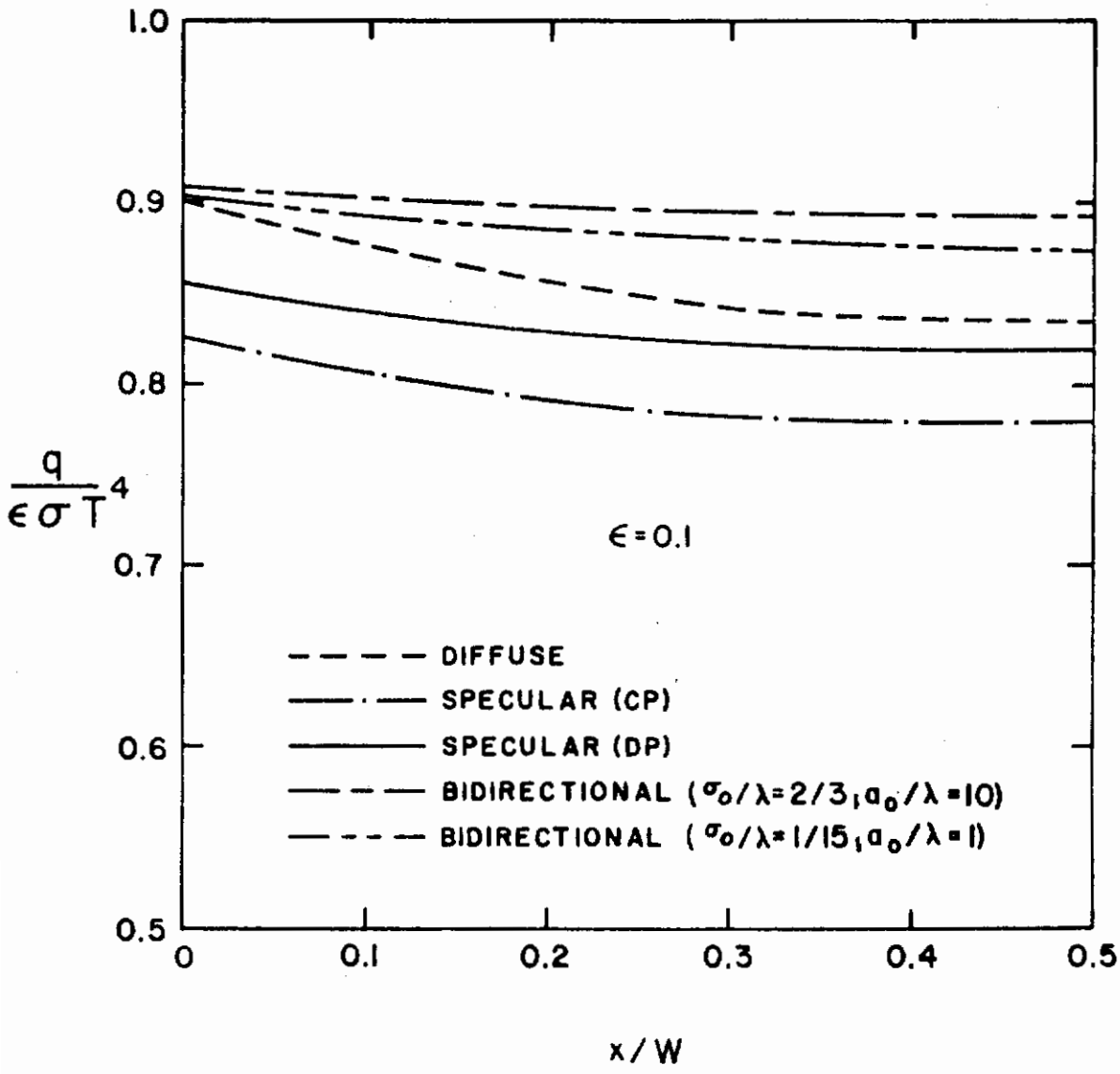

Figure 24

Local Heat Loss for Configuration 1. Identical Surfaces, $\epsilon_1=\epsilon_2=\epsilon$. $T_1=T_2=T$. H/W = 0.5, L/W = 2500.0

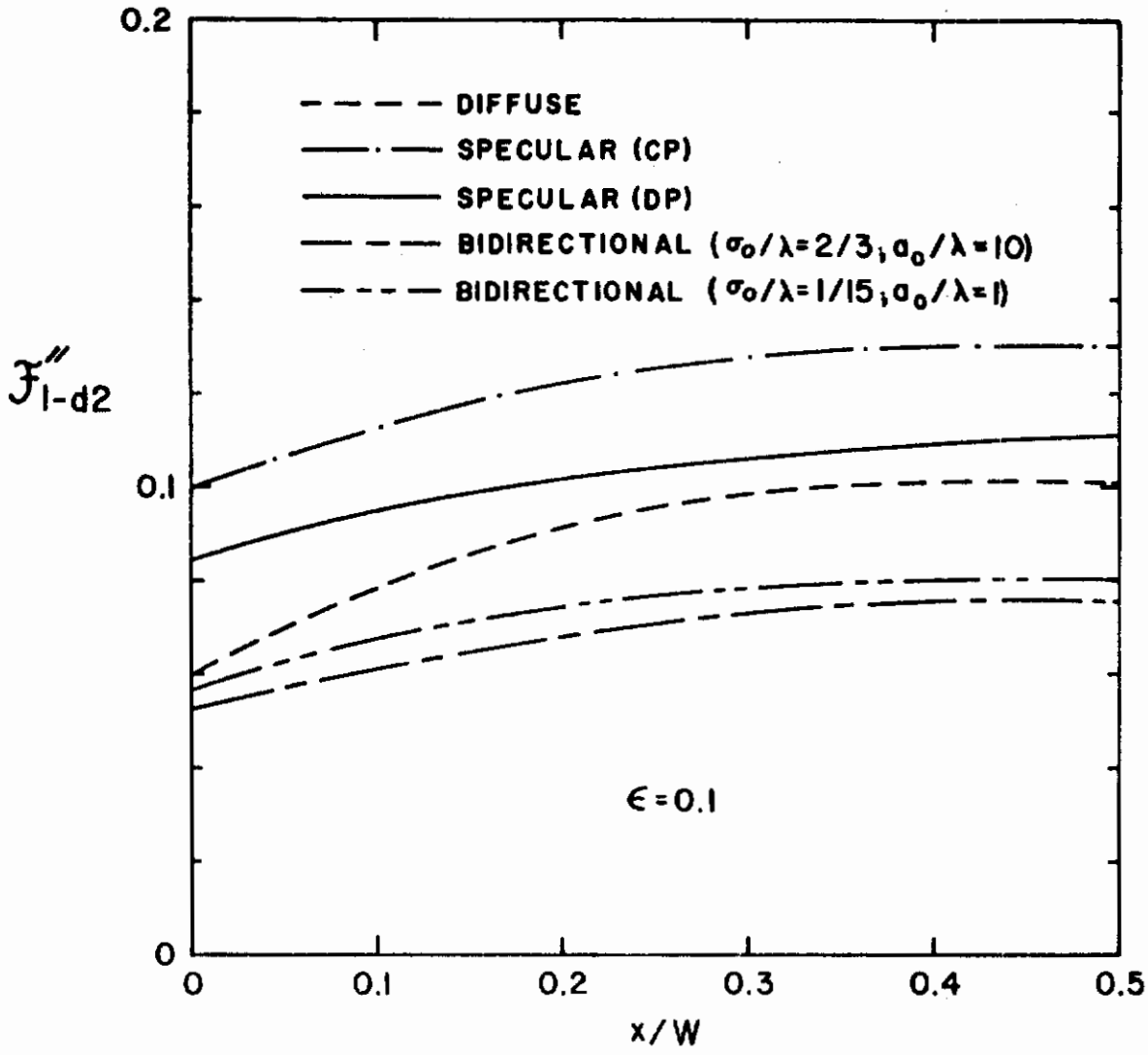

Figure 25

Absorption Factor $\mathcal{F}''_{1-d2}$ for Configuration 1; Identical Surfaces, $\epsilon_1=\epsilon_2=\epsilon$, H/W = 0.5, L/W = 2500.0

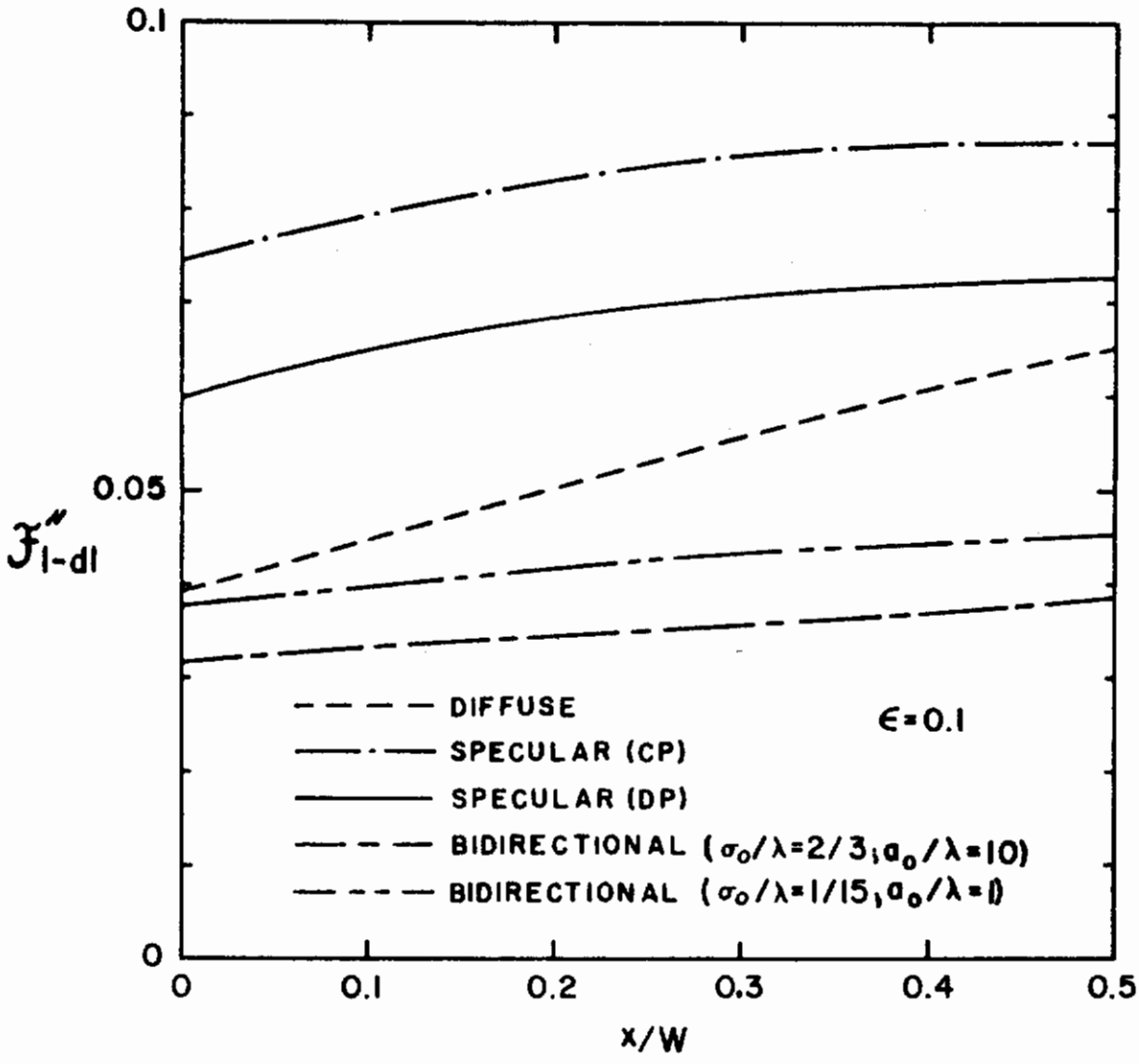

Figure 26

Absorption Factor $\mathcal{F}''_{1\text{-}dl}$ for Configuration 1; Identical Surfaces. $\epsilon_1 = \epsilon_2 = \epsilon$, H/W = 0.5. L/W = 2500.0

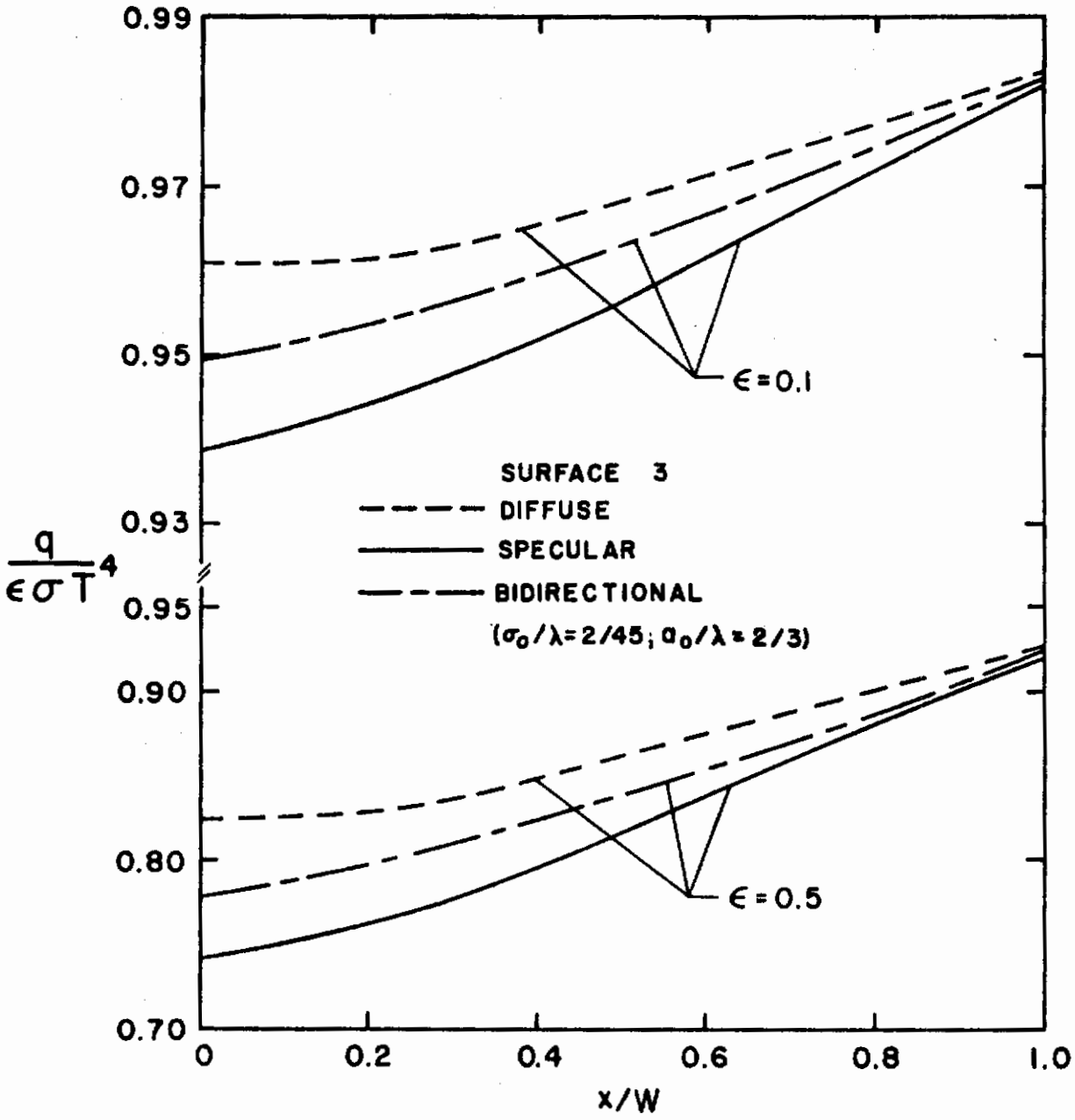

Figure 27

Local Heat Loss for Configuration 2; Diffuse Surfaces 1 and 2, $\epsilon_1 = \epsilon_2 = \epsilon$, $\rho_3 = 1.0$, $T_1 = T_2 = T$, $H/W = 1.0$, $Z/W = 0.5$, $L/W = 5000.0$

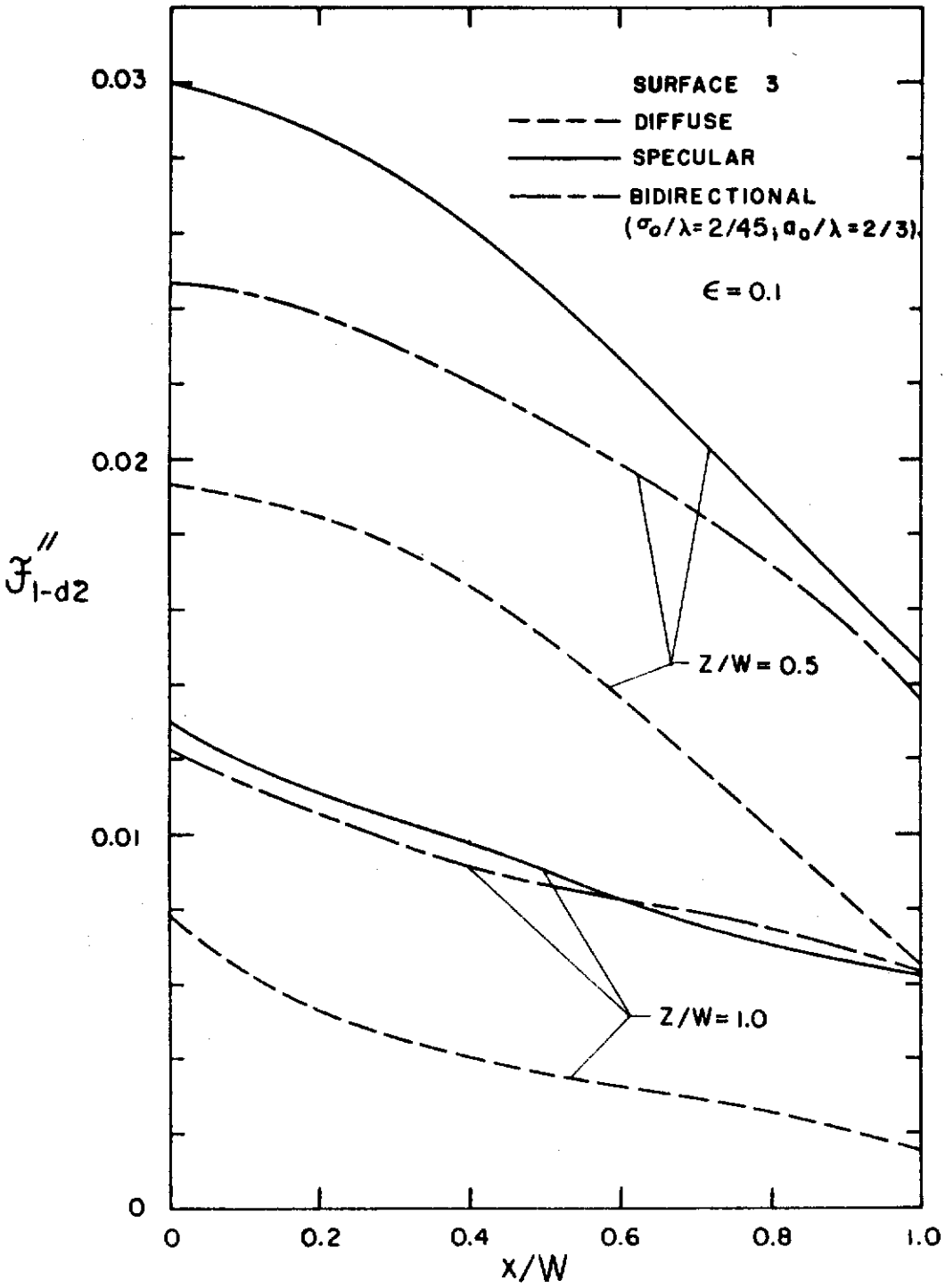

Figure 28

Absorption Factor $\mathcal{F}''_{1\text{-}d2}$ for Configuration 2; Diffuse Surfaces 1 and 2, $\epsilon_1 = \epsilon_2 = \epsilon$, $\rho_3 = 1.0$, H/W = 1.0, L/W = 5000.0

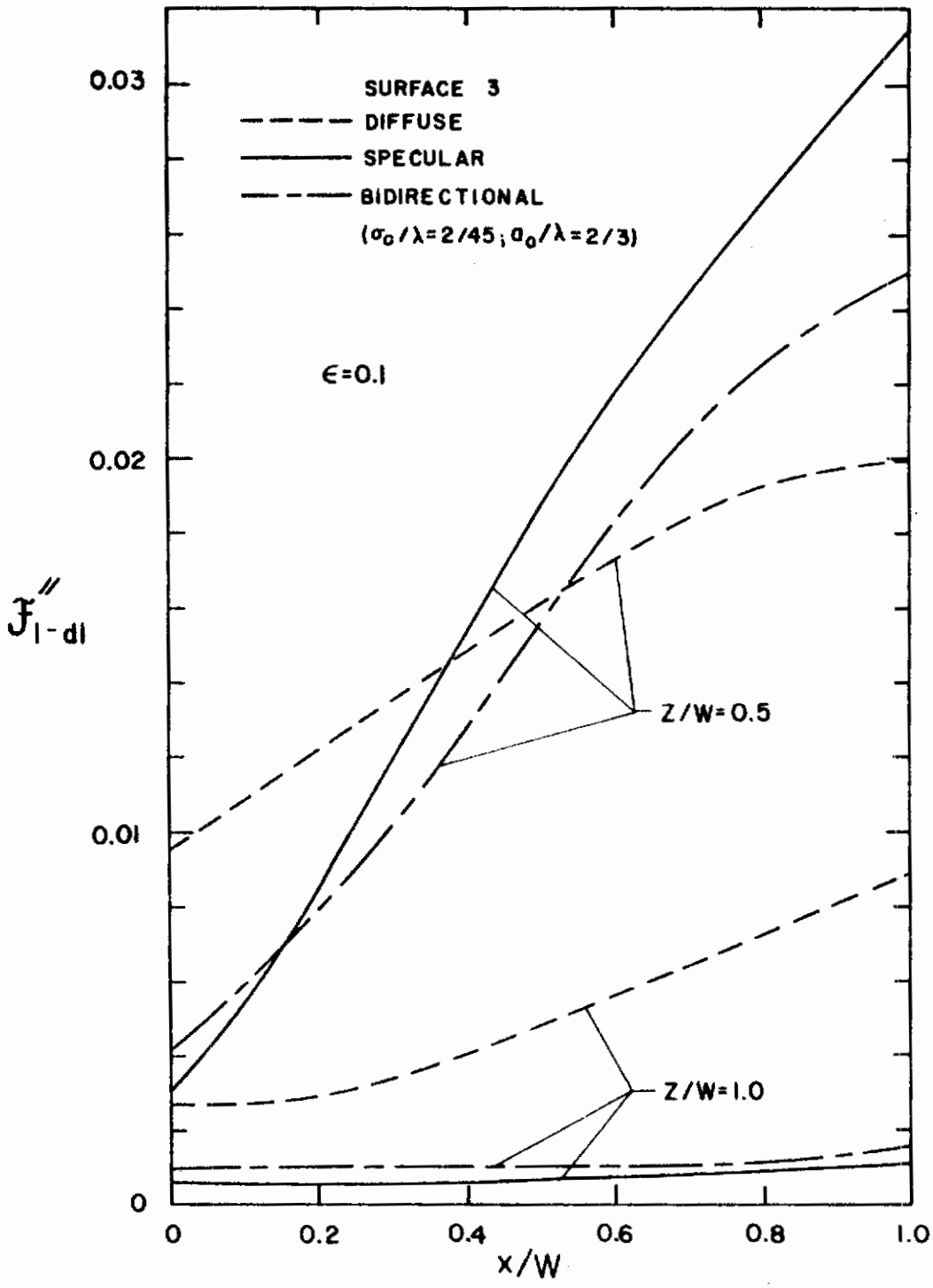

Figure 29

Absorption Factor $\mathcal{F}''_{1-d1}$ for Configuration 2; Diffuse Surfaces 1 and 2, $\epsilon_1 = \epsilon_2 = \epsilon$, $\rho_3 = 1.0$, H/W = 1.0, L/W = 5000.0

interchange. Inspection of the results reveals that for some configurations both $\mathcal{J}''_{1-d2}$ and $\mathcal{J}''_{1-d1}$ increase with increasing distance along the surface up to the center, see Figs. 25 and 26, while for others $\mathcal{J}''_{1-d1}$ increases and $\mathcal{J}''_{1-d2}$ decreases along the surface, see Figs. 28 and 29. These trends are obvious for the two particular configurations considered; however, in general no such simple conclusions can be made.

Comparison of absorption factors $\mathcal{J}''_{1-d2}$ based on different models shows that they may differ by as much as a factor of three; however, it is not possible to generalize this observation for different types of configurations. As Bevans and Edwards [13] have demonstrated it is possible to choose an extreme geometry for which the results would differ by many orders of magnitude depending on the model used for radiation surface characteristics. The largest differences between the results based on different models are expected to occur for very open arrangements when the dimensions of surfaces are very small compared to the distances between the surfaces.

Additional results for the local heat loss are given in Figs. 36 through 38. These as well as the results already presented are for identical surfaces 1 and 2. Before discussing the results in some detail it is desirable to review the configurations and the results reported earlier in the literature. For Configuration 1 local heat loss results have been reported by Sparrow et al. [25] for diffuse surfaces and by Eckert and Sparrow [6] for specularly reflecting constant property surfaces. The adjoint plate geometry (Configuration 3) has been considered by Sparrow et al. [25] for diffuse surfaces and by Eckert and Sparrow [6] for specular surfaces having constant properties and by Hering [14] for direction dependent properties. The dependence of the local heat loss for "open", "closed" and "intermediate" geometries has been systematically discussed by Sparrow et al. and needs no elaboration here.

Based on the results presented in the figures and some that are given in Reference 17 the following observations may be made:

1. For a given geometry the local heat loss is most nonuniform for black surfaces ($\epsilon = 1.0$) and becomes uniform for the limiting case of perfectly reflecting surfaces ($\rho \to 1$). For the former and very closed system, e. g., Configuration 1 where $(H/W) \to 0$, the ratio of heat loss at the edge of the plates to that at the center would be effectively infinite.

2. For open geometries the local heat loss from a surface is practically uniform over the surface and the presence of a second or additional surface plays a very minor role. As the system becomes more closed the local heat loss becomes more nonuniform.

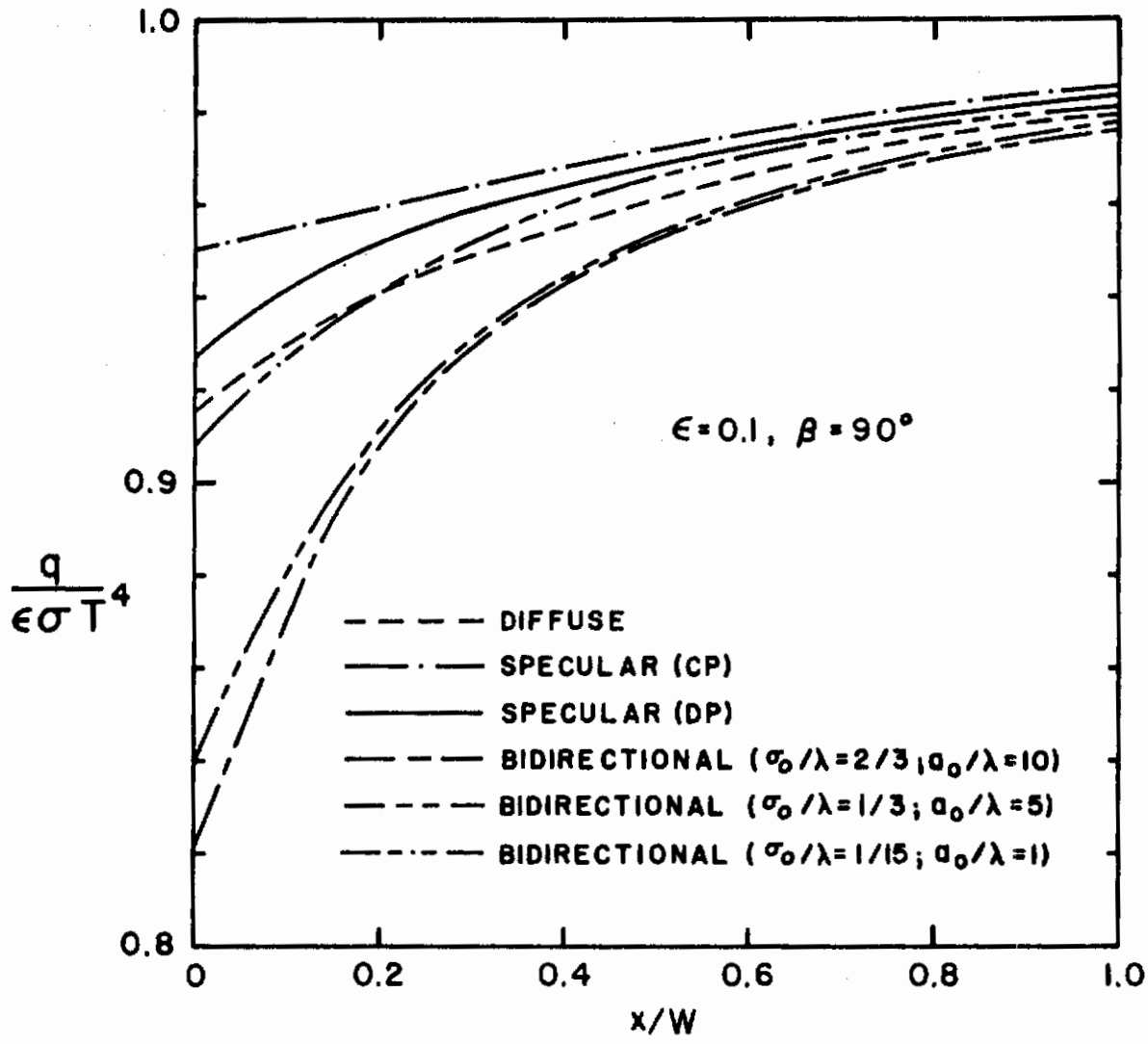

Figure 30

Local Heat Loss for Configuration 3; Identical Surfaces, $\epsilon_1 = \epsilon_2 = \epsilon$, $T_1 = T_2 = T$, L/W = 5000.0

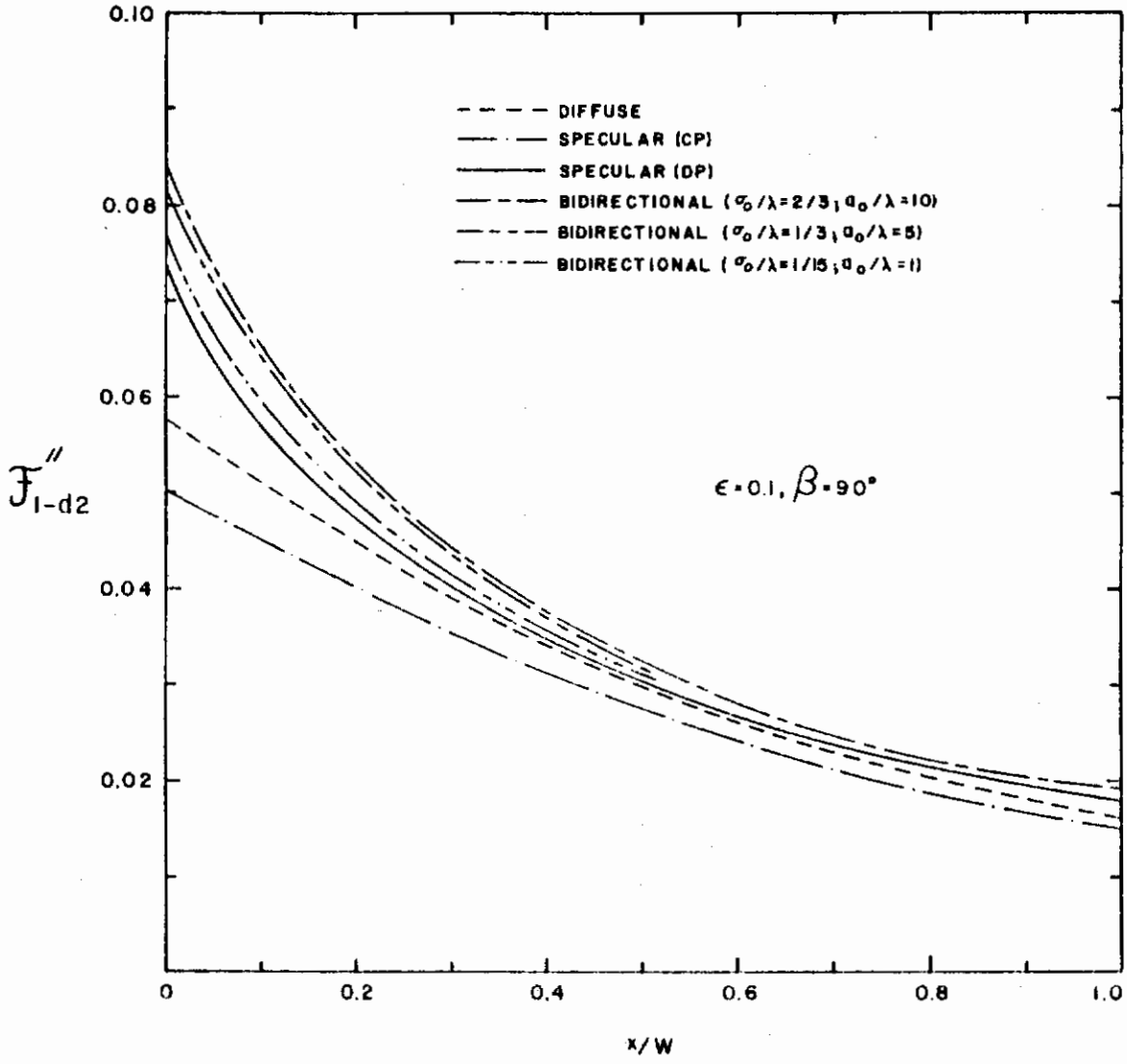

Figure 31

Absorption Factor $\mathcal{F}''_{1-d2}$ for Configuration 3;
Identical Surfaces, $\epsilon_1 = \epsilon_2 = \epsilon$
L/W = 5000.0

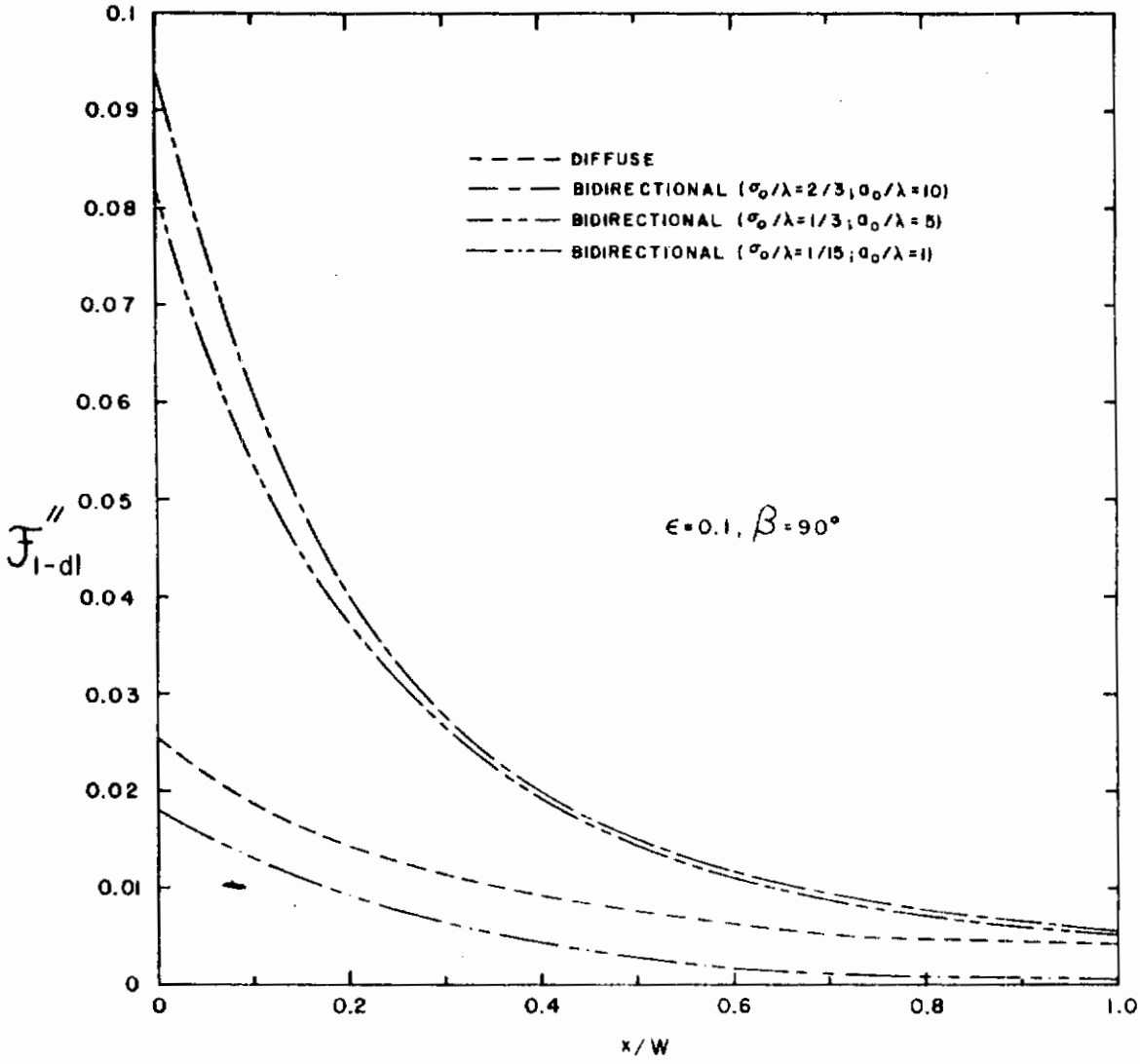

Figure 32

Absorption Factor $\mathcal{F}''_{1-dl}$ for Configuration 3; Identical Surfaces, $\epsilon_1 = \epsilon_2 = \epsilon$, L/W = 5000.0

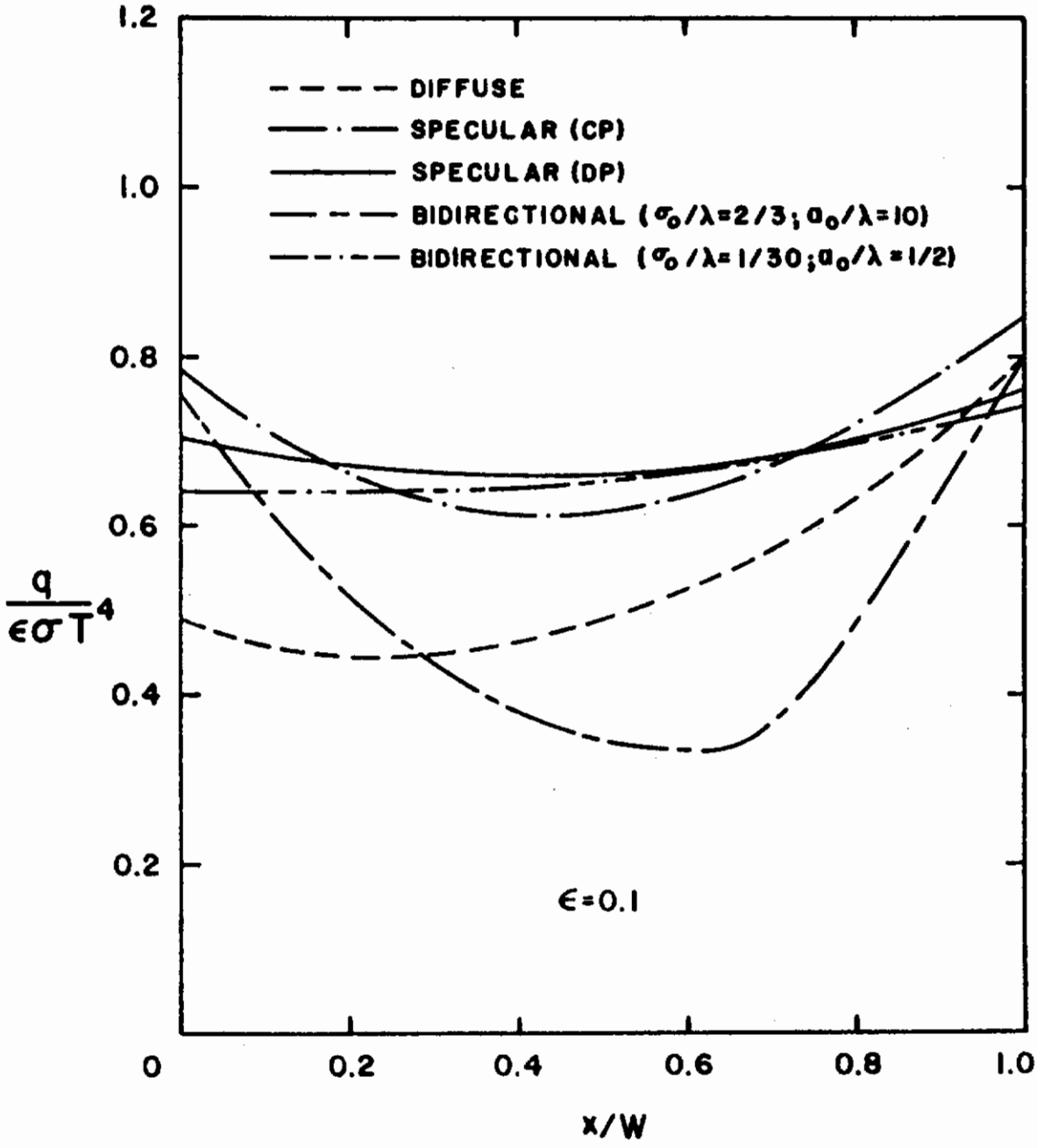

Figure 33

Local Heat Loss for Configuration 4; Surface 3 is Adiabatic, Diffuse and Perfect Reflector, Identical Surfaces 1 and 2, $\epsilon_1 = \epsilon_2 = \epsilon$, $T_1 = T_2 = T$, H/W = 0.25, L/W = 5000.0

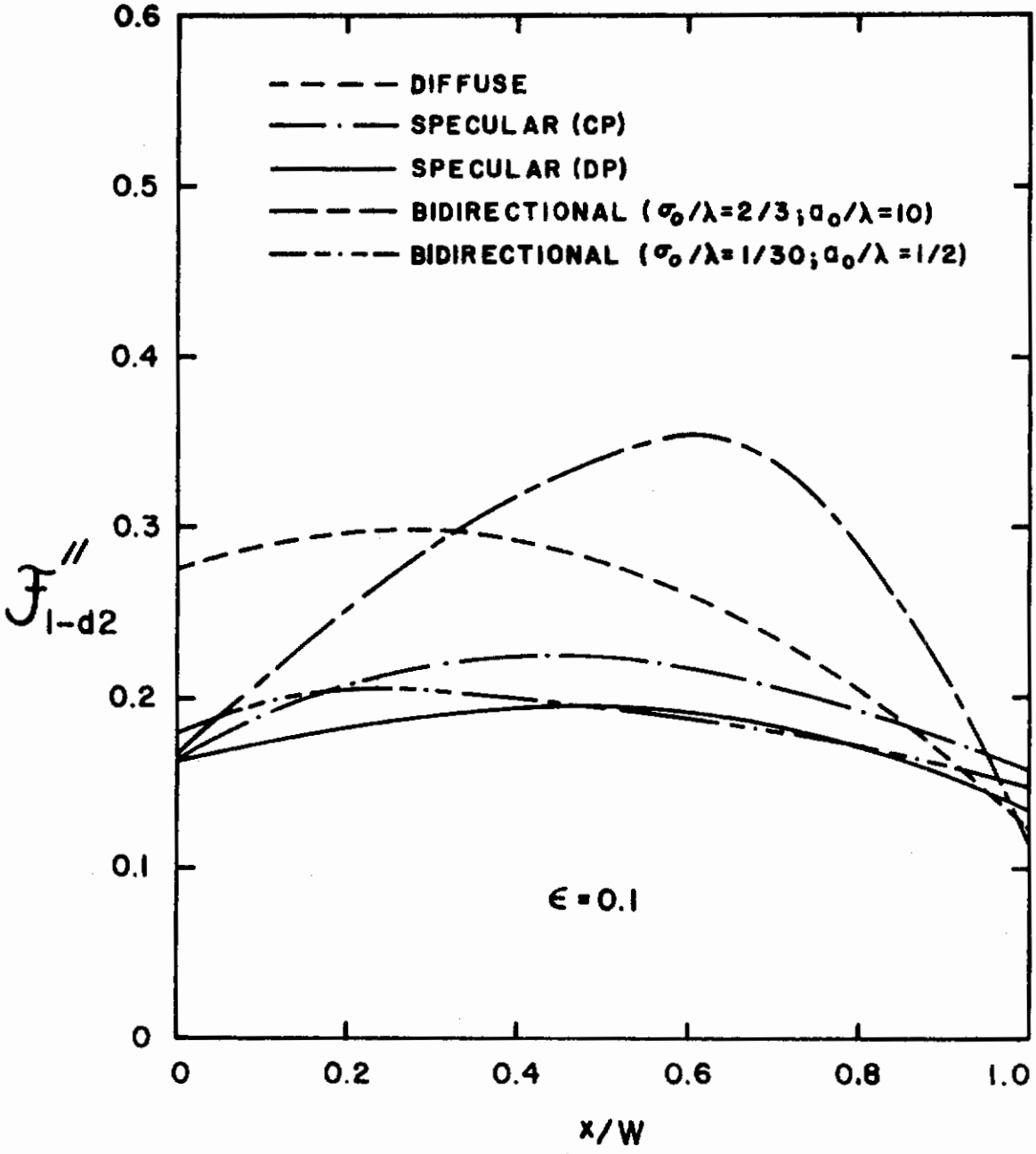

Figure 34

Absorption Factor $\mathcal{F}''_{1-d2}$ for Configuration 4; Surface 3 is Adiabatic, Diffuse and Perfect Reflector, Identical Surfaces 1 and 2. $\epsilon_1 = \epsilon_2 = \epsilon$, H/W = 0.25, L/W = 5000.0

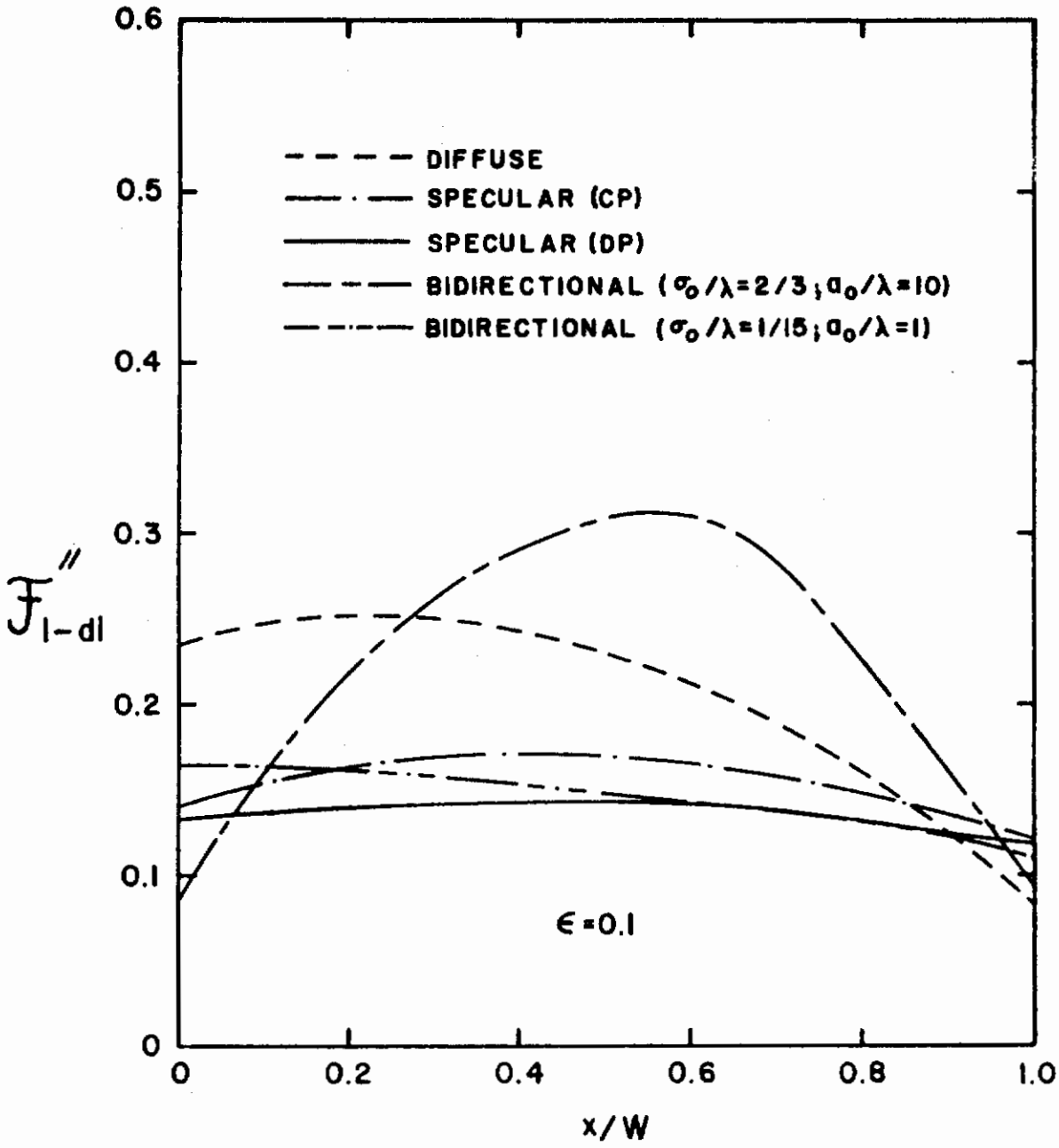

Figure 35

Absorption Factor $\mathcal{F}''_{1-dl}$ for Configuration 4; Surface 3 is Adiabatic, Diffuse and Perfect Reflector, Identical Surfaces 1 and 2. $\epsilon_1 = \epsilon_2 = \epsilon$, H/W = 0.25, L/W = 5000.0

3. The greatest difference between the predictions for $q/\epsilon\sigma T^4$ based on constant property models occurs at a position where the local heat loss is the smallest. The values differ in some instances, for example in Fig. 33, by more than a factor of two.

4. Regardless of the model chosen it is clear that for the two limiting cases either $\epsilon \to 1$ or $\epsilon \to 0$ at all the surfaces in the enclosure, the different models for radiation surface properties are expected to yield the same heat loss since there are no interreflections in the former and no absorptions in the latter enclosure. The largest difference between the predictions of q based on various models is expected to occur with intermediate values of ϵ.

5. Results show that the choice of the model is very important in analyzing local radiant interchange $Q_{di \to j}$ (i.e., net radiant exchange between an elementary area dA_i and a finite area A_j) particularly for open systems having highly reflecting surfaces.

6. The choice of the model is most critical and the greatest level of detail is required in describing the radiation characteristics when calculating local radiant heat loss at a highly reflecting surface which is a part of a closed system. The largest difference between the predictions of various models occurs at the position where the local heat loss is smallest.

7. The simple diffuse and specular constant property models can fail badly for a particular geometry and surface condition when the variation of properties with direction is not taken into account.

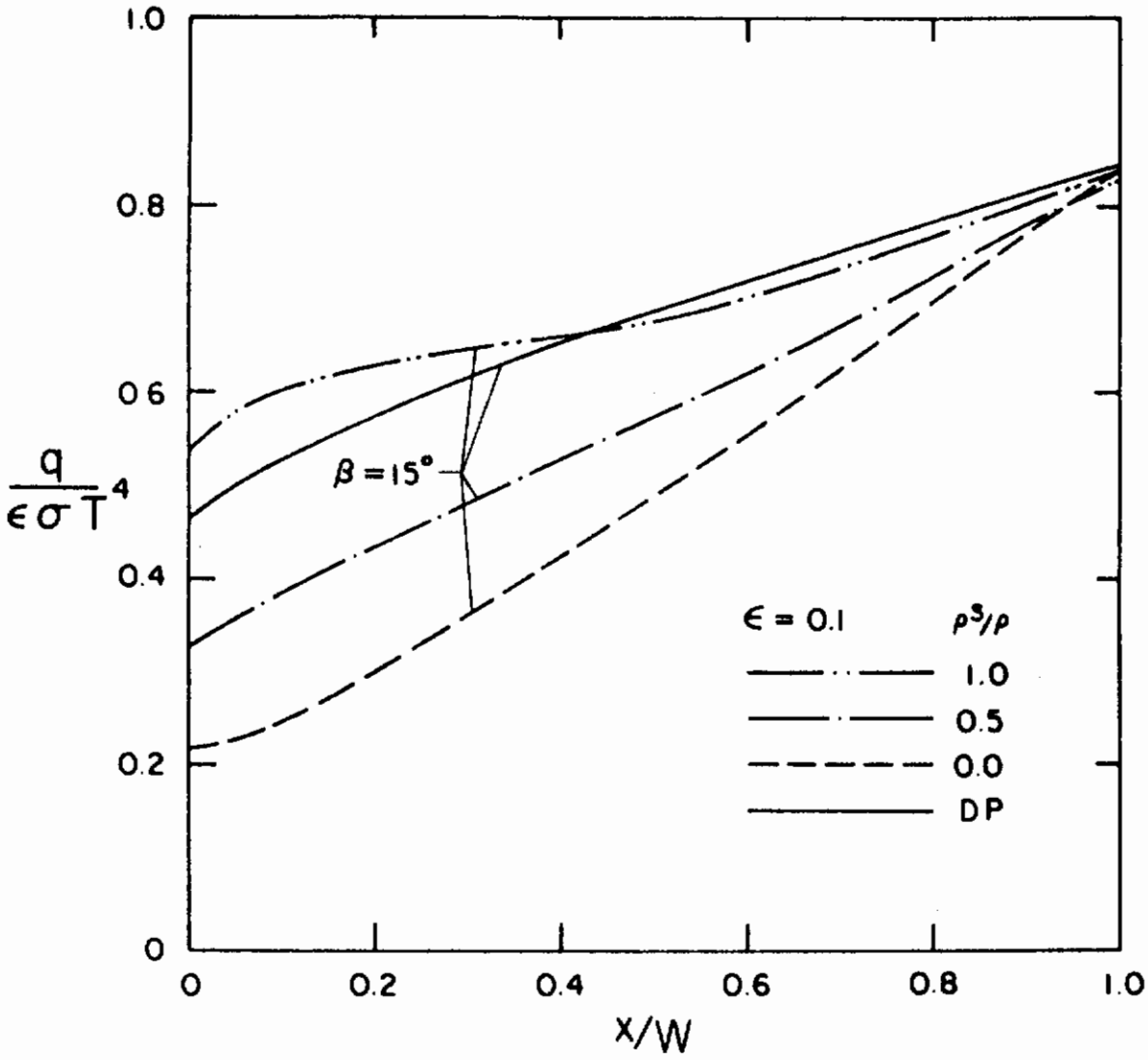

Figure 36

Local Heat Loss for Configuration 3; Identical Surfaces. $\epsilon_1 = \epsilon_2 = \epsilon$, $T_1 = T_2 = T$, L/W = 5000.0

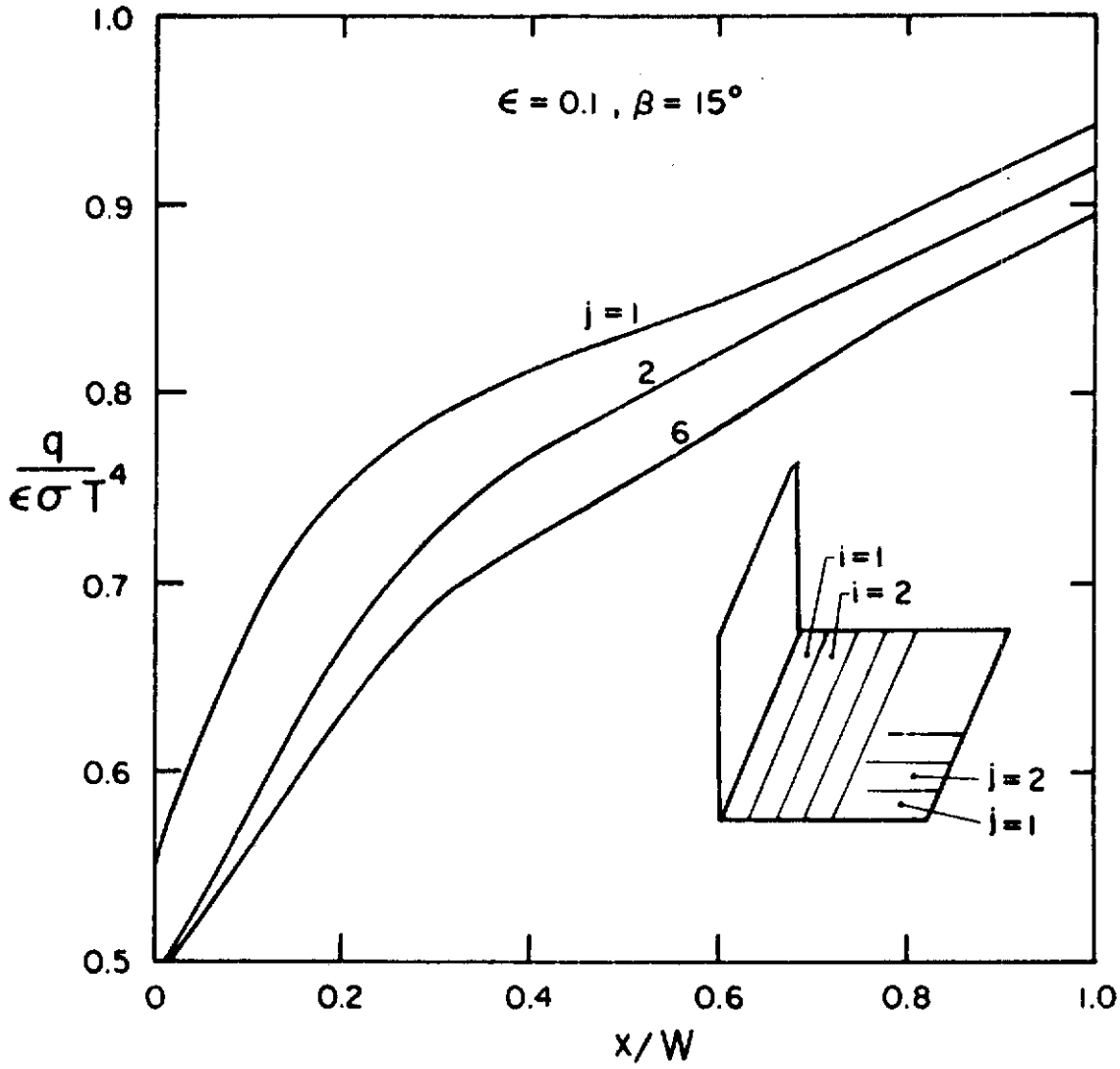

Figure 37

Local Heat Loss for Configuration 3; Specular (DP) Surfaces, $\epsilon_1 = \epsilon_2 = \epsilon$, $T_1 = T_2 = T$, L/W = 1.0 (i x j^1= 11^2x 11)

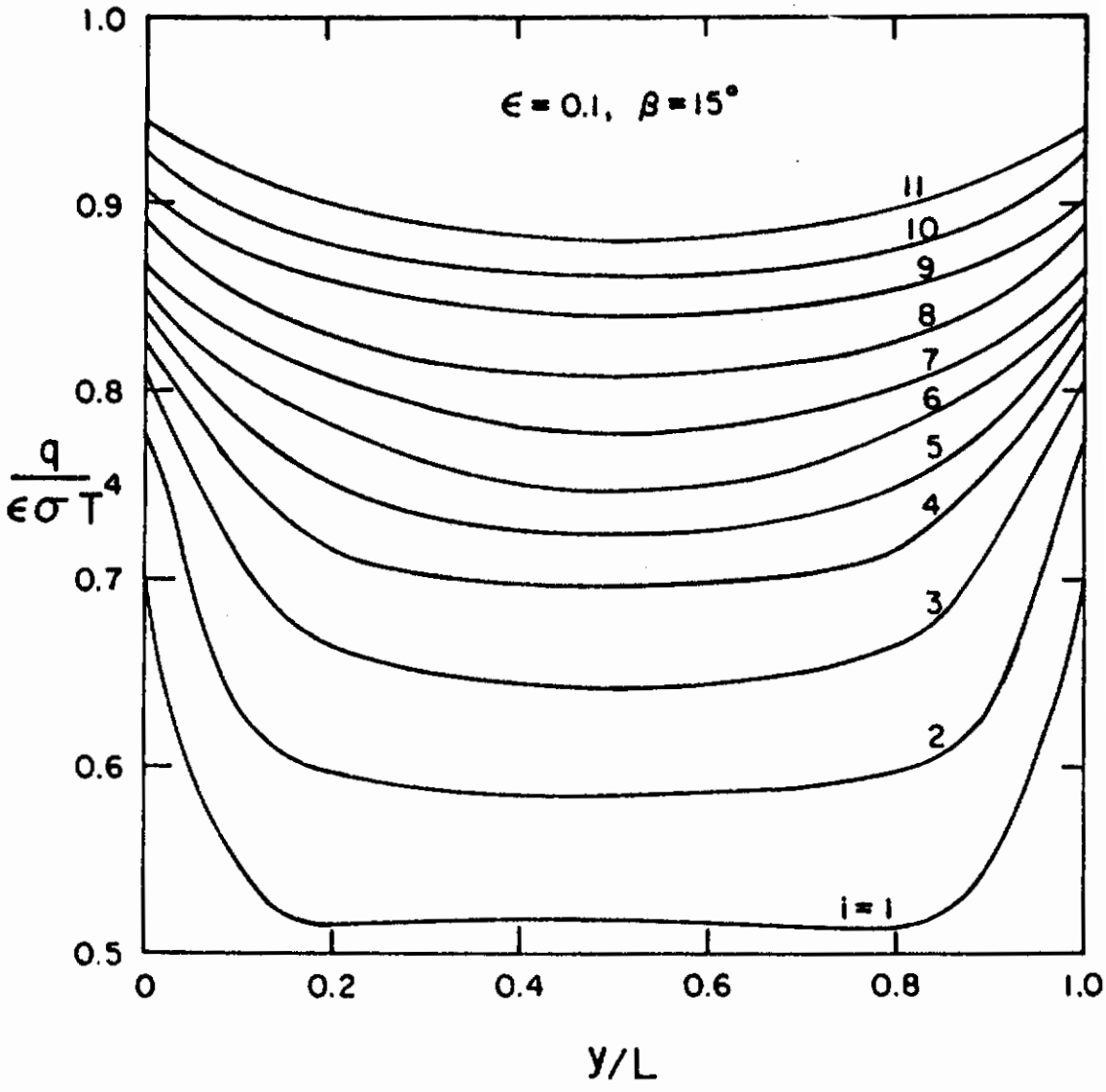

Figure 38

Local Heat Loss for Configuration 3; Specular (DP) Surfaces, $\epsilon_1 = \epsilon_2 = \epsilon$, $T_1 = T_2 = T$. L/W = 1.0 (i x j = 11 x 11)

7. CONCLUSIONS

As a result of the present analytical and experimental study of radiant heat transfer between simply arranged surfaces the following conclusions may be drawn.

1. Analytical results indicate that the diffuse and specular constant property analyses do not represent the upper and lower bounds on local radiant heat flux.

2. The simple diffuse analysis (where appropriate) yields good approximations to radiant heat transfer, especially considering the usual uncertainty of radiation surface properties. Even though the model is highly simplified, because of compensating effects, it can yield results for overall and local heat transfer of acceptable engineering accuracy. Particular care however should be exercised in analyzing radiant heat transfer at a surface which is primarily irradiated at large angles of incidence relative to the surface normal.

3. The local irradiation derived on the basis of the specular reflection constant property analysis with hemispherical properties yielded local irradiation values that differed in some instances by more than a factor of three from more realistic property models. The correct accounting for the variation of properties with direction for specularly reflecting surfaces, $(\sigma_o/\lambda_m)<<1$, is very important.

4. For large ratios of ρ^s/ρ the diffuse-specular constant property model suffers the same shortcomings as the specular model. Again, the dependence of the specular component of the hemispherical reflectivity must be accounted for in a more realistic radiant heat transfer analysis.

5. From the practical viewpoint, the directional emission and bidirectional reflection model for radiant heat transfer analysis is too complicated for use in engineering calculations. Even for the very simple configuration considered very extensive computations are needed and do not appear to be justifiable at the present time in view of the results obtained and the fact that detailed surface property information required to implement the real surface analysis, such as the spectral directional emissivity and the reflection distribution function of the participating surfaces, is generally not available for engineering materials.

6. An excellent compromise between reality, level of detail (where absolutely necessary) and computational effort appears to be the directional emission and reflection model with the diffuse and specular components of reflectivity depending on direction such that

$$\rho(\theta',\lambda) = \rho^{d}(\theta',\lambda) + \rho^{s}(\theta',\lambda)$$

All of the properties required by the analysis can be readily measured in the laboratory with existing instrumentation. Several laboratories in the country have this capability.

7. For the range of system parameters and surface materials considered the experimental data for the local irradiation agree remarkably well with the simple diffuse analysis. The predictions are within the maximum possible experimental error of the data. This is even true for materials approaching the optically smooth surface condition or when the ratio of the specular component of reflectivity to hemispherical reflectivity is large.

8. For surfaces approaching the optically smooth condition, for example, smooth electroplated gold, the experimental data does not fit the simple specular constant property analysis. The model appears to have certain severe limitations. Experimental data provides the verification of the importance of the directional effects for optically smooth surfaces.

9. For polished stainless steel or rough electroplated gold surfaces which have a large component of specular reflectivity the diffuse analysis is in closer agreement with the data than the diffuse-specular constant property analysis. The reason for this apparent failure is the same as for the simple specular analysis. It appears that if the diffuse-specular model is to be adopted for radiant heat transfer calculations at least the variation of the specular component of reflectivity with direction should be accounted for in some approximate manner.

10. The conclusions drawn above were based on the limited results obtained in the experimental and analytical phases of the program for the particular geometries, materials, and temperature levels. It appears from the Monte Carlo calculations that the configurations selected for radiant heat transfer analysis were not the most critical. These choices were primarily dictated by the computer time needed to perform the detailed computations. Therefore, care should be used in extending the results and conclusions to situations very much different from those studied here.

Based on the Monte Carlo calculations of radiant interchange among surfaces the following conclusions may be drawn:

1. For the type of radiation interchange problem considered in this study the Monte Carlo method provides a statistical approach that can be interpreted simply in terms of the physical processes and that has been extended to extreme generality. Moreover, the desired results can be expressed as overall and local absorption (radiation interchange) factors or overall and local heat flux distributions on the surface. The method can be readily adopted, with some additional complexity, for calculation of total radiant heat transfer on the spectral basis including the polarization effects.

2. For complex geometries or when the radiation characteristics of surfaces depend on direction, Monte Carlo simulation of radiant interchange problems is attractive. The method yields results that converge exactly (in the limit of many trials) to those of the specified physical problem. However, for very "open" systems, such as for Configuration 2 when Z/W is large, the method is very inefficient.

3. The choice of the model for predicting the overall heat loss from a surface is in general not very critical. The heat loss is generally within 25 percent of the simple diffuse analysis for both open and intermediate geometries.

4. The choice of the model and therefore the detail needed to describe the radiation characteristics of participating surfaces is not important in analyzing radiation interchange between two surfaces in a closed system when all surfaces have large emissivities. The differences between the predictions based on the various models was less than 10 percent.

5. The choice of the model and the detailed radiation characteristics are very critical in analyzing radiation interchange between two surfaces for very open systems having highly reflecting surfaces. The prediction of radiant heat interchange among two surfaces may differ by a factor of several or even many orders of magnitude.

6. The choice of the model is most critical and the greatest level of detail is required in describing the radiation characteristics for evaluating local heat loss at a highly reflecting surface which is a part of a closed system.

A number of new problem areas have evolved during the course of this research. This development of additional problems is expected in a study of this nature. A few areas which need further study are briefly discussed below.

1. The directional emission and reflection model F in which the directional reflectivity is resolved into diffuse and specular components is more realistic than the diffuse-specular constant property model C.

2. The development of simple experimental techniques for measuring the specular and diffuse components of directional reflectivity for engineering materials is needed if the model discussed above is to be applied successfully in more realistic heat transfer calculations.

3. The experimental work indicated a need for a small thermal (spectral or total) radiation detector that could be mounted flush with the surface and be nonselective to radiation regardless of incident direction and wavelength.

4. In experiments and analyses performed on a total basis it is difficult to separate the directional from the spectral effects.

In conclusion, the objectives of the research program have been satisfied, e.g., the accuracy and the validity of the commonly used simplified models for radiation surface characteristics have been examined both experimentally and analytically using more realistic and refined analysis.

REFERENCES

1. E. M. Sparrow, "On the Calculation of Radiant Interchange Between Surfaces," in Modern Developments in Heat Transfer (W. Ibele, Editor), pp. 181-212. Academic Press, London (1963).

2. E. Lax and M. Pirani, "Temperaturstrahlung Fester Körper", in Handbuch der Physik (H. Konen, Editor), Vol. XXI, pp. 190-272. Verlag von Julius Springer, Berlin (1929).

3. E. Eckert, "Messung der Reflexion von Wärmestrahlen an Technischen Oberflächen." Forsch. Gebiete Ingenieurw. 7, 265 (1936).

4. E. M. Sparrow, "Radiant Heat Transfer Between Surfaces," in Advances in Heat Transfer (J. P. Hartnett and T. F. Irvine, Jr., Editors) Vol. 2. pp. 399-452. Academic Press, New York (1965).

5. E. M. Sparrow and R. D. Cess, Radiation Heat Transfer. Brooks/Cole Publishing Company, Belmont, Calif. (1966).

6. E. R. G. Eckert and E. M. Sparrow, "Radiative Heat Exchange Between Surfaces with Specular Reflection." Int. J. Heat Mass Transfer 3, 42 (1961).

7. E. M. Sparrow, E. R. G. Eckert and V. K. Jonsson, "An Enclosure Theory for Radiative Exchange Between Specularly and Diffusely Reflecting Surfaces." Trans. ASME, J. Heat Transfer 84C, 294 (1962).

8. S. H. Lin and E. M. Sparrow, "Radiant Interchange Among Curved Specularly Reflecting Surfaces: Application to Cylindrical and Conical Cavities." Trans. ASME, J. Heat Transfer 87C, 299 (1965).

9. R. A. Seban, Discussion of Reference 7.

10. E. M. Sparrow and S. L. Lin, "Radiation Heat Transfer at a Surface Having both Specular and Diffuse Reflectance Components." Int. J. Heat Mass Transfer 8, 769 (1965).

11. A. F. Sarofim and H. C. Hottel, "Radiative Exchange Among Non-Lambert Surfaces," Trans. ASME, J. Heat Transfer 88C, 37 (1966).

12. G. L. Polyak, "Radiative Transfer Between Surfaces of Arbitrary Spatial Distribution of Reflection," Translation TT-9, School of Aeronautical and Engineering Sciences, Purdue University, Lafayette, Ind.; Translated

from Konvektivnyi i Luchistyi Teploobmen, pp. 118-132. Akad. Nauk SSSR, Moskva (1960).

13. J. T. Bevans and D. K. Edwards, "Radiation Exchange in an Enclosure with Directional Wall Properties," Trans. ASME, J. Heat Transfer 87C, 388 (1965).

14. R. G. Hering, "Radiative Heat Exchange Between Specularly Reflecting Surfaces with Direction Dependent Peroperties," in Proceedings of the Third International Heat Transfer Conference, Vol. V, pp. 200-206. AIChE, New York (1966).

15. J. R. Howell, "Calculation of Radiant Heat Exchange by the Monte Carlo Method," ASME Paper No 65-WA/HT-54.

16. R. C. Corlett, "Direct Numerical Simulation of Thermal Radiation in Vacuum," Trans. ASME, J. Heat Transfer 88C, 376 (1966).

17. J. S. Toor, "Radiant Heat Transfer Analysis Among Surfaces Having Direction Dependent Properties by the Monte Carlo Method," M. S. Thesis, Purdue University, Lafayette, Indiana (1967).

18. J. T. Bevans, et al., "Prediction of Space Vehicle Thermal Characteristics," Air Force Flight Dynamics Laboratory Technical Report AFFDL-TR-65-139, Wright-Patterson Air Force Base, Ohio (1966).

19. K. Elser, "Experimentalle Untersuchung des Strahlungsaustausches zwischen excentrischen Kugelflächen," Institut für Thermodynamik und Verbrennungsmotorenbau an der Eidgenossischen Technischen Hochschule in Zurich, Bericht Nr. 205 (1949).

20. B. Münch, Die Richtungsverteilung bei der Reflexion von Warmestrahlung und ihr Einfluss auf die Wärmeübertragung. Verlag Leeman, Zürich (1955).

21. T. J. Love and J. S. Gilbert, "Experimental Study of Radiant Heat Transfer Between Parallel Plates," Aerospace Research Laboratories Report ARL 66-0103, Wright-Patterson Air Force Base, Ohio (1966).

22. M. Born and E. Wolf, Principles of Optics, 2nd Edition. Pergamon Press, Oxford (1964).

23. D. K. Edwards and J. T. Bevans, "Effect of Polarization on Spacecraft Radiation Heat Transfer," AIAA Journal 3, 1323 (1965).

24. H. J. McNicholas, "Absolute Methods of Reflectometry," Nat. Bur. Stds., J. Research 1 29 (1928).

25. E. M. Sparrow, J. L. Gregg, J. V. Szel and P. Manos, "Analysis, Results, and Interpretation for Radiation Heat Transfer Between Some Simply Arrange Gray Surfaces," Trans. ASME, J. Heat Transfer 83C, 207 (1961).

26. R. G. Hering, "Radiative Heat Exchange and Equilibrium Surface Temperatures in a Space Environment, AIAA Paper No. 67-212 (1967).

27. P. Beckmann and A. Spizzichino, The Scattering of Electromagnetic Waves from Rough Surfaces. The Macmillan Company, New York (1963).

28. A. Houchens and R. G. Hering, "Bidirectional Reflectance of Rough Metal Surfaces," AIAA Paper No. 67-319 (1967).

29. H. Davies, "The Reflection of Electromagnetic Waves from a Rough Surface," Proc. Inst. Elect. Eng., Part III, 101, 209 (1954).

30. H. E. Bennet and J. O. Porteus, "Relation Between Surface Roughness and Specular Reflectance at Normal Incidence," J. Opt. Soc. Am. 51, 123 (1961).

31. H. von Helmholtz, Vorlesungen über der Theorie der Wärme, p. 161. J. A. Barth, Leipzig (1903).

32. N. F. Mott and H. Jones, The Theory of the Properties of Metals and Alloys. Dover Publications, New York (1958).

33. R. A. Seban, "The Emissivity of Transition Metals in the Infrared," Trans. ASME., J. Heat Transfer 87C, 173 (1965).

34. D. K. Edwards and N. B. de Volvo, "Useful Approximations for Spectral and Total Emissivity of Smooth Bare Metals," in Advances in Thermophysical Properties at Extreme Temperatures and Pressures, pp. 174-188. ASME, New York (1965).

35. J. R. Schornhorst, "An Analytical and Experimental Investigation of Radiant Heat Exchange Between Simply Arranged Surfaces," Ph. D. Thesis, Purdue University, Lafayette, Indiana (1967).

36. D. K. Edwards and I. Catton, "Radiation Characteristics of Rough and Oxidized Metals," in Advances in Thermophysical Properties at Extreme Temperatures and Pressures, pp. 189-199. ASME, New York (1965).

37. W. R. Wade and W. S. Slemp, "Measurements of Total Emittance of Several Refractory Oxides, Cermets, and Ceramics for Temperature from 600°F to 2,000°F," NASA Technical Note D-998 (1961).

38. R. C. Birkebak and E. R. G. Eckert, "Effects of Roughness of Metal Surfaces on Angular Distribution of Monochromatic Reflected Radiation," Trans. ASME, J. Heat Transfer 87C, 85 (1965).

39. T. J. Love and R. E. Francis, "Experimental Determination of Reflectance Function for Type 302 Stainless Steel," AIAA Paper No. 67-321 (1967).

40. R. E. Chupp and R. Viskanta, "Radiant Heat Transfer Between Concentric Spheres and Coaxial Cylinders," Trans. ASME, J. Heat Transfer 88C, 326 (1966).

41. M. M. Weiner, J. W. Tindall and L. M. Candell, "Radiative Interchange Factors by Monte Carlo," ASME Paper No. 65-WA/HT-51 (1965).

42. A. M. Herbert, Symposium on Monte Carlo Methods, John Wiley and Sons, Inc., New York (1956).

43. B. Gebhart, Heat Transfer, McGraw-Hill Book Co., Inc., New York (1961).

44. J. V. Uspensky, Introduction to Mathematical Probability, p. 131, McGraw-Hill Book Co., Inc., New York (1937).

45. F. B. Hildebrand, Methods of Applied Mathematics, Prentice-Hall, Inc., Englewood Cliffs, New Jersey (1952).

46. L. Fox, An Introduction to Numberical Linear Algebra, pp. 136-137, Oxford University Press, New York (1964).

47. A. H. Straud and P. Secret, Gaussian Quadrature Formulas, Prentice-Hall, Inc., Englewood Cliffs, New Jersey (1966).

APPENDIX A

Reduction of Integral Equation (3.9)

The aim of this appendix is to provide some details of reduction of the general integral equation for the spectral intensity of radiation. For the configuration shown in Fig. 3 which consists of two plane surfaces, infintely long (in the direction perpendicular to the plane of the figure), Eq(3.9) results in a pair of integral equations

$$I_1(x_1,\theta_1,\phi_1,\lambda) = \epsilon_1(x_1,\theta_1,\phi_1,\lambda) I_{b1}(x_1,\lambda) + \int_{A_1} f_1(x_1,\theta_1',\phi_1',\theta_1,\phi_1,\lambda) I_2(x_2,\theta_2,\phi_2,\lambda) K_{12} dA_2 \qquad (A.1)$$

and

$$I_2(x_2,\theta_2,\phi_2,\lambda) = \epsilon_2(x_2,\theta_2,\phi_2,\lambda) I_{b2}(x_2,\lambda) + \int_{A_1} f_2(x_2,\theta_2',\phi_2',\theta_2,\phi_2,\lambda) I_1(x_1,\theta_1,\phi_1,\lambda) K_{21} dA_1 \qquad (A.2)$$

if it is assumed that the surface temperature and properties are independent of the y coordinate. This is justifiable on the grounds that the plates are infinitely long in the y-direction and therefore y is no longer an independent variable of the problem. It remains now only to express the angles and the kernels in terms of the geometrical parameters and the coordinates of the two plates.

It is convenient to introduce dimensionless distances

$$\xi = x/L, \quad \eta = y/L, \quad \delta_1 = d_1/L, \; \delta_2 = d_2/L, \quad \gamma = h/L \qquad (A.3)$$

The angles of emission (or reflection) and incidence can after some manipulation be expressed in terms of the geometrical parameters of the problem and the dimensionless distance as

$$\theta_1 = \cos^{-1}[(\gamma + \xi_2 \sin\beta)/D_1] \qquad (A.4)$$

$$\theta_1' = \cos^{-1}[(\gamma + \xi_2' \sin\beta/D_1'] \qquad (A.5)$$

$$\phi_1 = \cos^{-1}(\eta_2/D_1) \tag{A.6}$$

$$\phi_1' = \cos^{-1}(\eta_2'/D_1') \tag{A.7}$$

where

$$D_1=[(\delta_2-\delta_1 + \xi_2\cos\beta - \xi_1)^2 + \eta_2^2 + (\gamma + \xi_2\sin\beta)^2]^{\frac{1}{2}} \tag{A.8}$$

$$D_1'=[(\delta_1-\delta_2 + \xi_1 - \xi_2'\cos\beta)^2 + (\eta_2')^2 + (\gamma + \xi_2'\sin\beta)^2]^{\frac{1}{2}} \tag{A.9}$$

and

$$\theta_2 = \cos^{-1}\left\{[\sin\beta(\delta_1-\delta_2+\xi_1) + \gamma\cos\beta]/D_2\right\} \tag{A.10}$$

$$\theta_2' = \cos^{-1}\left\{[\sin\beta(\delta_2-\delta_1+\xi_1) + \gamma\cos\beta]/D_2\right\} \tag{A.11}$$

$$\phi_2 = \cos^{-1}(\eta_1/D_2) \tag{A.12}$$

$$\phi_2' = \cos^{-1}(\eta_1'/D_2') \tag{A.13}$$

where

$$D_2=[(\delta_1-\delta_2+ \xi_1-\xi_2\cos\beta)^2 + \eta_1^2 + (\gamma + \xi_2\sin\beta)^2]^{\frac{1}{2}} \tag{A.14}$$

$$D_2'=[(\delta_2-\delta_1+ \xi_2\cos\beta-\xi_1')^2 + (\eta_1')^2 + (\gamma + \xi_2\sin\beta)^2]^{\frac{1}{2}} \tag{A.15}$$

The integral Eqs. (A.1) and (A.2) can be written as

$$I_1(\xi_1,\xi_2,\eta_2,\lambda) = \epsilon_1(\xi_1,\xi_2,\eta_2,\lambda)I_{b1}(\xi_1,\lambda) + \int_\infty^\infty\int_0^1 f_1(\xi_1,\xi_2,\eta_2,\xi_2',\eta_2',\lambda)I_2(\xi_2',\eta_2',\xi_1,\lambda)K_{12}d\xi_2'd\eta_2' \tag{A.16}$$

and

$$I_2(\xi_2,\xi_1,\eta_1,\lambda) = \epsilon_2(\xi_2,\xi_1,\eta_1,\lambda)I_{b2}(\xi_2,\lambda) + \int_\infty^\infty\int_0^1 f_2(\xi_2,\xi_1,\eta_1,\xi_1',\eta_1',\lambda)I_1(\xi_1',\eta_1',\xi_2,\lambda)K_{21}d\xi_1'd\eta_1' \tag{A.17}$$

respectively, where the kernels K_{12} and K_{21} are given by

$$K_{12} = (\gamma + \xi_2' \sin\beta)\,[\sin\beta(\delta_1 - \delta_2 + \xi_1') + \gamma\cos\beta]/(D_1')^4 \qquad \text{(A.18)}$$

$$K_{21} = (\gamma + \xi_2 \sin\beta)\,[\sin\beta(\delta_1 - \delta_2 + \xi_1') + \gamma\cos\beta]/(D_2')^4 \qquad \text{(A.19)}$$

APPENDIX B

Method of Solution of Integral Equation (3.12) or(3.13)

Since the kernels of Eqs. (3.12) and (3.13) are very complicated an exact analytical solution is not possible and a numerical solution is the best that can be obtained. This appendix describes such a solution of the integral equations along with the methods for determining the local irradiation and the local heat flux.

The methods for solving linear Fredholm integral equations of the second kind are well documented in the text of Hildebrand [45]. A review of some of the methods as they pertain to the solution of integral equations arising in problems of radiant interchange is given by Sparrow [4]. Variational methods are limited in that the form of the solution must be chosen and higher order approximations are very tedious. Finite differencing of the integral equation results in a system of algebraic equations, which in many instances requires the simultaneous solution of a large number of algebraic equations which may be ill-conditioned [46] as the results of Love and Gilbert [21] illustrate. The method of successive approximations lends itself readily to numerical computation. The drawbacks of this method are the large number of iterations required and the large number of points needed for numerical evaluation of integrals. However, the method of successive approximations appears to be the only suitable one and has been adopted for the solution of the integral equation.

The Gaussian quadrature was used for all numerical evaluations of integrals in the solution by the method of successive approximations. This quadrature is the most accurate available for the number of points used. Using the Gaussian quadrature the integrals with finite limits can be approximated as

$$\int_a^b f(x,\xi)\, d\xi \simeq \sum_{j=1}^{n} v_j\, f(x,\xi_j) \qquad (B.1)$$

where

$$\xi_j = \tfrac{1}{2}(b-a)y_j + \tfrac{1}{2}(b+a) \qquad (B.2)$$

$$v_j = \tfrac{1}{2}(b-a)\, u_j \qquad (B.3)$$

The weights u_j and the abscissas y_j have been taken from [47]. Similarly, the integrals with infinite limits can

be approximated by

$$\int_{-\infty}^{\infty} f(x,\eta)\, d\eta \simeq \sum_{j=1}^{n} w_j\, f(x,\eta_j) \qquad (B.4)$$

where again the weights w_j and the abscissas η_j tabulated in [48] were used. In terms of formulas (B.1) and (B.4) the double integrals were expressed as

$$\int_a^b \int_{-\infty}^{\infty} f(x,\xi,\eta)\, d\xi d\eta \simeq \sum_{i=1}^{n}\sum_{j=1}^{n} v_i w_j\, f(x,\xi_i,\eta_j) \qquad (B.5)$$

The numerical calculations were carried out on an IBM 7094 digital computer. In order to keep the computer time reasonable the radiation surface characteristics and the kernels had to be calculated once and stored in the core of the computer. As a result of this requirement and because $I(\xi_1,\xi_2,\eta_2)$ is a function of three independent variables, the maximum number of points that could be employed in carrying out the double integrations were n = 8.

In the calculations the successive approximation procedure was terminated after the convergence criteria

$$\left| \frac{I_i(\xi_1,\xi_2,\eta_2) - I_{i-1}(\xi_1,\xi_2,\eta_2)}{I_i(\xi_1,\xi_2,\eta_2)} \right| < 0.001 \qquad (B.6)$$

was satisfied. This convergence criteria was chosen so that the accuracy of the solution was consistent with the number of integration points employed. For the parallel plate geometry it was generally found that as the spacing to width ratio γ and the emissivity ϵ decreased the intensity of radiation leaving a surface $I(\xi_1,\xi_2,\eta_2)$ became greater, and the number of iterations required to achieve convergence increased. For values of $\gamma < 0.25$ the convergence was too prohibitative even on a very fast digital computer. Therefore, the smallest value γ for which results have been obtained by this method was 0.25. Models C, F and G needed the largest number of iterations to achieve convergence, particularly for small values of σ_o/λ or large values of a_o/λ. This was due to the presence of a prominent specular reflection component.

After the intensity of radiation leaving a surface $I(\xi_1,\xi_2,\eta_2)$ had been determined, the local irradiation was evaluated from Eq. (3.3) with the help of Eq. (3.7) using the same integration scheme previously discussed. The local heat loss was calculated from Eq. (3.1).

For the diffuse model A and the specular model B the

local heat loss results reported in References [25] and [6] respectively, were compared with those obtained by the present method for $\gamma = 1.0$ and were found to be in good agreement. However, there is no assurance of a comparable degree of accuracy for small values of $\gamma, \sigma_o/\lambda$ and/or large values of a_o/λ since the number of Gaussian points used for integration may have been insufficient. It is believed that the results obtained are accurate for engineering purposes, and if desired the precision can be improved by increasing the number of integration points and making the error criteria more strict. However, this was not justifiable in view of the purpose of the present study.

APPENDIX C

Discussion of Experimental Errors

An error estimate of the irradiation measurements is difficult and can only be qualitative. The basic reason for this is that it is impossible to accurately estimate the error introduced by the presence of the holes in front of the thermopiles. The effect of the hole is a function of the directional distribution of the incident flux, i.e., the geometry, the test surfaces and the temperatures. The thermopile calibration curves are only relative and not absolute since they were calculated by assuming the 3M and Pyromark black paints were diffuse emitters and reflectors.

In the irradiation measurements residual gases in the system did not have any effect on the measured fluxes since the radiation flux distribution for a given configuration is only a function of surface temperatures and properties. The measurements were made under vacuum conditions because the absence of convection is important in achieving a uniform temperature along and across the plate.

In the incident flux measurements the errors in the physical geometry are small. The estimated errors in h, d_1, d_2, β, and L are all less than 1 percent. The flux incident upon the thermopiles from the surroundings is also a small portion of the measured flux (less than $\frac{1}{2}$ percent), while the temperature error is approximately $\frac{1}{4}$ percent based on the absolute temperature scale.

Although the effect of the presence of the hole can not be estimated, an indication of its effect may be obtained from Fig. 11. On this graph a thermopile calibration curve, calculated as explained in Chapter 4 from the 3M and Pyromark painted plates, is compared to a similiar curve obtained from the cylindrical blackbody. The differences in the incident flux distributions from these two radiation sources is much greater than the differences in flux distributions obtained when using the test surfaces; however, the two calibration curves are within 2 percent of each other.

The total maximum or probable error in the calibration curves is impossible to calculate because of the complexity of the integral equations used in calculating the irradiation; therefore, only errors in each of the quantities used in computing the calibration curves will be discussed. The largest source of error in the calibration curves, beside the effect of the hole, is in determining surface temperatures. The temperature difference across the 3M paint film under high heat transfer rates may be as high as 8°F with an uncertainity of $\pm$ 50 percent due to the necessity of estimating the thermal conductivity of the paint. This leads to a

possible surface temperature error of 1 percent for the cold plate. The uncertainity in the temperature of the Pyromark coated hot plate is approximately $\frac{1}{2}$ percent due to the thinner coating. These temperature errors are compounded by the T^4 terms in the equations for the irradiation. The errors in the emissivities of the painted surfaces used in the calibration curve calculations are relatively high. The maximum errors in the emissivities of the 3M Black Velvet and Pyromark painted surfaces are 7 and 6 percent, respectively [34]. However, the errors in the surface temperatures in both the irradiation and emissivity measurements are primarily due to the difficulty in calculating the temperature drop across the paint. It is expected that these errors would be compensating and the probable errors in the calibration curves would be much lower.

An indication of the reproducability of the irradiation data is given by Fig. 12. On the graph with γ=0.75 the squares and circles represent data taken with different sets of thermopiles at the beginning and end of the experimental work, about three months apart. As shown on the graph the maximum difference between the two sets of data is 4.5 percent.

APPENDIX D

Tabulation of Experimental Data

The local surface temperatures are given in Table D-1 for two typical sets of data. The variation of temperature across the plate is seen to be small, and therefore in Tables D-2 through D-7 only the average surface temperatures are given. In view of the uncertainties in the radiation surface characteristics and other experimental errors, this appears to be reasonable.

Table D-1

Variation of Surface Temperature Across the Plate

a) Sandblasted Stainless Steel; $\gamma=0.75$, $\beta=\delta_1=\delta_2=0$

ξ	T_c(°F)	T_h(°F)
0	74.91	298.92
0.125	74.95	298.94
0.375	75.01	298.99
0.438	75.03	299.01

b) Smooth Gold; $\beta=90°$, $\gamma=\delta_1=0.25$, $\delta_2=0$

0.125	100.07	742.21
0.375	99.94	742.17
0.625	99.61	742.13
0.875	99.48	741.93

TABLE D-2

Experimental Local Irradiation Data for Sandblasted Stainless Steel; $\beta=\delta_1=\delta_2=0$

T_c(°F)	T_h(°F)	G_c^* ξ=0.063	ξ=0.125	ξ=0.25	ξ=0.375	ξ=0.438
		a) γ = 0.75				
50.0	49.8	0.674	0.707	0.802	0.843	0.847
50.0	50.0	0.681	0.741	0.816	0.849	0.866
75.0	298.9	2.51	2.65	3.00	3.13	3.16
75.0	299.2	2.69	2.78	3.19	3.26	3.23
100.0	650.0	10.9	11.6	13.1	13.3	13.4
		b) γ = 0.333				
50.0	50.0	1.21	1.32	1.65	1.71	1.76
75.0	249.6	3.34	3.59	4.38	4.58	4.57
100.0	700.4	19.9	21.5	26.1	27.6	27.9
		c) γ = 0.125				
50.0	50.0	1.85	2.25	2.70	2.83	2.91
75.0	200.1	3.74	4.47	5.28	5.24	5.35
100.0	605.0	19.7	22.7	26.9	26.8	27.8

TABLE D-3

Experimental Local Irradiation Data for Polished Stainless Steel; $\beta=\delta_1=\delta_2=0$

T_c(°F)	T_h(°F)	G_c^* ξ=0.063	ξ=0.125	ξ=0.25	ξ=0.375	ξ=0.438
		a) γ = 0.75				
50.0	50.0	0.894	0.913	1.06	1.07	1.11
75.3	300.0	3.37	3.45	3.94	4.01	4.04
100.0	700.2	17.3	18.2	20.7	20.9	21.3
		b) γ = 0.333				
50.0	50.0	1.79	1.93	2.41	2.55	2.62
75.0	250.0	4.83	5.28	6.46	6.80	6.85
100.0	700.4	32.2	35.4	43.4	43.9	44.3
		c) γ = 0.125				
50.0	50.0	3.57	4.22	5.49	5.93	6.13
75.0	200.1	7.40	8.76	10.7	10.8	11.3
100.0	586.9	37.0	44.1	50.6	53.2	56.3

TABLE D-4

Experimental Local Irradiation Data for Rough Gold; $\beta=\delta_1=\delta_2=0$

T_c(°F)	T_h(°F)	G^*_c ξ=0.063	ξ=0.125	ξ=0.250	ξ=0.375	ξ=0.438
			a) γ = 0.75			
50.0	50.0	0.949	0.976	1.05	1.14	1.14
75.0	299.0	4.34	4.64	5.01	5.37	5.36
100.0	700.4	20.4	21.9	23.9	25.5	25.7
			b) γ = 0.333			
50.0	50.0	2.27	2.43	3.00	3.19	3.21
75.0	249.7	6.85	7.43	8.87	9.45	9.46
100.0	700.7	42.8	47.4	57.8	60.8	61.4
			c) γ = 0.125			
50.0	50.0	5.95	7.21	9.53	10.0	10.5
75.0	204.2	12.7	15.1	19.9	21.7	22.1
100.0	607.0	70.8	80.8	108.0	111.0	113.0

TABLE D-5

Experimental Local Irradiation Data for Smooth Gold; $\beta=\delta_1=\delta_2=0$

T_c(°F)	T_h(°F)	G^*_c ξ=0.063	ξ=0.125	ξ=0.25	ξ=0.375	ξ=0.438
			a) γ = 0.75			
50.0	50.0	0.948	0.991	1.08	1.09	1.13
75.0	299.2	3.44	3.58	3.99	4.05	4.13
100.0	700.4	16.1	16.4	18.1	18.6	18.8
			b) γ = 0.333			
50.0	50.0	2.12	2.32	2.80	3.03	3.06
700.3	100.0	30.8	35.6	41.9	44.6	46.5
			c) γ = 0.125			
50.0	50.0	5.28	6.78	8.38	9.66	9.27
75.0	249.8	13.9	16.1	20.7	21.9	22.5
100.0	693.5	84.5	95.5	116.0	119.0	120.0

TABLE D-6

Experimental Local Irradiation Data for PV100 White Paint; $\beta=\delta_1=\delta_2=0$

T_c(°F)	T_h(°F)	G_c^* ξ=0.063	ξ=0.125	ξ=0.25	ξ=0.375	ξ=0.438
		a) γ = 0.75				
50.0	50.0	0.493	0.523	0.568	0.599	0.604
100.0	309.4	1.63	1.67	1.92	2.04	2.06
		b) γ = 0.125				
50.0	50.0	0.893	1.00	1.09	1.12	1.13
100.0	295.8	2.76	3.03	3.32	3.39	3.50

TABLE D-7

Experimental Local Irradiation for Perpendicular Plates; $\beta=90°$, $\gamma=\delta_1=0.25$, $\delta_2=0$

T_c(°F)	T_h(°F)	G_c^* ξ=0.125	ξ=0.375	ξ=0.50	ξ=0.75	ξ=0.938
		a) Sandblasted Stainless Steel				
50.0	50.0	0.319	0.277	0.268	0.209	0.165
74.5	363.9	2.00	1.74	1.65	1.30	1.08
99.9	703.4	7.56	6.59	6.28	5.00	3.88
		b) Polished Stainless Steel				
50.0	50.0	0.322	0.284	0.277	0.198	0.164
75.0	368.9	2.35	2.02	1.85	1.39	1.56
100.0	878.2	17.4	14.7	13.4	11.3	10.4
		c) Rough Gold				
50.0	50.0	0.362	0.331	0.288	0.241	0.227
75.0	353.1	3.04	2.69	2.24	2.00	1.57
99.8	865.0	17.1	15.5	14.0	12.2	11.6
		d) Smooth Gold				
50.0	50.0	0.326	0.286	0.268	0.224	0.202
75.0	352.7	1.92	1.70	1.57	1.31	1.14
99.8	742.2	8.23	7.42	6.82	5.68	5.07

TABLE E-1

Overall Absorption Factors for Configuration 1
with L/W = 0.5 and $\epsilon_1 = \epsilon_2 = \epsilon$

a) $\mathcal{F}_{12}$

ϵ	H/W	CP			DP	BP(v_o/λ;a_o/λ)		
		D*	D	S	S	2/3;10	1/6;5/2	1/30;1/2
	2.0	.0326	.0334	.0328	.0356	.0352	.0352	.0357
	.5	.258	.254	.252	.286	.284	.285	.288
	.25	.459	.459	.458	.499	.496	.496	.498
0.9	.05	.785	.790	.788	.812	.812	.815	.812
	.025	.844	.850	.852	.865	.863	.865	.866
	.005	.895	.895	.893	.911	.912	.917	.912
	2.0	.0181	.0177	.019	.0165	.0168	.0169	.017
	.5	.146	.140	.150	.146	.140	.141	.143
	.25	.272	.278	.280	.272	.250	.254	.267
0.5	.05	.533	.549	.542	.535	.491	.507	.524
	.025	.593	.611	.599	.595	.560	.580	.589
	.005	.651	.659	.652	.656	.647	.65	.649
	2.0	.00362	.00367	.0048	.0022	.00255	.0026	.003
	.5	.031	.031	.037	.0243	.0207	.0204	.0213
	.25	.064	.069	.075	.0556	.0422	.0428	.0458
0.1	.05	.22	.258	.238	.206	.128	.142	.174
	.025	.31	.363	.326	.300	.200	.222	.264
	.005	.461	.489	.461	.463	.403	.425	.454

b) $\mathcal{F}_{11}$

	2.0	.000118	.00007	.0009	.00087	.00009	.0001	.0008
	.5	.0074	.0067	.0103	.00553	.0024	.0028	.00453
	.25	.0234	.0222	.0226	.0148	.009	.0098	.0137
0.9	.05	.068	.0671	.0668	.0521	.0419	.0485	.0518
	.025	.0784	.0760	.0732	.0651	.0519	.06	.0645
	.005	.0882	.089	.0911	.0743	.0689	.0678	.0723
	2.0	.000327	.00053	.0028	.00267	.000	.000	.0022
	.5	.0209	.0195	.0329	.028	.0138	.0139	.0246
	.25	.0693	.0719	.0765	.0752	.0471	.0494	.0689
0.5	.05	.231	.237	.228	.235	.189	.204	.232
	.025	.276	.2754	.278	.278	.243	.260	.278
	.005	.320	.316	.323	.314	.306	.315	.322
	2.0	.000118	.00013	.00145	.00153	.0001	.00011	.00047
	.5	.0079	.0087	.00738	.00967	.00353	.00333	.0068
	.25	.0295	.0336	.0434	.0324	.0127	.0139	.0233
0.1	.05	.172	.205	.187	.155	.0835	.092	.130
	.025	.259	.314	.265	.239	.14	.173	.207
	.005	.409	.435	.414	.408	.348	.371	.381

TABLE E-2

Overall Absorption Factors for Configuration 1

with L/W = 2500.0 and $\epsilon_1 = \epsilon_2 = \epsilon$

a) $\mathcal{F}_{12}$

ϵ	H/W	CP			DP	BP(a_o/λ;a_o/λ)		
		D*	D	S	S	2/3;10	1/6;5/2	1/30;1/2
	2.0	.213	.216	.219	.236	.236	.237	.235
	.5	.558	.551	.556	.605	.602	.601	.604
	.25	.707	.707	.706	.741	.740	.742	.742
0.9	.05	.864	.867	.867	.883	.886	.888	.885
	.025	.886	.889	.887	.901	.905	.906	.902
	.005	.904	.905	.905	.917	.92	.922	.92
	2.0	.120	.119	.135	.128	.116	.12	.123
	.5	.342	.334	.354	.344	.329	.33	.335
	.25	.461	.460	.461	.459	.430	.435	.450
0.5	.05	.615	.628	.621	.617	.593	.61	.608
	.025	.640	.650	.646	.641	.628	.641	.635
	.005	.661	.665	.666	.667	.663	.66	.66
	2.0	.0247	.025	.04	.031	.0196	.0199	.0261
	.5	.089	.0918	.122	.0996	.063	.0689	.0829
	.25	.154	.166	.182	.159	.104	.1139	.138
0.1	.05	.356	.403	.371	.343	.246	.2802	.32
	.025	.425	.462	.424	.421	.341	.370	.397
	.005	.502	.515	.499	.505	.481	.490	.509

b) $\mathcal{F}_{11}$

	2.0	.00501	.00493	.011	.00793	.00353	.004	.0073
	.5	.0345	.0337	.0353	.0231	.0173	.0178	.0216
	.25	.0552	.0513	.0515	.0415	.0317	.034	.039
0.9	.05	.0882	.0796	.0824	.0672	.0581	.061	.0641
	.025	.0864	.0865	.0865	.0743	.066	.0675	.0725
	.005	.090	.089	.0897	.0784	.074	.0738	.0756
	2.0	.0141	.0137	.0355	.0334	.0165	.0167	.0278
	.5	.105	.110	.127	.120	.083	.0914	.111
	.25	.180	.184	.188	.189	.142	.154	.182
0.5	.05	.292	.286	.287	.291	.265	.28	.293
	.025	.312	.308	.308	.311	.298	.30	.315
	.005	.329	.325	.326	.323	.320	.327	.33
	2.0	.00525	.00533	.0227	.0195	.00554	.00473	.0143
	.5	.0498	.0496	.0858	.0675	.0345	.0357	.0457
	.25	.108	.117	.146	.117	.0631	.0695	.0884
0.1	.05	.305	.346	.308	.290	.205	.2253	.264
	.025	.373	.412	.380	.359	.288	.306	.340
	.005	.450	.458	.454	.445	.425	.432	.433

TABLE E-3

Overall Absorption Factors for Configuration 2:
Surfaces 1 and 2 are Diffuse and Surface 3
is Adiabatic and Perfectly Reflecting with
H/W = 1.0 and L/W = 1.0

a) $\mathcal{F}'_{12}$

ϵ	Z/W	CP		BP($c_o/\lambda : a_o/\lambda$)				
		D	S	2/3;10	1/6;5/2	1/15;1	2/45;2/3	1/30;1/2
1.0	0.5	.0239	.050	.0296	.0311	.0352	.0398	.0423
0.5	0.5	.0122	.0251	.0156	.0162	.0176	.020	.0213
0.1	0.5	.00248	.00528	.00328	.00347	.00358	.00405	.00427
1.0	1.0	.0058	.0201	.0156	.0173	.0178	.0175	.0186
0.5	1.0	.0030	.0103	.00824	.0088	.0085	.00883	.0092
0.1	1.0	.000458	.00215	.00152	.00166	.00192	.00188	.00195

b) $\mathcal{F}'_{11}$

1.0	0.5	.0281	.0343	.015	.0158	.0215	.0307	.0281
0.5	0.5	.014	.0179	.007	.0075	.0104	.0158	.0138
0.1	0.5	.00271	.00396	.00139	.00145	.0022	.00295	.00328
1.0	1.0	.0091	.0000	.00064	.00081	.000292	.00689	.0000
0.5	1.0	.00437	.0001	.00038	.00042	.000153	.0000972	.0000
0.1	1.0	.000842	.0000417	.0000833	.0000417	.0000556	.0000292	.0000278

TABLE E-4

Overall Absorption Factors for Configuration 2; Surfaces 1 and 2 are Diffuse and Surface 3 is Adiabatic and Perfectly Reflecting with H/W = 1.0 and L/W = 5000.0

a) $\mathcal{F}'_{12}$

ϵ	Z/W	CP		BP(σ_o/λ;a_o/λ)	
		D	S	1/3;5	2/45;2/3
1.0	0.5	.111	.180	.145	.159
0.5	0.5	.0632	.102	.0825	.0902
0.1	0.5	.0143	.0236	.0181	.0203
1.0	1.0	.0363	.0907	.0842	.0821
0.5	1.0	.0195	.0457	.0419	.0443
0.1	1.0	.00406	.00918	.00845	.00893

b) $\mathcal{F}'_{11}$

1.0	0.5	.124	.118	.0854	.125
0.5	0.5	.0704	.0731	.0525	.0647
0.1	0.5	.0158	.0179	.0122	.0154
1.0	1.0	.0476	.00	.004	.0205
0.5	1.0	.0247	.00225	.0394	.0044
0.1	1.0	.00513	.000812	.00111	.0012

TABLE E-5

Overall Absorption Factor for Configuration 3
with L/W = 1.0 and $\epsilon_1 = \epsilon_2 = \epsilon$

a) $\mathcal{F}'_{12}$

ϵ	β^*	CP			DP	BP(σ_o/λ;a_o/λ)		
		D*	S	D	S	2/3;10	1/6;5/2	1/30;1/2
	15	----	.703	.716	.737	.733	.746	.744
	45	.436	.442	.443	.459	.445	.448	.450
0.9	60	.335	.333	.340	.345	.344	.346	.340
	90	.180	.180	.179	.169	.172	.172	.168
	135	.043	.0438	.0452	.0284	.0319	.0278	.0294
	15	----	.457	.477	.461	.43	.441	.454
	45	.280	.253	.268	.247	.242	.242	.242
0.5	60	.192	.185	.203	.184	.192	.190	.184
	90	.101	.1001	.1005	.0989	.0994	.0994	.0979
	135	.025	.0248	.0238	.0245	.0276	.0264	.0252
	15	----	.143	.208	.141	.107	.129	.144
	45	.06	.051	.0698	.0506	.0515	.0518	.0502
0.1	60	.0418	.0327	.0464	.0339	.0374	.0366	.0346
	90	.0207	.0189	.0206	.0208	.0216	.021	.0203
	135	.0048	.0044	.0049	.009	.00925	.00889	.00939

b) $\mathcal{F}'_{11}$

	15	----	.0553	.0603	.0367	.0377	.0362	.036
	45	.0214	.017	.0251	.00913	.017	.0136	.00887
0.9	60	.0124	.0071	.0153	.00329	.0127	.0087	.00356
	90	.0036	.00	.00483	.00	.00634	.0034	.000446
	135	.00036	.00	.000233	.00	.00187	.00573	.000011
	15	----	.179	.20	.183	.166	.165	.177
	45	.060	.0453	.0765	.0525	.0709	.0646	.0503
0.5	60	.0357	.0216	.0483	.0243	.0498	.042	.0233
	90	.0101	.00	.0136	.00	.018	.0151	.00183
	135	.00101	.00	.000867	.00	.00408	.00185	.000128
	15	----	.0973	.162	.0973	.064	.072	.102
	45	.025	.0181	.0389	.0194	.0258	.0236	.0197
0.1	60	.014	.0071	.0202	.0119	.0188	.0167	.0115
	90	.0037	.00	.0054	.00	.00809	.00674	.000725
	135	.00036	.00	.0002	.00	.00296	.00161	.0000606

Table E-6

Overall Absorption Factors for Configuration 3

with L/W = 5000.0 and $\epsilon_1 = \epsilon_2 = \epsilon$

a) $\mathcal{F}_{12}$

ϵ	$\beta°$	CP			DP	BP(σ_o/λ;a_o/λ)		
		D*	S	D	S	2/3;10	1/6;5/2	1/30;1/2
	15	.788	.783	.784	.807	.797	.81	.805
	45	.558	.554	.560	.568	.564	.566	.559
0.9	60	.451	.451	.453	.452	.443	.452	.440
	90	.264	.265	.261	.244	.248	.247	.246
	135	.0685	.0696	.0705	.0433	.0488	.0437	.0442
	15	.536	.528	.549	.526	.475	.504	.521
	45	.341	.322	.353	.318	.317	.325	.318
0.5	60	.267	.249	.270	.250	.254	.252	.247
	90	.150	.147	.152	.148	.15	.155	.150
	135	.0381	.0389	.0395	.0393	.0403	.0427	.0412
	15	.224	.178	.272	.188	.1313	.175	.194
	45	.0893	.0663	.101	.074	.0753	.080	.0742
0.1	60	.0627	.0498	.068	.0503	.0579	.0576	.0516
	90	.0315	.0294	.0318	.0342	.0374	.0369	.0348
	135	.0077	.0075	.0080	.0173	.0169	.017	.0177

b) $\mathcal{F}_{11}$

	15	.0686	.0668	.0695	.0466	.0586	.052	.045
	45	.0344	.0277	.0363	.0142	.0442	.0289	.0139
0.9	60	.0226	.0114	.0240	.00533	.036	.0215	.00583
	90	.00773	.00	.0081	.00	.0242	.0113	.000495
	135	.000522	.00	.00035	.00	.00864	.00191	.000014
	15	.233	.223	.247	.223	.233	.226	.218
	45	.105	.0706	.110	.0773	.143	.120	.075
0.5	60	.0667	.0336	.0734	.0371	.108	.0849	.0372
	90	.0219	.00	.025	.00	.058	.0403	.0024
	135	.00145	.00	.0020	.00	.0134	.00531	.000184
	15	.176	.129	.223	.137	.107	.119	.146
	45	.0496	.0270	.0629	.0314	.0548	.0474	.0335
0.1	60	.0282	.0101	.037	.0203	.0417	.0345	.0203
	90	.0083	.00	.0102	.00	.0244	.0166	.00122
	135	.000524	.00	.00055	.00	.0103	.00445	.000249

TABLE E-7

Overall Absorption Factors for Configuration 4:
Surface 3 is Adiabatic, Diffuse and Perfect Reflector,
Identical Surfaces 1 and 2, $\epsilon_1 = \epsilon_2 = \epsilon$, L/W = 5000.0

a) $\mathcal{J}'_{12}$

ϵ	H/W	CP		DP	BP(σ_o/λ;a_o/λ)		
		D	S	S	2/3;10	1/6;5/2	1/30;1/2
	4.0	.1302	.126	.136	.137	.138	.137
0.9	1.0	.451	.448	.478	.483	.472	.478
	.25	.760	.752	.785	.780	.783	.788
	4.0	.0795	.0767	.0734	.0742	.0724	.0735
0.5	1.0	.286	.28	.272	.299	.301	.276
	.25	.535	.503	.502	.49	.535	.519
	4.0	.0321	.0221	.0177	.0137	.0135	.015
0.1	1.0	.123	.0859	.070	.114	.103	.0673
	.25	.255	.202	.179	.285	.279	.188

b) $\mathcal{J}'_{11}$

	4.0	.0985	.096	.0886	.0941	.090	.0938
0.9	1.0	.105	.113	.0934	.101	.103	.0936
	.25	.106	.103	.0794	.0895	.085	.0837
	4.0	.0621	.0688	.0697	.0671	.0647	.0706
0.5	1.0	.123	.127	.124	.165	.161	.130
	.25	.257	.224	.227	.273	.255	.241
	4.0	.0143	.0217	.0225	.0178	.0176	.0221
0.1	1.0	.0474	.0597	.0518	.0952	.0843	.0486
	.25	.209	.157	.136	.240	.230	.146

Unclassified

Security Classification

DOCUMENT CONTROL DATA - R&D

(Security classification of title, body of abstract and indexing annotation must be entered when the overall report is classified)

1. ORIGINATING ACTIVITY (Corporate author)
School of Mechanical Engineering
Purdue University
Lafayette, Indiana 47907

2a. REPORT SECURITY CLASSIFICATION
Unclassified

2b. GROUP

3. REPORT TITLE
Analysis and Experiment of Radiant Heat Exchange Between Simply Arranged Surfaces

4. DESCRIPTIVE NOTES (Type of report and inclusive dates)
TR

5. AUTHOR(S) (Last name, first name, initial)
Viskanta, Raymond
Schornhorst, James R.
Toor, Jaswant S.

6. REPORT DATE
July 1967

7a. TOTAL NO. OF PAGES
114

7b. NO. OF REFS
47

8a. CONTRACT OR GRANT NO.
AF 33(615)-2362

b. PROJECT NO.
6146

c.

d. 614616

9a. ORIGINATOR'S REPORT NUMBER(S)
AFFDL-TR-67-94

9b. OTHER REPORT NO(S) (Any other numbers that may be assigned this report)

10. AVAILABILITY/LIMITATION NOTICES
Distribution of this abstract is unlimited.

11. SUPPLEMENTARY NOTES

12. SPONSORING MILITARY ACTIVITY
Air Force Flight Dynamics Laboratory
Wright-Patterson Air Force Base, Ohio

13. ABSTRACT
The work reported herein covers the effort to improve the accuracy and to provide some confidence in the analytical methods for predicting radiant heat exchange among surfaces having nonelementary emission and reflection characteristics. The study consisted of an examination of the validity of commonly used simplified methods of radiant heat transfer analysis, measurements of local irradiation at a surface and Monte Carlo calculations to estimate what level of detail is important in the description of the radiation characteristics of surfaces.

The radiant heat transfer problem was first formulated for a general enclosure with as few simplifying assumptions as possible and then specialized to a very simple configuration. Solutions for the local radiant heat flux and incident flux were obtained for seven different models approximating the radiation characteristics of surfaces.

The local irradiation measurements were made for sandblasted stainless steel, electropolished stainless steel, rough electroplated gold, smooth electroplated gold, and PV 100 white paint over the temperature range from 50°F to 850°F. The predictions of the local incident flux using the diffuse, specular, and diffuse-specular models have been compared with experimental results.

The Monte Carlo results showed that under some conditions the choice of the model for radiation surface characteristics can be very critical for both the local heat transfer and overall radiant interchange calculations.

DD FORM 1473

Unclassified

Security Classification

Unclassified

Security Classification

KEY WORDS	LINK A		LINK B		LINK C	
	ROLE	WT	ROLE	WT	ROLE	WT
Radiant Heat Transfer						

INSTRUCTIONS

1. ORIGINATING ACTIVITY: Enter the name and address of the contractor, subcontractor, grantee, Department of Defense activity or other organization *(corporate author)* issuing the report.

2a. REPORT SECURITY CLASSIFICATION: Enter the overall security classification of the report. Indicate whether "Restricted Data" is included. Marking is to be in accordance with appropriate security regulations.

2b. GROUP: Automatic downgrading is specified in DoD Directive 5200.10 and Armed Forces Industrial Manual. Enter the group number. Also, when applicable, show that optional markings have been used for Group 3 and Group 4 as authorized.

3. REPORT TITLE: Enter the complete report title in all capital letters. Titles in all cases should be unclassified. If a meaningful title cannot be selected without classification, show title classification in all capitals in parenthesis immediately following the title.

4. DESCRIPTIVE NOTES: If appropriate, enter the type of report, e.g., interim, progress, summary, annual, or final. Give the inclusive dates when a specific reporting period is covered.

5. AUTHOR(S): Enter the name(s) of author(s) as shown on or in the report. Enter last name, first name, middle initial. If military, show rank and branch of service. The name of the principal author is an absolute minimum requirement.

6. REPORT DATE: Enter the date of the report as day, month, year, or month, year. If more than one date appears on the report, use date of publication.

7a. TOTAL NUMBER OF PAGES: The total page count should follow normal pagination procedures, i.e., enter the number of pages containing information.

7b. NUMBER OF REFERENCES: Enter the total number of references cited in the report.

8a. CONTRACT OR GRANT NUMBER: If appropriate, enter the applicable number of the contract or grant under which the report was written.

8b, 8c, & 8d. PROJECT NUMBER: Enter the appropriate military department identification, such as project number, subproject number, system numbers, task number, etc.

9a. ORIGINATOR'S REPORT NUMBER(S): Enter the official report number by which the document will be identified and controlled by the originating activity. This number must be unique to this report.

9b. OTHER REPORT NUMBER(S): If the report has been assigned any other report numbers *(either by the originator or by the sponsor)*, also enter this number(s).

10. AVAILABILITY/LIMITATION NOTICES: Enter any limitations on further dissemination of the report, other than those imposed by security classification, using standard statements such as:

(1) "Qualified requesters may obtain copies of this report from DDC."

(2) "Foreign announcement and dissemination of this report by DDC is not authorized."

(3) "U. S. Government agencies may obtain copies of this report directly from DDC. Other qualified DDC users shall request through _____."

(4) "U. S. military agencies may obtain copies of this report directly from DDC. Other qualified users shall request through _____."

(5) "All distribution of this report is controlled. Qualified DDC users shall request through _____."

If the report has been furnished to the Office of Technical Services, Department of Commerce, for sale to the public, indicate this fact and enter the price, if known.

11. SUPPLEMENTARY NOTES: Use for additional explanatory notes.

12. SPONSORING MILITARY ACTIVITY: Enter the name of the departmental project office or laboratory sponsoring *(paying for)* the research and development. Include address.

13. ABSTRACT: Enter an abstract giving a brief and factual summary of the document indicative of the report, even though it may also appear elsewhere in the body of the technical report. If additional space is required, a continuation sheet shall be attached.

It is highly desirable that the abstract of classified reports be unclassified. Each paragraph of the abstract shall end with an indication of the military security classification of the information in the paragraph, represented as *(TS), (S), (C), or (U)*

There is no limitation on the length of the abstract. However, the suggested length is from 150 to 225 words.

14. KEY WORDS: Key words are technically meaningful terms or short phrases that characterize a report and may be used as index entries for cataloging the report. Key words must be selected so that no security classification is required. Identifiers, such as equipment model designation, trade name, military project code name, geographic location, may be used as key words but will be followed by an indication of technical context. The assignment of links, rules, and weights is optional.

Unclassified

Security Classification